

# Polarized Neutron Reflectometry

C. F. Majkrzak,<sup>1</sup> K. V. O'Donovan,<sup>1,2,3</sup> N. F. Berk<sup>1</sup>

<sup>1</sup>Center for Neutron Research,  
National Institute of Standards and Technology,  
Gaithersburg, MD 20899, USA

<sup>2</sup>University of Maryland, College Park, MD 20742, USA

<sup>3</sup>University of California, Irvine, CA 92697

April 16, 2004

# Contents

<b>1</b>	<b>Polarized Neutron Reflectometry</b>	<b>3</b>
1.1	Introduction . . . . .	3
1.2	Fundamental Theory of Neutron Reflectivity . . . . .	6
1.2.1	Wave Equation in Three Dimensions . . . . .	8
1.2.2	Refractive Index . . . . .	10
1.2.3	Specular Reflection from a Perfectly Flat Slab: The Wave Equation in One Dimension . . . . .	11
1.2.4	Specular Reflection from a Film with a Nonuniform SLD Profile . . . . .	16
1.2.5	Born Approximation . . . . .	18
1.2.6	Nonspecular Reflection . . . . .	19
1.3	Spin-Dependent Neutron Wave Function . . . . .	21
1.3.1	Neutron Magnetic Moment and Spin Angular Momentum	21
1.3.2	Explicit Form of the Spin-Dependent Neutron Wave Function . . . . .	22
1.3.3	Polarization . . . . .	24
1.3.4	Selecting a Neutron Polarization State . . . . .	26
1.3.5	Changing a Neutron's Polarization . . . . .	28
1.4	Spin-Dependent Neutron Reflectivity . . . . .	36
1.4.1	Spin-Dependent Reflection from a Magnetic Film in Vacuum Referred to Reference Frame of Film . . . . .	37
1.4.2	Magnetic Media Surrounding Film . . . . .	53
1.4.3	Coordinate System Transformation . . . . .	55
1.4.4	Selection Rules "of Thumb" . . . . .	58
1.4.5	Three-Dimensional Polarization Analysis . . . . .	61
1.4.6	Elementary Spin-Dependent Reflectivity Examples . .	63
1.5	Experimental methods . . . . .	66

1.6	An Illustrative Application of PNR . . . . .	70
1.6.1	Symmetries of Reflectance Matrices . . . . .	70
1.6.2	Basis-Independent Representation . . . . .	73
1.6.3	Front-Back Reflectivity of Idealized Twists . . . . .	75
1.6.4	PNR of Actual Systems . . . . .	80
	Appendix . . . . .	85
	Bibliography . . . . .	96

# Chapter 1

## Polarized Neutron Reflectometry

### 1.1 Introduction

Advances in our understanding of the structure and properties of matter have so often depended upon finding the right probe for studying a given problem. This was appreciated long ago, at the beginning of the evolution of modern science. In his masterpiece *Faust*, Johann Wolfgang von Goethe wrote about the legend of Doctor Faust, who bargained his immortal soul to the Devil, Mephistopheles, in exchange for unlimited knowledge. Early in the story, Faust ponders the relationship between humankind and the universe (Part I, Scene I):[1]

*Mysterious even in open day,  
Nature retains her veil, despite our clamors:  
That which she doth not willingly display  
Cannot be wrenched from her with levers, screws, and hammers.*

Fortunately, for anyone in the 21st century interested in the structure of condensed matter on the atomic and nanometer length scales, the considerable efforts of our predecessors have led to the development of a remarkable collection of sophisticated and exquisitely sensitive probes (far surpassing the capabilities of levers, screws, and hammers). These newfound tools are so powerful, in fact, that making a pact with Mephistopheles may no longer be necessary!

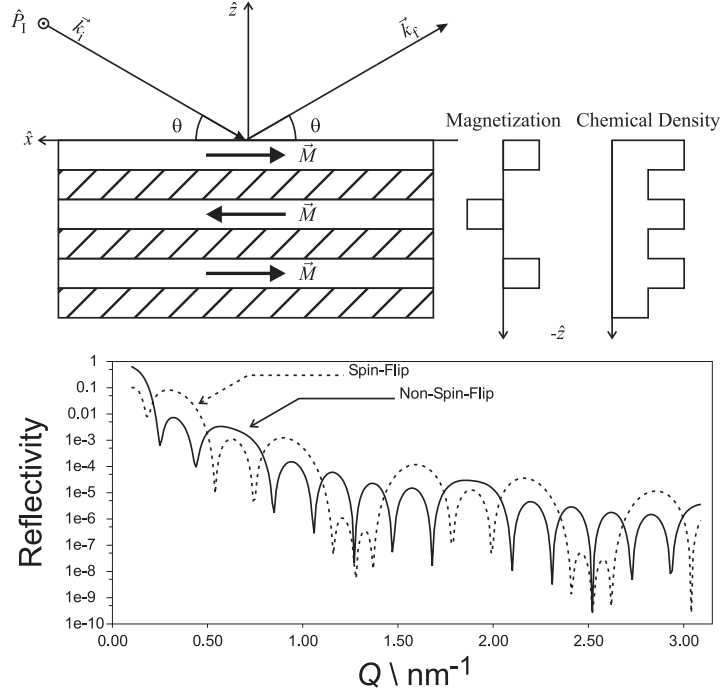


Figure 1.1: Schematic illustration of the structural information which can be deduced from a polarized neutron reflectivity measurement, performed under specular conditions, on a typical model magnetic film. The film is flat and composed of alternating layers of ferromagnetic (the magnetization direction in a given layer is indicated by an arrow) and nonmagnetic material. The reflected intensity, measured as a function of the glancing angle of incidence  $\theta$  or wavevector transfer  $Q$ , can be analysed to obtain the in-plane average of the chemical composition and vector magnetization as a function of depth along the surface normal, with subnanometer resolution under certain conditions, as is described in detail in the text. Reflectivities for a polarized incident beam can be differentiated according to whether the spin state of the neutron changes (“flips”) upon reflection from a magnetic film. In this particular example, the relative orientations of incident neutron polarization  $\hat{P}_1$  and layer magnetizations  $\vec{M}$  are such that the non-spin-flip reflectivity contains information only about the chemical compositional depth profile whereas the spin-flip reflectivity reveals the vector magnetization depth profile.

Polarized neutron reflectometry (PNR) is one such probe that is particularly well suited for determining the nanostructures of magnetic thin films and multilayers. Different types of magnetometers ordinarily yield only average magnetization values, integrated over the entire volume of the specimen, whereas other probes which do possess a higher degree of spatial resolution, such as scanning electron microscopy with polarization analysis (SEMPA) [2], are specifically surface sensitive because their relatively strong interaction with matter limits penetration. Together with magnetic x-ray scattering, PNR provides a unique means of “seeing” the vector magnetization with extraordinary spatial detail well beneath the surface. For neutrons this sensitivity to atomic magnetic moments comes about because the neutron itself possesses a magnetic moment and neutrons can be obtained with a wavelength comparable to interatomic distances. More specifically, the specular reflection of polarized neutrons, namely, coherent elastic scattering for which the angles of incidence and reflection of the neutron wavevector relative to a flat surface are of equal magnitude, can be analysed to yield the in-plane average of the vector magnetization depth profile along the surface normal. By measuring the reflectivity (the ratio of reflected to incident intensities) over a sufficiently broad range of wavevector transfer  $\vec{Q}$ , subnanometer spatial resolution can be achieved. The specular geometry is depicted schematically in Figure 1.1. Furthermore, by tilting  $\vec{Q}$  away from the surface normal, the resulting projection of  $\vec{Q}$  parallel to the surface of the film allows in-plane fluctuations of the magnetization, which give rise to nonspecular scattering, to be sensed. Unlike optical or electron microscopy, neutron and x-ray reflectometry do not directly provide real-space images of the objects of interest. Because neutron and x-ray wavelengths are of the order of the dimensions of the objects being viewed, the information about shape and composition that is contained in the reflected radiation pattern, including the vector magnetization depth profile, must be extracted by mathematical analysis.

Given the ability to obtain the vector magnetization profile by PNR, a multilayered structure composed of ferromagnetic films separated by intervening layers of another material can be systematically studied to reveal various fundamental magnetic behaviors. For instance, the strength and range of the interlayer magnetic interaction between ferromagnetic layers can be examined as a function of layer thickness, crystallographic orientation, the strain associated with lattice mismatch (in single-crystalline films), the electronic states (*e.g.*, super-, normal-, semi-conducting or insulating) and magnetic

configurations (co- and noncollinear) of the intervening layers, and on chemical interdiffusion (*e.g.*, of hydrogen). Investigations of magnetic domain size and orientation and the effects of finite layer thickness can also be performed by measuring both specular and nonspecular spin-dependent scattering.

A broad range of related problems of fundamental scientific and technological interest involving magnetic thin films can be addressed using PNR, especially when employed in conjunction with other techniques such as magnetic x-ray reflectometry and complementary real-space probes. Nonetheless, the realization of this research potential depends to a certain extent on the capability of growing nanostructures with atomic scale precision by a variety of thin-film vapor deposition techniques, *e.g.*, molecular beam epitaxy.

It is not the purpose of this chapter to review the multitude of magnetic thin film systems which have been studied with PNR. There exists a substantial literature on this subject, including a number of review articles [3, 4]. The primary goal here, rather, is to describe the fundamental concepts of the theory and experimental methodology of PNR. As it turns out, a significant fraction of the description of the basic reflection process for polarized neutrons can be applied to magnetic x-ray reflection and to more general reflectometry studies involving nonmagnetic materials.

## 1.2 Fundamental Theory of Neutron Reflectivity

For our purposes, we can (fortunately) ignore the intricate internal workings of the quarks comprising a neutron having an energy in the millielectron volt range and concentrate on only a few resultant properties that are relevant to its interaction with condensed matter. As it happens, we can accurately represent the neutron, according to quantum mechanics, in the simplest of terms as a plane wave of wavevector  $\vec{k}$  propagating undistorted through free space, as represented in Figure 1.2. Because we are concerned with elastic scattering processes in which the neutron in interacting with matter or magnetic field neither gains nor loses energy (*i.e.*, the total energy of the neutron is conserved), the neutron wave function and corresponding time-independent Schrödinger wave equation of motion do not exhibit any explicit dependence on time. (This does not imply, however, that the neutron has zero velocity.) We will defer discussion of the neutron spin and magnetic interactions until

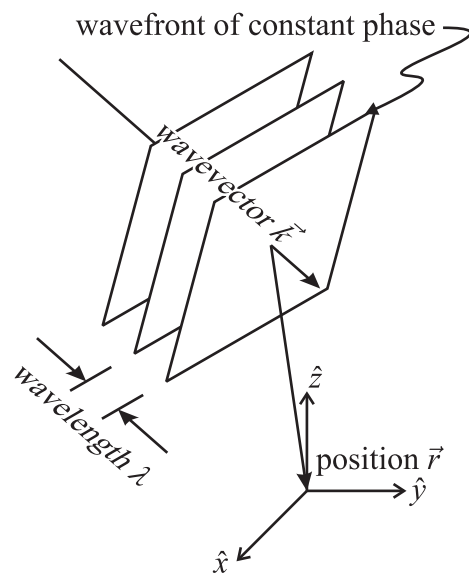


Figure 1.2: Idealized representation of a neutron as a plane wave propagating in space (the planar wavefronts of constant phase are assumed to extend laterally to infinity).

Section 1.3. General discussions of the specular reflection of waves in one dimension can be found in such texts as Merzbacher [5] and Born and Wolf [6]. Early discussions of specular reflection specific to neutrons can be found in a number of works including those of Yamada *et al.* [7] and Croce and Pardo [8].

### 1.2.1 Wave Equation in Three Dimensions

The mathematical representation of a neutron plane wave in three dimensions is given by

$$\Psi(\vec{k}, \vec{r}) = e^{i\vec{k}\cdot\vec{r}} \quad (1.1)$$

where the neutron wavevector  $\vec{k} = k_x\hat{x} + k_y\hat{y} + k_z\hat{z}$  and its position in space  $\vec{r} = x\hat{x} + y\hat{y} + z\hat{z}$ . The square of the modulus of the neutron wavefunction,  $|\Psi|^2 = \Psi^*\Psi$ , is interpreted as the probability that a given neutron can be found at a specific location in space with a particular momentum  $mv = h/\lambda = \hbar k$  (where  $m$  is the neutron mass,  $v$  its velocity,  $\lambda$  its wavelength,  $h$  is Planck's constant, and  $\hbar = h/(2\pi)$ ). The description of the neutron as a single plane wave implies that it extends infinitely in all directions. A more realistic representation would be a wavepacket consisting of a coherent superposition of plane waves, having a distribution of different wavevectors, which results in a localization in space consistent with a corresponding uncertainty in momentum—an inescapable quantum phenomenon (see, for example, the text by Merzbacher [5]). Nonetheless, in regard to the wave equation of interest, for the problem at hand (Equation 1.2 below), it turns out that the single, plane-wave representation of the neutron is remarkably accurate in practice. Thus, unless necessary to do otherwise, we will treat the neutron so.

Now the neutron interacts with matter primarily through a nuclear potential and a magnetic potential which affect the magnitude of  $\vec{k}$ . The strengths of these potentials are effectively characterized by scalar “coherent” scattering lengths, although for the magnetic coupling a scattering-angle-dependent “form factor” is also necessary at sufficiently high wavevector transfers (due to the relatively extended spatial distribution of unpaired electron spin density which gives rise to the magnetic potential). We will ignore absorptive as well as incoherent interactions for the time being and also make the assumption throughout that any nuclear spins in the materials considered are completely disordered (see, *e.g.*, the book by Bacon [9] for a discussion). To

properly account for the neutron magnetic moment and its interaction with a magnetic potential requires that the neutron be represented by a more complicated wave function consisting of two components, each of which has the form of a plane wave. Discussion of the magnetic interaction will be postponed until Section 1.3.

At present there exist no coherent neutron sources analogous to a photon laser: the neutrons in a beam can be taken to be independent of and effectively noninteracting with one another. Therefore, we can avoid the concept of beams altogether in describing the reflection process and focus on one neutron at a time, as represented by a plane wave, and compute probabilities that a neutron is, say, reflected or transmitted by a particular film structure.

Since we are concerned here with structural (instead of vibrational) information, we can limit our considerations to elastic scattering processes, as mentioned earlier. Thus, a time-independent Schrödinger wave equation predicts the evolution of a single neutron plane wave in its interaction with material:

$$\left[ -\frac{\hbar^2}{2m}\nabla^2 + V(\vec{r}) \right] \Psi = E\Psi \quad (1.2)$$

where

$$\nabla^2 = \frac{\partial^2}{\partial x^2} + \frac{\partial^2}{\partial y^2} + \frac{\partial^2}{\partial z^2} \quad (1.3)$$

and where the first term of the Hamiltonian operator in the brackets on the left-hand side of Equation 1.2 represents the kinetic energy while the second term accounts for the potential energy  $V$  of the neutron. Outside of a material medium, the potential energy is zero. On the right-hand side (RHS) of the equation,  $E$  expresses the total energy of the neutron, which is taken to be conserved for the static nonabsorbing potentials which we are considering here. (A description of the quantum mechanics pertinent to the neutron reflection process can be found, for example, in the text by Merzbacher [5].) Now in vacuum,  $V(\vec{r}) = 0$  so that the total energy  $E$  of the neutron is equal to the kinetic energy alone. Consequently,

$$E_0 = \frac{1}{2}mv_0^2 = \frac{\hbar^2 k_0^2}{2m} \quad (1.4)$$

where the subscript “0” signifies the value for free space. For now we will assume that matter can be described as a continuous distribution without an atomic scale granularity. That this is in fact a valid assumption can be

demonstrated by calculation for model film structures using the reflectivity formula to be derived below. Within a continuous medium of density  $N$  (number of scattering centers, *e.g.*, atoms, per unit volume), the potential energy is given by [10, 11]

$$V = \frac{2\pi\hbar^2}{m}Nb = \frac{2\pi\hbar^2}{m}\rho \quad (1.5)$$

where it is assumed that the material consists of only a single isotope of a given element possessing a coherent scattering length  $b$  and  $\rho$  is defined as the scattering length density (SLD). If absorption were present, then the scattering length would include an imaginary component, but, as stated above, such a possibility will be ignored for the discussion here since it only complicates the derivations without adding any essential insight in most cases; for neutron reflection, absorption is rarely an appreciable effect. For multicomponent materials the SLD can be generalized to

$$\rho = \sum_{j=1}^M N_j b_j \quad (1.6)$$

where  $M$  is the number of distinct types of isotopes present.

Now because the total energy of the neutron is conserved in an elastic process, we can equate the kinetic energy of the neutron in vacuum with the constant total energy  $E$  within any material medium. Then, substituting the RHS's of Equations 1.4 and 1.5 into Equation 1.2 and simplifying, we obtain the three-dimensional wave equation

$$[\nabla^2 + k_0^2 - 4\pi\rho] \Psi = 0. \quad (1.7)$$

### 1.2.2 Refractive Index

We can impose conservation of energy once again to define a neutron refractive index analogous to that employed in ordinary light optics. In vacuum,  $E$  is given by Equation 1.4, whereas within a medium

$$E = \frac{\hbar^2 k^2}{2m} + \frac{2\pi\hbar^2}{m}\rho. \quad (1.8)$$

Equating the RHS's of Equations 1.4 and 1.8 we get a relationship between the neutron wavevector  $k$  inside and  $k_0$  outside of the medium of scattering length density  $\rho$ :

$$k^2 = k_0^2 - 4\pi\rho. \quad (1.9)$$

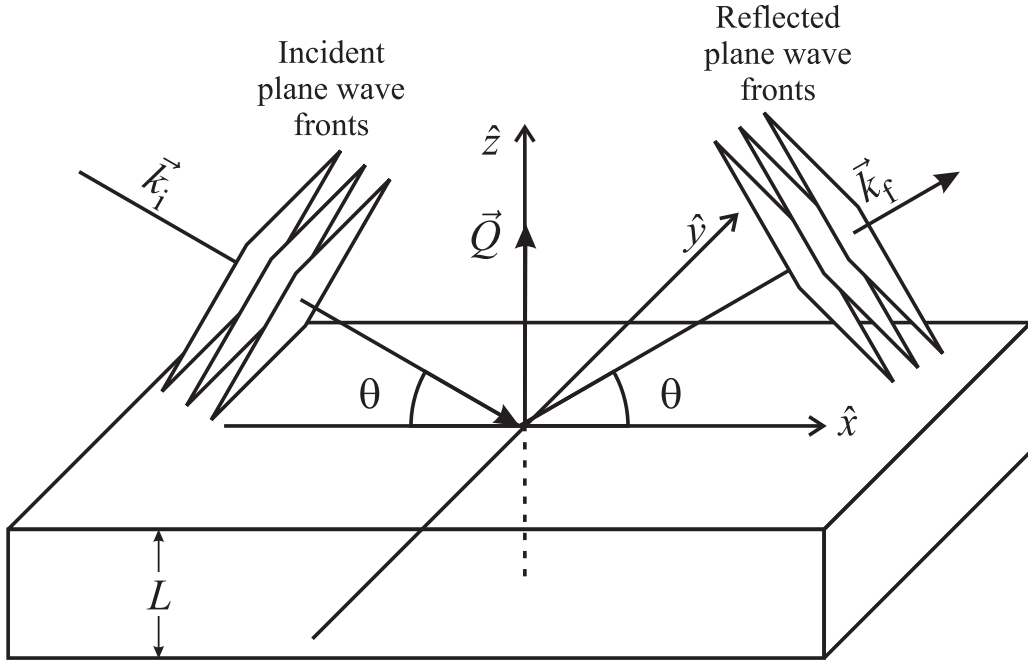


Figure 1.3: Diagram of the specular reflection of a plane wave from a homogeneous flat slab of thickness  $L$  (and of infinite lateral extent in the  $xy$  plane).

The refractive index  $n$  is defined as the ratio  $k/k_0$  so that

$$n(k_0) = \sqrt{1 - 4\pi\rho/k_0^2} \quad (1.10)$$

and  $k = nk_0$ . Thus, we can write Equation 1.7 alternatively as

$$[\nabla^2 + k^2] \Psi = 0. \quad (1.11)$$

### 1.2.3 Specular Reflection from a Perfectly Flat Slab: The Wave Equation in One Dimension

Consider next the reflection of a neutron plane wave from an idealized slab of material of thickness  $L$  and infinite lateral extent in the plane of the film, as depicted in Figure 1.3. This slab is perfectly flat, smooth, and homogeneous. In Figure 1.3, the reflection of the wave is depicted to be

specular in nature, *i.e.*, as mentioned earlier, the angles of incidence and reflection are equal in magnitude. It will be shown in the following discussion that this specular condition is indeed the only possibility for reflection if there are no material density fluctuations along  $x$  or  $y$  in plane and the density is a function of  $z$  alone, along the surface normal: *i.e.*,  $\rho(x, y, z) = \rho(z)$ . (Here, since  $|\vec{k}_i| = |\vec{k}_f|$ ,  $\vec{Q} = \vec{k}_f - \vec{k}_i$  implies that  $|\vec{Q}| = 2k_0 \sin(\theta)$ . We will have to solve the general equation of motion 1.11 for a nonuniform SLD, specifically for a region of space where abrupt changes in the potential occur along  $z$ .

To determine the physical constraints on the mathematical solution, let us first assume that we are in another region of space where the SLD has a uniform but nonzero value everywhere. In this particular case the solution to Equation 1.11 has the particularly simple form of a plane wave

$$\begin{aligned} \Psi(\vec{r}) &= \Psi(x, y, z) = \psi(x)\psi(y)\psi(z) \\ &\parallel \parallel \\ e^{i\vec{k}\cdot\vec{r}} &= e^{i(k_x x + k_y y + k_z z)} = e^{ik_x x} e^{ik_y y} e^{ik_z z} \end{aligned} \quad (1.12)$$

which, when substituted into Equation 1.11 yields an identity which can be recast, using the expanded form of Equation 1.9, as

$$k_x^2 + k_y^2 + k_z^2 + 4\pi\rho = k_{0x}^2 + k_{0y}^2 + k_{0z}^2. \quad (1.13)$$

Now let us return to the case in which the SLD is zero everywhere except for a slab of thickness  $L$  perpendicular to the  $z$  axis wherein  $\rho = \rho(z)$  only so that  $d\rho/dx$  and  $d\rho/dy$ , which are proportional to the gradients of the potential in the respective directions (see Equation 1.5), are zero. Thus, no force can be exerted on the neutron along the  $x$  or  $y$  directions and the momentum and corresponding wavevector components along  $x$  and  $y$  must be conserved as “constants of the motion”; *i.e.*,  $k_x = k_{0x}$  and  $k_y = k_{0y}$ . Consequently,  $k_z^2 = k_{0z}^2 - 4\pi\rho$ . Therefore, for a slab of material that is of uniform density in plane, the reflection must be specular in nature—a result which is, in fact, valid for any distribution of SLD that is a function only of  $z$  across a slab of finite thickness. The wave equation describing the motion of the neutron in the reflection process then reduces to one dimension, as can be verified by substituting the wave function

$$\Psi(\vec{r}) = e^{ik_{0x}x} e^{ik_{0y}y} \psi(z) \quad (1.14)$$

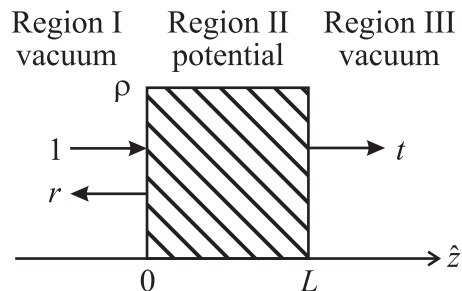


Figure 1.4: Pictorial representation of specular reflectivity from a homogeneous slab as a one-dimensional problem.

into Equation 1.11 which then produces

$$\left[ \frac{\partial^2}{\partial z^2} + k_{0z}^2 - 4\pi\rho(z) \right] \psi(z) = 0. \quad (1.15)$$

When  $\rho(z)$  is constant everywhere, Equation 1.15 has the simple one-dimensional plane wave solution  $\psi(z) = e^{\pm ik_z z}$ . From Equation 1.10, a special refractive index  $n_z = n_z(k_{0z})$  can now be defined which is associated with  $k_z$  along the  $z$  axis:

$$k_z = n_z k_{0z} = k_{0z} \sqrt{1 - 4\pi\rho(z)/k_{0z}^2}. \quad (1.16)$$

Having reduced specular reflection to a one-dimensional problem, we can now proceed to find a solution for reflection from the uniform slab of finite thickness. Look at Figure 1.4 where the slab of Figure 1.3 is shown schematically in cross section, with a thickness  $L$  and with a constant SLD  $\rho$ . We can partition space into three distinct regions: Region I extending from  $z = -\infty$  to the boundary of the potential at  $z = 0$ ; Region II from  $z = 0$  to  $z = L$  in which the SLD is  $\rho$ ; and Region III from  $z = L$  to  $z = \infty$ . (Note that in following a commonly adopted convention of having the wave incident from left to right, the  $+z$  axis has been extended into Region III of the transmitted wave, opposite to that which was adopted in Figure 1.3; we will follow the new convention for the present discussion only.)

The wave function  $\psi_I$  in Region I can be written as the sum of an incident plane wave of unit amplitude propagating to the right and a reflected wave of amplitude  $r$  moving back to the left:

$$\psi_I = 1e^{+ik_1 z} + re^{-ik_1 z} \quad (1.17)$$

where  $k_I$  denotes the wavevector in Region I as given by Equation 1.16. Note, however, that we have dropped the subscript  $z$  from here on for simplicity! In Region II,  $\psi_{II}$  is given by

$$\psi_{II} = ce^{+ik_{II}z} + de^{-ik_{II}z} \quad (1.18)$$

where  $c$  and  $d$  are the undetermined amplitudes of the waves moving to the right and left within the slab medium, respectively, both having wavevector  $k_{II}$  along  $z$ . The value of  $k_{II}$  is given by Equation 1.16 with nonzero  $\rho(z)$ . Finally, in Region III there exists only a solitary transmitted plane wave propagating to the right with amplitude  $t$  and wavevector  $k_{III}$  (again, entirely along  $z$  with the  $z$  subscript omitted):

$$\psi_{III} = te^{+ik_{III}z}. \quad (1.19)$$

Recall that the square of the modulus of the wave function represents the probability of finding the neutron somewhere in space. Thus, in order to conserve the number of neutrons, the probability density current must be conserved, which, in turn, requires that the wave function be continuous across any boundary, such as occurs at  $z = 0$  and  $z = L$  in Figure 1.4. (For a general discussion of probability density currents, see, for example, the quantum mechanics text by Merzbacher [5].) In addition, conservation of momentum requires that the first derivative of the wave function also be continuous at a boundary between regions of differing SLD. These two boundary conditions lead to four relations among  $r$ ,  $t$ ,  $c$ , and  $d$ . That is, upon setting  $\psi_I = \psi_{II}$  and  $d\psi_I/dz = d\psi_{II}/dz$  at  $z = 0$  as well as  $\psi_{II} = \psi_{III}$  and  $d\psi_{II}/dz = d\psi_{III}/dz$  at  $z = L$ , we obtain

$$1 + r = c + d \quad (1.20)$$

$$(k_I/k_{II})(1 - r) = c - d \quad (1.21)$$

$$ce^{+ik_{II}L} + de^{-ik_{II}L} = te^{+ik_{III}L} \quad (1.22)$$

$$ce^{+ik_{II}L} - de^{-ik_{II}L} = (k_{III}/k_{II})te^{+ik_{III}L}. \quad (1.23)$$

We can solve for  $c$  and  $d$  in terms of  $(1 + r)$  and  $(1 - r)$  using Equations 1.20 and 1.21 and then substitute the resulting expressions into Equations 1.22 and 1.23, thereby eliminating the explicit appearance of  $c$  and  $d$ . The term containing  $t$  can be isolated to one side of each of the two equations. If the quantities  $(1 + r)$  and  $(1 - r)$  are then factored out on the other side of each

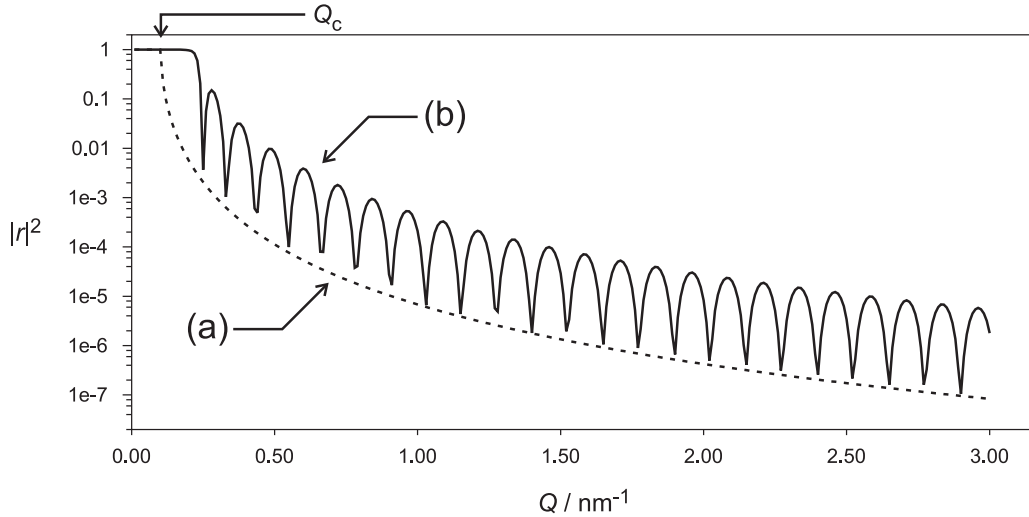


Figure 1.5: Reflectivity *vs.*  $Q$  for: a) a semi-infinite substrate of single-crystalline Si; and b) a uniform 500 Å thick (nonmagnetic) film of Ni on a semi-infinite Si substrate. Note the flat region of total or mirror reflection below a critical value of  $Q$ . The oscillations of the reflectivity in b) are called Kiessig fringes and result from the self-interference of the neutron wave as it is simultaneously reflected from the front and back of the Ni film.

equation, the resultant expressions can be rearranged in matrix form as

$$\begin{pmatrix} t \\ ik_{\text{III}}t \end{pmatrix} e^{+ik_{\text{III}}L} = \begin{pmatrix} \cos(k_{\text{II}}L) & \sin(k_{\text{II}}L)/k_{\text{II}} \\ -k_{\text{II}}\sin(k_{\text{II}}L) & \cos(k_{\text{II}}L) \end{pmatrix} \begin{pmatrix} 1+r \\ ik_{\text{I}}(1-r) \end{pmatrix} \quad (1.24)$$

where the  $z$  components of the neutron wavevectors in the three different regions of space are given by Equation 1.16 (remember that the  $z$  subscripts on the  $k$ 's have been dropped). Equation 1.24 represents a pair of simultaneous equations from which both the reflection and transmission amplitudes  $r$  and  $t$  can be solved for in terms of the thickness and SLD of the material slab and its surrounding media (which may be vacuum, in which case  $n_z = 1$ ). The matrix of sine and cosine functions which contain the information about the scattering properties of the slab is referred to as the transfer matrix.

In Figure 1.5 is shown the reflectivity  $|r|^2$  *vs.* the wavevector transfer  $Q$  for two SLD profiles, one simply for a substrate with a perfectly smooth surface boundary and the other for the same semi-infinite substrate but with

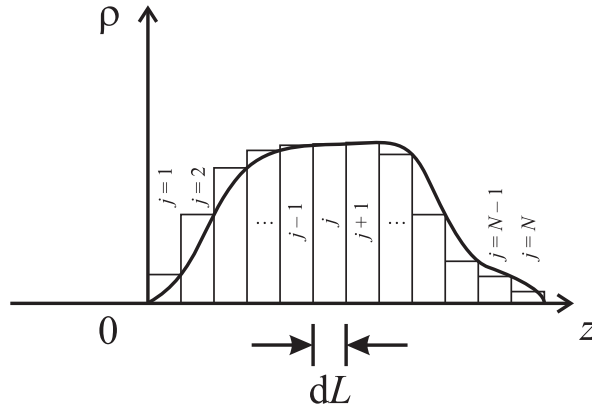


Figure 1.6: Arbitrary SLD profile divided into  $N$  bins of thickness  $dL$ . The SLD is taken to be constant across the width of each bin. The larger the number of bins, the smaller the bin width and the more accurate the rectangular representation becomes.

a single homogeneous layer deposited on its surface. The oscillations of the reflectivity curve corresponding to the layer of finite thickness are known as Kiessig fringes and result from wave interference between the front and back film interfaces. Note the flat region of total or mirror reflection between the origin and a certain critical value of the wavevector transfer designated  $Q_c$ .  $Q_c$  can be determined for any substrate SLD  $\rho$  from Equation 1.16 by computing the value of  $k_{0z}(Q = 2k_{0z})$  for which the argument of the square root vanishes (*i.e.*,  $k_{0z}^2 = 4\pi\rho(z)$ ).

#### 1.2.4 Specular Reflection from a Film with a Nonuniform SLD Profile

The preceding treatment for a single slab of material of uniform SLD can be extended to any arbitrary profile by dividing the slab into  $N$  bins of width  $dL$  along  $z$  as shown in Figure 1.6. The SLD is taken to be constant across the width of any given bin so that the continuity conditions on the wave function and its derivative at each boundary between adjacent bins can be applied successively. That is, follow the same procedure used in arriving at Equation 1.24, except that the wave function within bin  $j + 1$ , written in general terms simply as  $\psi(j + 1)$ , is set equal to that of the  $j$ th bin at

the boundary between the two bins (at  $z = j \, dL$ ): similarly,  $\psi(j - 1) = \psi(j)$  at  $z = (j - 1) \, dL$ . Doing likewise for the wave function derivatives leads to a relationship similar to Equation 1.24, but between any pair of wavefunctions (and corresponding derivatives) across an intervening bin of width  $dL$ . With this relation, the wavefunction can be stepped across the entire film width from the front to back interface, thereby connecting  $r$  and  $t$  as in Equation 1.24. In fact, the resultant solution for the general piecewise continuous SLD profile yields an expression identical to Equation 1.24 except that the following product form of the transfer matrix, representing the entire film thickness, replaces that for the single slab:

$$\begin{pmatrix} A & B \\ C & D \end{pmatrix} = M_N M_{N-1} \cdots M_j \cdots M_2 M_1 \quad (1.25)$$

where the matrix  $M_j$  corresponds to the  $j$ th bin of the film and has the explicit form of the transfer matrix appearing in Equation 1.24 for a single slab. Note the order of the matrix multiplication:  $M_1$  corresponds to the bin or layer in contact with the region of space containing the incident and reflected waves whereas  $M_N$  is next to the space in which the transmitted wave is found. Thus, the general solution for the reflection amplitude  $r$  is obtained by substituting the composite transfer matrix of Equation 1.25 for the single slab matrix in Equation 1.24. This exact or so-called “dynamical” expression for the specular reflection amplitude has proven to be remarkably accurate in a wide range of practical applications in the study of thin films. Equation 1.24 is readily solved numerically and is computationally stable for the relatively large numbers of bins into which a film may be divided.

What ultimately determines the number of bins into which a film of a given total thickness should be divided is the range of wavevector transfer  $Q$  over which reflectivity data can be measured. The general rule of thumb is that a bin width  $dL$ , which is a measure of spatial resolution in the SLD depth profile, is commensurate with a maximum wavevector transfer  $Q = \pi/dL$  (this is a known property associated with Fourier transforms of real-valued functions; see, for example, Reference [12] for a discussion in the specific context of neutron reflectometry).

It was stated at the beginning of Section 1.2.1 that it is the square of the modulus of the neutron wavefunction which corresponds to the probability of finding a neutron at a given location in space with a particular momentum:  $|\psi|^2$  represents a measurable quantity. Thus, it is  $|r|^2$  which can be directly measured as an intensity in a neutron detector. Although it

is straightforward to obtain a prediction of  $|r|^2$  from a value of  $r$  calculated using Equation 1.24, solving the inverse problem of extracting the SLD profile from measured  $|r|^2$  via Equation 1.24 is another matter altogether. The conventional approach is to employ a nonlinear least-squares numerical analysis to fit calculated values of the reflectivity based on model or trial SLD profiles, using Equation 1.24, to measured reflectivity data. Even when satisfactory fits are obtained, the uniqueness of the solution is not guaranteed. Recent development of reference layer techniques do, however, make it possible to determine the reflection amplitude exactly, from which a direct unambiguous inversion can be performed to extract the SLD profile directly (for a review of these methods see, for example, Reference [12]).

Nonetheless, insofar as typical studies of magnetic films and multilayers are concerned, the chemical structure and composition are often known to a sufficient degree or can be determined independently from a combination of nonpolarized neutron and x-ray reflectivity measurements. Such knowledge can then in certain cases compensate for part of the explicit phase information lost in having only  $|r|^2$  instead of  $r$  when determining vector magnetization profiles.

### 1.2.5 Born Approximation

The exact one-dimensional solution for the specular reflectivity which was derived above is valid at all wavevector transfers  $Q$ . However, at large enough values of  $Q$ , especially towards values corresponding to diffraction peaks arising from atomic interplanar spacings in crystalline materials, the incident neutron wavefunction is not significantly distorted from its free-space form in its interaction with the scattering medium. In this limit, an approximation, attributed to Born, and also referred to as the “kinematic” approximation, can be made in which the form of the wavefunction within the scattering medium is replaced by that in vacuum. The Born approximation turns out to be applicable even in certain circumstances in reflectometry at lower values of  $Q$ , including the analysis of scattering from periodic superlattices. In other instances, it is valuable for qualitatively explaining more complicated scattering phenomena and concepts. Although we will not make extensive use of the Born approximation, it is particularly helpful when describing nonspecular reflection in the next section.

Perhaps the most straightforward way to illustrate the Born approximation is to begin with the integral form of the expression for the one-

dimensional reflection amplitude  $r$ . An alternative expression for the specular reflection amplitude to that which we derived from a solution of a differential wave equation in previous sections is (see, for example, the derivation in Reference [13]):

$$r(Q) = \frac{4\pi}{iQ} \int_{-\infty}^{+\infty} \psi(Q, z) \rho(z) e^{-ik_{0z}z} dz \quad (1.26)$$

where  $Q = 2k_{0z}$  for specular scattering from a flat slab of infinite lateral extent.  $\psi(Q, z)$  represents the neutron wave function within the scattering medium, which exists, say, between  $z = 0$  and  $z = L$ . The useful representation of  $r$  given by Equation 1.26 will be generalized for magnetic films and polarized beams in Section 1.4.1. To make the Born approximation, we simply replace  $\psi$  in Equation 1.26 with  $\exp(-ik_{0z}z)$ . Then,

$$r_{\text{BA}}(Q) = \frac{4\pi}{iQ} \int_{-\infty}^{+\infty} \rho(z) e^{-iQz} dz \quad (1.27)$$

so that the SLD  $\rho(z)$  and  $r_{\text{BA}}(Q)$  are related to one another by a Fourier transform.

The three-dimensional analog of Equation 1.27 for the slab geometry is [14]:

$$r_{\text{BA}}(\vec{Q}) = \frac{4\pi}{iQ_z S} \iiint_{-\infty}^{+\infty} \rho(\vec{r}) e^{-i\vec{Q}\cdot\vec{r}} d^3r \quad (1.28)$$

where  $S$  is a surface area in the plane of the slab (ideally approaching infinity).

### 1.2.6 Nonspecular Reflection

Looking back at Figure 1.3, we can imagine tilting  $\vec{Q}$  away from the slab normal, which implies that the angles of incidence and reflection are no longer equal, so that a component of the wavevector transfer lies in plane. Thus, if any density variations exist along the in-plane directions, *i.e.*, in the  $xy$  plane, then reflected intensity will be observed at directions of  $\vec{Q}$  other than normal to the surface as described, in the Born approximation, by Equation 1.28. Although the description of nonspecular scattering is relatively straightforward in those cases in which the Born approximation is valid, the complications which arise when it is not can be formidable. More rigorous treatments of nonspecular scattering are a subject of considerable ongoing research (see, for example, References [15, 16]) and are beyond the scope of this

chapter. The emphasis here is on specular reflection for two reasons. First, and perhaps foremost, a thorough understanding of the theory and methods of specular reflectometry is not only an end in itself, but also provides a necessary conceptual foundation for further investigation of nonspecular scattering. Second, to date, reflectometry studies of magnetic films and multilayers have predominantly involved specular measurements, concentrating on properties related to the in-plane average vector magnetization depth profile and related interlayer coupling. Thus, much has been and can continue to be learned from the specular reflectometry work alone. Nonetheless, it is important to realize the potential usefulness of nonspecular reflectivity measurements in the investigation of magnetic phenomena, for example, that relate to in-plane domain structure in layered media. The reader is encouraged to learn more about nonspecular reflectivity from the references cited above, as well as more recent literature.

Before continuing, however, it is worthwhile to discuss both what distinguishes specular and nonspecular components of the reflectivity on one hand, as well as what connects them on the other. Because what we are about to demonstrate holds true in both the exact theory and Born approximations, we will adopt the latter description for its relative transparency. Equation 1.28, which expresses the reflection amplitude in three dimensions for a sample with the characteristic slab shape, can be rewritten, for the specular condition where  $Q_x = Q_y = 0$ , in an equivalent form in which the in-plane and out-of-plane components are explicitly separated:

$$r_{\text{BA}}(Q_x = 0, Q_y = 0, Q_z) = \frac{4\pi}{iQ_z} \int_{-\infty}^{+\infty} e^{-iQ_z z} \left[ \frac{1}{S} \iint_{-\infty}^{+\infty} \rho(x, y, z) dx dy \right] dz. \quad (1.29)$$

The term in square brackets in the integrand of Equation 1.29 is simply the in-plane average of the three-dimensional scattering length density where  $S$  is the in-plane area which approaches infinity as the limits of integration on  $x$  and  $y$  do. This can be defined as  $\bar{\rho}(z)$ :

$$\bar{\rho}(z) \equiv \frac{1}{S} \iint_{-\infty}^{+\infty} \rho(x, y, z) dx dy. \quad (1.30)$$

Thus  $\bar{\rho}(z)$  *always* gives rise to specular scattering for  $Q$  perpendicular to the surface, *i.e.*, along the  $z$  direction. The shape of the nonspecular reflectivity curve along a direction parallel to the surface is determined by the spatial distribution of the compositional inhomogeneity in the plane of the

film. Although the specular reflectivity can reveal the presence of nonsharp boundaries between layers of different SLD in the depth profile, only the non-specular reflectivity manifests the nature of that gradation, *i.e.*, whether the variation in SLD is due, for example, to interdiffusion of two or more isotopes on an atomic scale or, alternatively, to the presence of much larger contiguous regions of the different constituents in plane (*e.g.*, islands of one material in a sea of the other). The former possibility would give rise to a relatively broader distribution of scattering along an in-plane nonspecular direction than would the latter.

### 1.3 Spin-Dependent Neutron Wave Function

Up to this point we have deliberately ignored the magnetic moment of the neutron in order to simplify the presentation of those aspects of the reflection process which are common to both nuclear and magnetic interactions of the neutron with condensed matter. We will now examine the interaction between the magnetic moment of the neutron and the atomic moments which are present in magnetic films.

#### 1.3.1 Neutron Magnetic Moment and Spin Angular Momentum

The magnetic moment of the neutron is associated with an intrinsic “spin” angular momentum which is quantized such that the neutron can occupy only one of two discrete energy states within a given magnetic field. The energies  $E$  corresponding to these states are found to be

$$E_{\pm,\text{magnetic}} = \mp\mu \left| \vec{B} \right| \quad (1.31)$$

where  $\mu$  is the magnitude of the neutron magnetic moment ( $\mu = -1.913$  nuclear magnetons or  $-1.913 \times 5.051 \times 10^{-27}$  Joule/Tesla) and  $B$  is the magnetic induction (which can be treated classically for our purposes: see, for example, the discussion by Mezei [17] of the implications of a magnetic interaction which is proportional to the magnetic induction  $B$  as opposed to the field intensity  $H$ ). The corresponding spin angular momentum  $\mathcal{S}$  of the neutron is  $\mathcal{S} = \pm\hbar/2$ , where  $\hbar$  is Planck’s constant divided by  $2\pi$  (hence the classification of a neutron as a Fermion or “spin half” particle). A consequence of

the quantum nature of the neutron spin and moment is that the two allowed, discrete values of either the spin or moment can be projected only along the direction of a magnetic field, which defines an axis of quantization (and which can have any continuous direction in real space). A theoretical description which properly accounts for the observation that along a continuously variable direction in space only a discrete pair of values of the magnetic moment can occur, can be formulated using the mathematical construct known as a spinor. The spinor represents the contribution of the property of spin to a complete wavefunction describing the overall state of the neutron. A spinor is a two-component column (or row) matrix which can act on and be acted upon by other matrices describing certain physical operations such as rotations in space. The matrix formalism is a powerful symbolic means of representing the simultaneous equations which are necessary to mathematically account for the observed quantum behavior of the spin. The discussion of spin which immediately follows is based on well-known principles of quantum mechanics; more complete accounts can be found in any of a number of texts (see, for example, Merzbacher [5], for an exceptionally clear and thorough explanation of spin).

### 1.3.2 Explicit Form of the Spin-Dependent Neutron Wave Function

The wave function describing a general state of the neutron can be written as:

$$\Psi(\vec{r}, \mathcal{S}) = C_+ \begin{pmatrix} 1 \\ 0 \end{pmatrix} \Psi_+(\vec{r}) + C_- \begin{pmatrix} 0 \\ 1 \end{pmatrix} \Psi_-(\vec{r}) \quad (1.32)$$

where  $|C_+|^2 = C_+^* C_+$  and  $|C_-|^2 = C_-^* C_-$  are the probabilities of finding the neutron in the “+” or spin “up” and “-” or spin “down” states, respectively (in general,  $C_+$  and  $C_-$  are complex numbers satisfying  $|C_+|^2 + |C_-|^2 = 1$ ). Note, however, that the spatial component wave functions,  $\Psi_+$  and  $\Psi_-$ , are different from one another in the presence of a magnetic field. Because of the magnetic energy (Equation 1.31), the refractive index for neutrons in a magnetic field is two-valued, *i.e.*, the refractive index given by Equation 1.10 for a purely nuclear medium, must now be generalized to include a magnetic contribution:

$$n_{\pm} = \sqrt{1 - 4\pi(\rho_N \pm \rho_M)/k_0^2} \Rightarrow n_{z\pm} = \sqrt{1 - 4\pi(\rho_N \pm \rho_M)/k_{0z}^2} \quad (1.33)$$

where the magnetic scattering length density  $\rho_M$  is given by

$$\rho_M = \mp \frac{m}{2\pi\hbar^2} \mu B \quad (1.34)$$

and where the “+” and “−” subscripts denote the neutron spin state and “N” and “M” refer to the nuclear and magnetic components of the SLD, respectively (see also Equation 1.5). Therefore, in a magnetic medium,  $k_{\pm} = n_{\pm}k_0$  so that

$$\Psi_{\pm} = e^{+i\vec{k}_{\pm}\cdot\vec{r}} = e^{+in_{\pm}\vec{k}_0\cdot\vec{r}}. \quad (1.35)$$

As we shall soon see, however, the vectorial nature of the magnetic field and the spinor character of the neutron spin wave function, in combination, give rise to a far more complicated (but, on the other hand, more interesting) interaction than what the birefringent property of the refractive index alone might at first suggest.

It can be shown (see, for instance, Merzbacher [5]) that the magnetic moment and intrinsic spin angular momentum of the neutron can be correctly represented by the operators indicated in Equations 1.36 and 1.37, respectively:

$$\check{\mu} = -\mu\check{\sigma} \quad (1.36)$$

$$\check{\mathcal{S}} = \frac{\hbar}{2}\check{\sigma} \quad (1.37)$$

where  $\check{\phantom{x}}$  indicates a matrix operator. The operator  $\check{\sigma}$  consists of three  $2 \times 2$  component matrices, each of which is directed along one of the three orthogonal spatial axes:

$$\begin{aligned} \check{\sigma} &= \check{\sigma}_x\hat{x} + \check{\sigma}_y\hat{y} + \check{\sigma}_z\hat{z} \\ &= \begin{pmatrix} 0 & 1 \\ 1 & 0 \end{pmatrix} \hat{x} + \begin{pmatrix} 0 & -i \\ i & 0 \end{pmatrix} \hat{y} + \begin{pmatrix} 1 & 0 \\ 0 & -1 \end{pmatrix} \hat{z} \end{aligned} \quad (1.38)$$

where the  $z$  axis has been specifically chosen to correspond to the direction of any magnetic field which might exist at the position in space where the neutron is found. (The component operators of Equation 1.38 are known as the Pauli matrices, in honor of their inventor. It would be difficult to overstate the fundamental importance of his conceptual achievement in constructing a mathematical framework to describe the inherently quantum phenomenon of spin with quantitative accuracy. A detailed exposition of this theory is

given in the chapters on spin in the text by Merzbacher [5] and is highly recommended.)

The magnetic field direction, here explicitly taken to lie along  $z$ , thus plays a special role as the adopted axis of quantization. Any procedure which results in a determination of the neutron spin state in effect projects the full magnitude of the neutron moment along the magnetic field axis, pointing either up or down (+ or -).

Now the spin dependence of the neutron wave function can be specified by a column vector  $\chi$  normalized such that:

$$\chi^{*\text{T}}\chi = \chi^\dagger\chi = (C_+^* \ C_-^*) \begin{pmatrix} C_+ \\ C_- \end{pmatrix} = |C_+|^2 + |C_-|^2 = 1 \quad (1.39)$$

where \* denotes complex conjugation and T signifies taking the transpose (column to row). A direction in space can always be found for which the neutron has unit probability of residing in a pure + or - state. Consequently, any interaction, whether with an individual atom or macroscopic magnetic field region, which affects the spin state of the neutron can be represented by an appropriately constructed rotation operator  $\check{U}_R$  acting through a certain angle  $\epsilon$  about a particular axis  $\hat{\eta}$ [5]:

$$\check{U}_R(\epsilon, \hat{\eta}) = \check{I} \cos(\epsilon/2) - i\hat{\eta} \cdot \check{\sigma} \sin(\epsilon/2) = e^{-i(\epsilon/2)\hat{\eta} \cdot \check{\sigma}} \quad (1.40)$$

where  $\check{I}$  is the identity matrix.

One of the underlying principles of quantum theory is that every physically measurable quantity corresponds to the expectation (or average) value of a corresponding operator. For any operator  $\check{A}$  which affects only the spin component of the single neutron wave function directly,

$$\langle \check{A} \rangle \equiv \chi^\dagger \check{A} \chi = (C_+^* \ C_-^*) \begin{pmatrix} A_{11} & A_{12} \\ A_{21} & A_{22} \end{pmatrix} \begin{pmatrix} C_+ \\ C_- \end{pmatrix}. \quad (1.41)$$

### 1.3.3 Polarization

A quantity of great conceptual value is the polarization  $\hat{P}$ , a unit vector which, as will be seen below, can be imagined to point along the axis of the neutron's spin or magnetic moment (parallel or antiparallel, respectively). There exists, in fact, a formal isomorphism between the two-state quantum system describing the neutron spin in an abstract space and the description

of a classical moment in real space, as characterized by an analogous polarization vector [18]. It can be shown that the ordinary, three-dimensional, real space polarization vector  $\hat{P}$  has components given by the expectation values of the Pauli matrices appearing in Equation 1.38:

$$\begin{aligned}\hat{P} &= P_x \hat{x} + P_y \hat{y} + P_z \hat{z}; \\ P_x &= \langle \check{\sigma}_x \rangle = 2\text{Re}(C_+^* C_-); \\ P_y &= \langle \check{\sigma}_y \rangle = 2\text{Im}(C_+^* C_-); \text{ and} \\ P_z &= \langle \check{\sigma}_z \rangle = |C_+|^2 - |C_-|^2.\end{aligned}\tag{1.42}$$

Thus the rectangular components of the polarization vector are proportional to the corresponding expectation values of the components of the moment operator  $\check{\mu}$ . Note, in particular, that  $P_z$  is the relative probability of finding the neutron in one of the two basis states (along the quantization axis defined by the magnetic field, which was stipulated to lie along the  $z$  direction).

Another quantity which can be of particular use in dealing with statistical ensembles of systems (where each identical system represents an individual neutron) is the density matrix  $\check{\rho}$ . It is formed by the tensor product  $\chi\chi^\dagger$  (not to be confused with the inner product  $\chi^\dagger\chi$  of Equation 1.39) and contains all of the information which it is possible to know, in principle, about the spin state of an individual neutron:

$$\chi\chi^\dagger = \begin{pmatrix} C_+ \\ C_- \end{pmatrix} \begin{pmatrix} C_+^* & C_-^* \end{pmatrix} = \begin{pmatrix} C_+ C_+^* & C_+ C_-^* \\ C_- C_+^* & C_- C_-^* \end{pmatrix} \equiv \check{\rho}.\tag{1.43}$$

Using the density matrix operator, Equation 1.41 can be rewritten as

$$\langle \check{A} \rangle \equiv \text{trace} \left( \begin{pmatrix} C_+ C_+^* & C_+ C_-^* \\ C_- C_+^* & C_- C_-^* \end{pmatrix} \begin{pmatrix} A_{11} & A_{12} \\ A_{21} & A_{22} \end{pmatrix} \right) = \text{trace} (\check{\rho} \check{A}).\tag{1.44}$$

With some further manipulation involving Equations 1.38 and 1.42,  $\check{\rho}$  can also be expressed in terms of  $\check{\sigma}$  and the polarization vector  $\hat{P}$ :

$$\check{\rho} = \frac{1}{2} \left( \check{I} + \hat{P} \cdot \check{\sigma} \right).\tag{1.45}$$

One other parameterization of the polarization vector  $\hat{P}$ , by a pair of real parameters  $\theta$  and  $\phi$ , can help to visualize certain phenomena. A general spin state can be specified with  $C_+ = \cos(\theta/2)$  and  $C_- = \exp(i\phi) \sin(\theta/2)$ , since

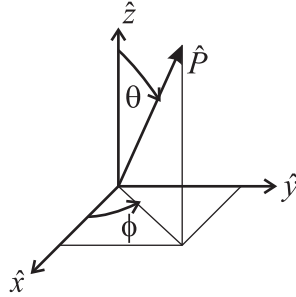


Figure 1.7: Three-dimensional neutron polarization vector  $\hat{P}$  referred to rectangular coordinate axes.

$|C_+|^2 + |C_-|^2 = 1$  and the phase angle  $\phi$  can still be chosen arbitrarily (see, for example, Blum [19]). Equation 1.42 can then be rewritten as

$$\begin{aligned}
 P_x &= \sin \theta \cos \phi \\
 P_y &= \sin \theta \sin \phi \\
 P_z &= \cos \theta
 \end{aligned}
 \tag{1.46}$$

where the real parameters  $\theta$  and  $\phi$  can be interpreted as the polar angles of the polarization vector  $\hat{P}$  with  $\theta$  the angle between  $\hat{P}$  and the  $z$  axis as shown in Figure 1.7. Note that it is easy to show that  $P^2 = P_x^2 + P_y^2 + P_z^2 = 1$  using Equation 1.46. Table 1.1 compares the values of  $C_+$  and  $C_-$  for several corresponding values of  $P_x$ ,  $P_y$ , and  $P_z$ .

Before moving on to a derivation of the complete set of equations of motion which govern spin-dependent neutron reflection from magnetic materials, we can use what we have learned thus far about reflection from nonmagnetic media and the spin-dependent neutron wave function to examine several important consequences of the spin on the observable behavior of the neutron.

### 1.3.4 Selecting a Neutron Polarization State

Recall our discussion at the end of Section 1.2.3 regarding mirror reflection below a critical value  $Q_c$ , as obtained for a semi-infinite substrate of nuclear SLD  $\rho$  and illustrated in Figure 1.5. Suppose now that the substrate is composed of a ferromagnetic material with a magnetization that is saturated in the plane of the film along the direction of a relatively small applied magnetic

$P_x$	$P_y$	$P_z$	$\theta$	$\phi$	$C_+$	$C_-$
0	0	1	0	0	1	0
0	0	-1	$\pi$	0	0	1
1	0	0	$\pi/2$	0	$1/\sqrt{2}$	$1/\sqrt{2}$
0	1	0	$\pi/2$	$\pi/2$	$1/\sqrt{2}$	$i/\sqrt{2}$

$C_+ = \cos(\theta/2)$ ;  $C_- = \sin(\theta/2) [\cos \phi + i \sin \phi]$

Table 1.1: Parameters describing a selection of different neutron polarizations.

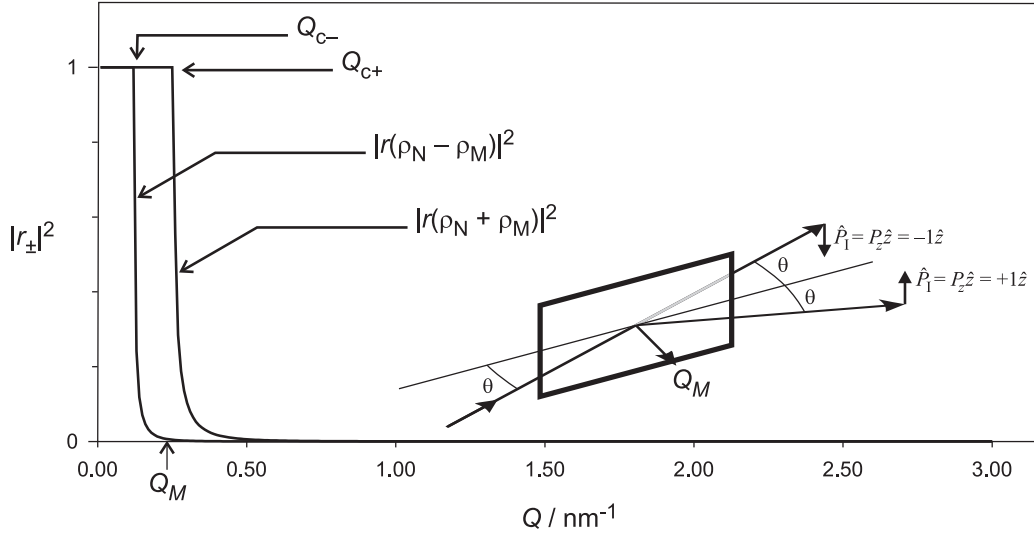


Figure 1.8: Neutron reflectivity for a saturated ferromagnetic Fe mirror. Two critical scattering vectors are observed, one corresponding to the sum of nuclear and magnetic SLDs, the other to their difference (the lower value). The magnetic guide field, which defines an axis of quantization for the neutron, is applied in the plane of the mirror surface, perpendicular to the wavevector transfer; the magnetization of the Fe is assumed to lie along the applied magnetic field (the magnitude of the guide field is taken to be negligible in comparison to the magnetization of the Fe). In this configuration, the reflectivity is non-spin-flip.

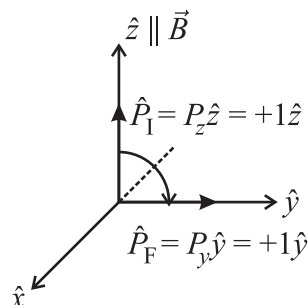


Figure 1.9: Rotation of the neutron polarization vector  $\hat{P}$  by  $90^\circ$ , as discussed in the text.

field in the space surrounding this substrate. We saw that in the presence of a magnetic field the neutron refractive index becomes double-valued, as given by Equation 1.33. This immediately implies the occurrence of two critical  $Q$  values (or angles), one corresponding to  $(\rho_N + \rho_M)$ , and the other to  $(\rho_N - \rho_M)$ . This birefringent property can be used to obtain a neutron with almost unit probability of being polarized in one of its basis states if  $\rho_M$  is sufficiently large and the neutron is reflected at a  $Q$  between the critical values: reflected neutrons will be in one spin state and transmitted neutrons in the other. (Better yet, if  $\rho_N \leq \rho_M$ , then only one spin state is mirror-reflected between  $Q = 0$  and  $Q = Q_c$ ). A practical case is shown for an Fe substrate in Figure 1.8. This interference between nuclear and magnetic SLDs is the basis of neutron polarizing devices made of mirrors or thin-film multilayers, as well as single crystals [20, 21]. Polarization efficiencies approaching unity can be achieved in practice using such reflection devices.

### 1.3.5 Changing a Neutron's Polarization

In the previous section we showed how to take a neutron in any unknown polarization state and, by reflection from a saturated ferromagnetic film, prepare it to be in an essentially pure spin + or “up” state, along the direction coincident with that of the applied magnetic field, often referred to as the “guide” field which defines the axis of quantization  $z$  along the neutron beam from one region of space to another. Later, in Section 1.4.1, we will explicitly label the states corresponding to “up” and “down” along the guide field with the symbols  $\uparrow$  and  $\downarrow$ , respectively. How can we effect a change from this

initial pure spin state,  $\hat{P}_I = P_z \hat{z} = +1\hat{z}$ , to one in which the final neutron polarization points in another direction, say  $\hat{P}_F = P_y \hat{y} = +1\hat{y}$ , as schematically represented in Figure 1.9? Mathematically, the rotation operator  $\check{U}_R$ , defined in Equation 1.40, can be used to identify rotations in space that would accomplish this transformation. Examination of Figure 1.9 suggests the obvious possibility of a  $-90^\circ$  rotation about  $x$  (*i.e.*,  $90^\circ$  CW; the adopted right-hand-rule convention implies that CCW is positive). In this particular case Equation 1.40 gives

$$\check{U}_R(\epsilon = -\pi/2, \hat{n} = \hat{x}) = \tag{1.47}$$

$$\begin{pmatrix} 1 & 0 \\ 0 & 1 \end{pmatrix} \cos(-\pi/4) - i \begin{pmatrix} 0 & 1 \\ 1 & 0 \end{pmatrix} \sin(-\pi/4) = \frac{1}{\sqrt{2}} \begin{pmatrix} 1 & i \\ i & 1 \end{pmatrix}.$$

Then

$$\begin{aligned} \chi_F &= \check{U}_R \chi_I = \check{U}_R \begin{pmatrix} C_{+I} \\ C_{-I} \end{pmatrix} = \check{U}_R \begin{pmatrix} 1 \\ 0 \end{pmatrix} \\ &= \frac{1}{\sqrt{2}} \begin{pmatrix} 1 & i \\ i & 1 \end{pmatrix} \begin{pmatrix} 1 \\ 0 \end{pmatrix} = \begin{pmatrix} 1/\sqrt{2} \\ i/\sqrt{2} \end{pmatrix} = \begin{pmatrix} C_{+F} \\ C_{-F} \end{pmatrix} \end{aligned} \tag{1.48}$$

where Equation 1.42 immediately identifies  $\chi_I$  as corresponding to  $\hat{P}_I = +P_z \hat{z} = +1\hat{z}$  and  $\chi_F$  to  $\hat{P}_F = +P_y \hat{y} = +1\hat{y}$ .

## Precession

How can the rotation of the neutron polarization described mathematically in the preceding discussion be realized physically? The answer is by employing magnetic fields which vary in magnitude and direction over different regions of space along the neutron's trajectory (time-varying fields are also employed in practice, but to understand their use requires an equation of motion that is explicitly time-dependent; a complication that we have chosen to avoid since it is not necessary for describing the elastic scattering processes that we are primarily interested in here). Consider then a neutron plane wave propagating, say, along the  $y$  axis in the positive direction, where the magnetic guide field  $B_{GF}$  points along  $+z$  in a Region I (where  $y < 0$ ), along  $-x$  in Region II (where  $0 < y < L$ ), and back up again parallel to  $+z$  in Region III (where  $y > L$ ), all of which is indicated in Figure 1.10. Thus, the magnetic guide field changes direction abruptly at  $y = 0$  and at  $y = L$ . (For the present discussion, it is assumed that the magnetic field

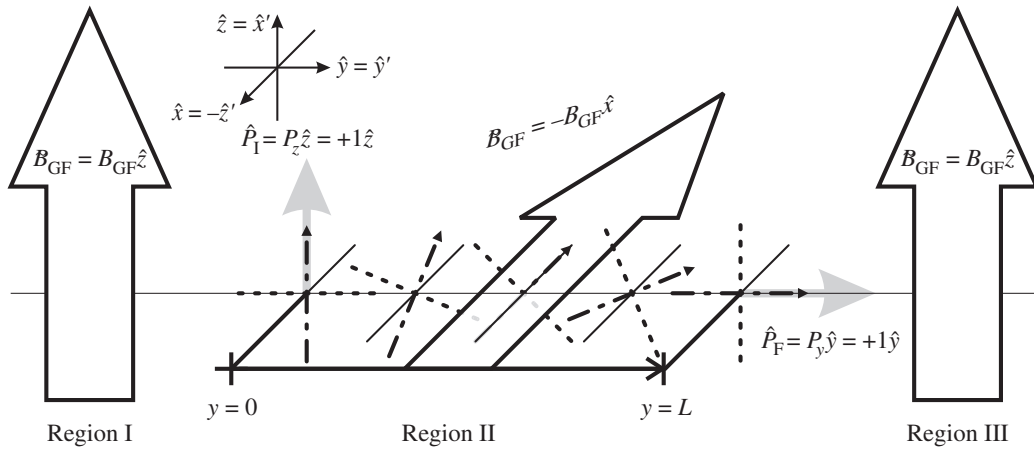


Figure 1.10: Process for rotating the polarization by  $90^\circ$ . A neutron in the  $+$  spin eigenstate in Region I has a polarization vector  $\hat{P} = P_z \hat{z}$  where the quantization axis, defined by a magnetic guide field  $B_{GF}$ , is directed along  $+z$ . As the neutron propagates along  $y$ , it crosses from Region I to Region II at  $y = 0$  where the magnetic guide field abruptly changes direction by  $90^\circ$ . This so-called “sudden” transition results in the neutron polarization being initially orthogonal to the new guide field direction in Region II. As the neutron traverses Region II its polarization precesses about the magnetic field direction. If the distance  $L$  and the magnitude of the constant field are properly selected, then the neutron polarization will be rotated by  $90^\circ$  in its passage from  $y = 0$  to  $y = L$ . The neutron then makes a sudden transition from Region II to Region III at  $y = L$ , where the guide field in Region III is oriented back along the same direction as in Region I. The neutron polarization is initially along  $y$  in Region III and will again precess, but now about the original  $z$  axis. Consult the corresponding text for further discussion.

strengths involved and the orientation of the neutron wavevector relative to boundaries between adjacent field regions are such that no appreciable reflection occurs.) In quantum theory, the passage of the neutron wave function across an infinitesimally thin boundary separating regions of space wherein the magnetic field points in different directions induces a “sudden” transition in its polarization state. A sudden transition means, for the conditions depicted in Figure 1.10, that if the neutron has a polarization  $\hat{P} = +P_z\hat{z} = +1\hat{z}$  in Region I, then just across the boundary with Region II at  $y = 0$  it finds itself still pointing along  $+z$  but now orthogonal to the new magnetic guide field direction which is parallel to  $-x$ . (See a text on quantum mechanics, *e.g.*, Reference [22], for further discussion of the circumstances under which it is justified to assume a “sudden” transition as opposed to one that is “adiabatic,” *i.e.*, one for which the neutron spin and moment follow and stay aligned with the changing magnetic field direction.) A change of neutron polarization with respect to the magnetic field direction can be effected via a sudden transition in the laboratory, for example, by passage of a neutron beam through a thin current sheet [20]. From the neutron’s perspective, this is equivalent to an abrupt change in the applied field.

Now once inside Region II, we need to consider what happens to the neutron wave function as a consequence of the change in direction of the magnetic field. It is essential to realize that within this region, a new quantization direction is established by the physical presence of a magnetic field pointing along the  $-x$  axis. The convention which has been adopted is to designate the field direction as the  $z$  axis; thus, we call it  $z'$  in Region II so as to distinguish it from the former  $z$  axis. By maintaining  $y = y'$ , the former  $z$  axis becomes  $x'$ . These labeling changes are also indicated in Figure 1.10.

The wavefunction describing the neutron in Region II is obtained from Equations 1.32 and 1.35 (note that here  $k_0 = k_{0y}$ ):

$$\psi(y) = C_+ \begin{pmatrix} 1 \\ 0 \end{pmatrix} + C_- \begin{pmatrix} 0 \\ 1 \end{pmatrix} = C_{+0} e^{+in_+ k_0 y} \begin{pmatrix} 1 \\ 0 \end{pmatrix} + C_{-0} e^{+in_- k_0 y} \begin{pmatrix} 0 \\ 1 \end{pmatrix} \quad (1.49)$$

where the refractive indices are different in the presence of the magnetic field and are given by Equation 1.33 with  $\rho_N$ , in this instance, equal to zero;  $\rho_M$  is obtained from Equation 1.34. At  $y = 0$ ,  $\hat{P} = +P_{x'}\hat{x}' = +1\hat{x}'$  so that  $C_{+0} = 1/\sqrt{2}$  and  $C_{-0} = 1/\sqrt{2}$ .

From Equation 1.49 we then obtain

$$\begin{aligned} C_+ &= C_+(y) = C_{+0} [\cos(n_+ k_0 y) + i \sin(n_+ k_0 y)] \\ &= \frac{1}{\sqrt{2}} [\cos(n_+ k_0 y) + i \sin(n_+ k_0 y)] \end{aligned} \quad (1.50)$$

with a similar expression for  $C_-$ . Using Equations 1.42 then gives us the following expressions for how the polarization components evolve with position in Region II (recall that the  $y$  axis has not changed, so that  $y' = y$ ):

$$\begin{aligned} P_{x'}(y) &= 2\text{Re}(C_+^* C_-) \\ &= \cos(n_+ k_0 y) \cos(n_- k_0 y) + \sin(n_+ k_0 y) \sin(n_- k_0 y) \\ &= \cos((n_- - n_+) k_0 y); \\ P_{y'}(y) &= \sin((n_- - n_+) k_0 y); \\ P_{z'}(y) &= 0. \end{aligned} \quad (1.51)$$

This rotation of the polarization components  $P_{x'}$  and  $P_{y'}$  in Region II is known as precession. Note in particular that the  $z'$  component remains unchanged at zero value. The argument of the sine or cosine functions in the RHS of Equation 1.51 is the precession angle  $\Delta\phi$  in radians:  $\Delta\phi = (n_- - n_+) k_0 y$ . In the absence of a magnetic field ( $n_- = n_+$ ), no precession occurs. Or, if  $C_{+0} = 1$  and  $C_{-0} = 0$ , which would have been the case had the magnetic guide field remained along the original  $z$  axis, instead of being rotated by  $90^\circ$  through Region II, then  $P_z$  would have remained  $+1$ .

Neutron precession can also take place if nuclei with spin-dependent nuclear coherent scattering lengths (associated not with the atomic electron moments of our primary interest, but rather with net *nuclear* magnetic moments), are aligned (see Reference [23]). Ferromagnetically ordered nuclear magnetic moments also give rise to different  $+$  and  $-$  refractive indices. Early discussions of precession, viewed in the way we have just described as a “beating” phenomenon arising from the interference between the two spin basis states of the neutron wave function, can be found in Reference [23] and also in the text by Gurevitch and Tarasov [24].

Now the precession angle  $\Delta\phi(y)$  can be directly related to the magnitude of  $\vec{B}$  by

$$\begin{aligned} \Delta\phi(y) &= (n_- - n_+) k_0 y = \\ &= \left( \sqrt{1 - 2m\mu B/(\hbar k_0)^2} - \sqrt{1 + 2m\mu B/(\hbar k_0)^2} \right) k_0 y, \quad (1.52) \\ |\Delta\phi(y)| &\simeq (2m\mu B/(\hbar k_0)^2) k_0 y = (2\mu B/(mv_0^2)) k_0 y \end{aligned}$$

where the approximate expression (obtained by expanding the square root and keeping the first two terms) is good enough for many purposes involving the design of instrumental devices for effecting rotations of the polarization. (For Fe,  $B \simeq 2.2$  Tesla or 22 000 Gauss with corresponding  $p = 0.6 \times 10^{-12}$  cm and  $\rho_M = 5.09 \times 10^{-6} \text{ \AA}^{-2}$ .) For instance, the  $\pi/2$  rotation depicted in Figure 1.10 could be accomplished for  $k_0 = 2.67 \text{ \AA}^{-1}$  ( $\lambda = 2.35 \text{ \AA}$ ; speed  $v = 1683$  m/s) with  $B = 0.005$  Tesla or 50 Gauss, and  $L = 0.577$  cm. A spin “flipping” device based upon this principle can be constructed from ordinary aluminum wire in the form of a rectangular solenoid and is commonly employed in PNR [25, 26].

As mentioned earlier, the derivation of the precession angle above assumed, implicitly, that there was no appreciable reflection of the neutron wave at the boundary  $y = 0$  where the magnetic field abruptly changed direction and that the wave continued along  $+y$ . In Section 1.4, an equation of motion will be derived which can account for such possibilities and which is, in fact, general enough to treat almost all eventualities. We will explore the polarization dependence of reflection from magnetic films and multilayers there.

### General Means of Rotating and Analyzing the Polarization

We have so far described two devices with which we can manipulate the neutron polarization. First, a magnetized mirror can be employed to select the component or projection of the polarization along the direction defined by the applied magnetic field. Following convention, this quantization axis is taken to coincide with  $z$ . Secondly, adjacent regions of space with effectively infinitesimally thin boundaries can be established so that the direction and magnitude of the magnetic field change abruptly; such constructions enable controlled rotations of the polarization via precession. We have, therefore, the means for not only creating a particular neutron polarization, but also for analyzing any arbitrary polarization vector by appropriate combination of rotations and reflections as will be illustrated next.

Consider the diagram in Figure 1.11 showing a particular initial polarization  $\hat{P}_1$  at the boundary between Region I and Region II at  $y = 0$  where the magnetic guide field is directed along  $z$ . If a mirror reflecting device, similar to that shown in Figure 1.8, with an in-plane magnetization directed along  $z$  was inserted at an appropriate angle  $\theta_M$  (between the two critical angles  $\theta_{c-}$  and  $\theta_{c+}$ ) at  $y = 0$  in the path of the neutron (propagating along  $+y$ ), it would

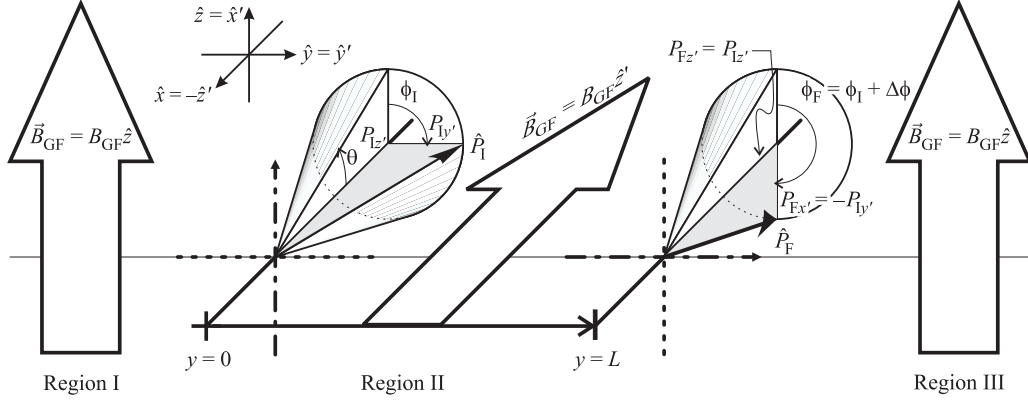


Figure 1.11: Magnetic guide field configuration along the neutron trajectory ( $y$  axis) similar to that shown in Figure 1.10, but for a more general initial neutron polarization at  $y = 0$ . Note that as the neutron polarization precesses through Region II, its projection along the field direction ( $z'$  axis) remains constant. The component along the  $y'$  axis, however, is rotated to point along the  $-x'$  axis at  $y = L$ .

select out the  $P_z$  component of the neutron polarization. Since  $P_z$  represents the probability of finding a single neutron in the  $+$  spin state, it would be necessary to measure the basis spin states of an ensemble of neutrons, *i.e.*, a beam of neutrons with identical wavevector and polarization state, in order to determine the value of  $P_z$ . For example, if  $P_z = 0.5$ , then for 100 neutrons incident on the mirror in this configuration, the most probable outcome would be to detect 75 reflected neutrons, corresponding to the  $+$  spin state; the remaining 25 neutrons, occupying the  $-$  spin state, would be transmitted through the mirror. ( $P_z = |C_+|^2 - |C_-|^2 = (75/100) - (25/100) = 0.5$ ).

For reasons to do with the spatial extent and angular divergences of the beam encountered in practice, which typically can differ significantly in two orthogonal directions, a magnetic mirror normally can be efficiently oriented along only one particular direction. Thus, to find the  $P_x$  and  $P_y$  components of the polarization, a controlled rotation of  $\hat{P}$  must first be induced.

In order to effect the rotation required, for example, to make the  $y$  component in Region I point along  $-z$  in Region III at  $y = L$ , consider the rotation of  $\hat{P}_1$  to  $\hat{P}_F$  in Figure 1.11. Using Equation 1.46 we can write the components of the final polarization in the primed coordinate system in Region II,

in which  $-\hat{x} \rightarrow \hat{z}'$ ,  $\hat{y} \rightarrow \hat{y}'$  and  $\hat{z} \rightarrow \hat{x}'$  as

$$\begin{aligned} P_{F_{x'}} &= \sin \theta \cos(\phi_I + \Delta\phi) \\ P_{F_{y'}} &= \sin \theta \sin(\phi_I + \Delta\phi) \\ P_{F_{z'}} &= \cos \theta \end{aligned} \quad (1.53)$$

where the precession angle  $\Delta\phi$  is again given by Equation 1.52. Because  $\theta$  and the  $z'$  (parallel to  $-\hat{x}$ ) components of  $\hat{P}_I$  and  $\hat{P}_F$  are constant along the field (and rotation) axis, Equation 1.53 can be rewritten as

$$\begin{aligned} P_{F_{x'}} &= \sin \theta \cos(\phi_I) \cos(\Delta\phi) - \sin \theta \sin(\phi_I) \sin(\Delta\phi) \\ &= P_{I_{x'}} \cos(\Delta\phi) - P_{I_{y'}} \sin(\Delta\phi) \end{aligned} \quad (1.54)$$

or, in matrix notation for all three components,

$$\begin{pmatrix} P_{F_{x'}} \\ P_{F_{y'}} \\ P_{F_{z'}} \end{pmatrix} = \begin{pmatrix} \cos(\Delta\phi) & -\sin(\Delta\phi) & 0 \\ \sin(\Delta\phi) & \cos(\Delta\phi) & 0 \\ 0 & 0 & 1 \end{pmatrix} \begin{pmatrix} P_{I_{x'}} \\ P_{I_{y'}} \\ P_{I_{z'}} \end{pmatrix}. \quad (1.55)$$

The equation above is a prescription of general applicability for rotating the polarization in the geometry of Figure 1.11.

Thus, in practice, to determine the component  $P_{I_y}$  in Figure 1.11, we would first establish an orthogonal magnetic field along the  $-x$  direction in Region II and rename the  $-x$  axis  $z'$ . By choosing the proper magnitudes of  $B_{GF}$  and  $L$  for a given  $k_0$ , the neutron would arrive in Region III at  $y = L$  with the  $y$  component of its original polarization rotated by  $\pi/2$ , now lying along the  $-z$  axis of the original coordinate system. In Region III the guide field could be oriented along the original  $+z$  and a magnetized mirror placed at  $L$ . The initial component  $P_{I_y}$ , rotated to  $P_{F_z}$ , would be analyzed (since it was rotated to  $-\hat{P}_z = -1\hat{z}$ , it will be transmitted by the mirror). The  $x$  component of the original  $\hat{P}_I$  at  $y = 0$  could also be “projected out” along  $z$ , but in practice two sequential rotations of  $\pi/2$ , one about the  $+z$  (or  $+x'$ ) axis followed by another about  $-x$  (or  $+z'$ ) would be required. The pair of rotations is necessary because of the practical requirement of abruptly changing the magnetic field direction across an effectively infinite planar boundary defined by the wire coils of a flat solenoid. (Again, any component of  $\vec{B}$  normal to the plane of the wire coils would have to be continuous across the boundary between the interior and exterior of the solenoid whereas the parallel component can change direction abruptly at this interface.)

Let us summarize the principal results regarding polarization. It is possible to measure only whether a given neutron is in the  $+$  or  $-$  spin basis state along a quantization direction established by a magnetic field, which, by convention, is taken to lie along the  $z$  axis of the frame of reference. This measurement can be performed in practice, for example, with a spin-state-sensitive magnetic mirror. However, the corresponding  $z$  component of the three-dimensional polarization vector  $\hat{P}$  can be deduced only by making a sufficient number of measurements, to be statistically accurate to the desired degree, on a collection or ensemble of identical neutron systems (*i.e.*, neutrons having the same wavevector and polarization). The  $x$  and  $y$  components of the polarization can be determined similarly, but by first rotating the polarization the requisite amount(s) about the appropriate field direction(s) and then projecting out the desired component by reflection from a magnetic mirror, as done for the  $z$  component. In the analysis of spin-dependent reflection from magnetic films, discussed in the following section, performing rotations of the polarization relative to different coordinate systems, associated with instrument and sample, will be required.

## 1.4 Spin-Dependent Neutron Reflectivity

As discussed in Section 1.2, to correctly describe the motion of a neutron through a region of space in which a nonmagnetic potential exists that is strong enough to significantly distort the incident neutron wavefunction, an exact solution of the Schrödinger wave equation is necessary. This so-called dynamical theory can be augmented to include magnetic interactions if we take into account the spin-dependent nature of the neutron wavefunction described in Section 1.3. Measurements of the spin-dependent neutron specular reflectivity can be analysed to obtain not only the chemical compositional depth profile, but the in-plane vector magnetization depth profile as well. Although there have been more recent treatments, the dynamical theory of polarized neutron diffraction from magnetic crystals was fully developed many years earlier by Mendiratta and Blume [27], Sivardiere [28], and Belyakov and Bokun [29], among others. Scharpf [30] extended the dynamical theory to the continuum limit, where the scattering potential can be represented by a SLD, while Felcher *et al.* [31] and Majkrzak and Berk [32, 33] made specific application of the dynamical theory to polarized neutron reflectivity measurements of magnetic films and multilayers. Here we will present

a derivation of the dynamical theory for the specular reflection of polarized neutrons from magnetic materials in the continuum limit which parallels that for the nonmagnetic case presented in Section 1.2. This theory is applicable not only to PNR, but also to macroscopic devices such as resonance spin flippers [34] and to transmission neutron depolarization studies [35].

### 1.4.1 Spin-Dependent Reflection from a Magnetic Film in Vacuum Referred to Reference Frame of Film

We have seen in Section 1.3 that the neutron wavefunction must be described, in general, as a linear superposition of two plane waves, one corresponding to the + spin basis state and the other to the – state. Given the existence of two different spin states, a general magnetic interaction potential must account for two qualitatively different types of possible scattering processes: one which results in a change in the initial spin state and another which does not. Consequently, the description of specular reflection from a flat magnetic thin film structure now requires a pair of second-order, coupled, one-dimensional differential wave equations:

$$\begin{aligned} \left[ -\frac{\hbar^2}{2m} \frac{\partial^2}{\partial z^2} + V_{++}(z) - E \right] \psi_+(z) + V_{+-}(z) \psi_-(z) &= 0 \\ \left[ -\frac{\hbar^2}{2m} \frac{\partial^2}{\partial z^2} + V_{--}(z) - E \right] \psi_-(z) + V_{-+}(z) \psi_+(z) &= 0 \end{aligned} \quad (1.56)$$

where, as in the nonmagnetic case, the total energy  $E$  of the neutron is conserved so that there is no explicit time dependence. In matrix notation we can write Equation 1.56 as

$$\left[ -\frac{\hbar^2}{2m} \frac{\partial^2}{\partial z^2} \begin{pmatrix} 1 & 0 \\ 0 & 1 \end{pmatrix} + \begin{pmatrix} V_{++}(z) & V_{+-}(z) \\ V_{-+}(z) & V_{--}(z) \end{pmatrix} - E \begin{pmatrix} 1 & 0 \\ 0 & 1 \end{pmatrix} \right] \begin{pmatrix} \psi_+ \\ \psi_- \end{pmatrix} = 0 \quad (1.57)$$

where the net potential operator  $\check{V} = \check{V}_N + \check{V}_M$  has a magnetic contribution  $\check{V}_M$  written in terms of the Pauli matrices of Equation 1.38 as

$$\begin{aligned} \check{V}_M &= \check{\mu} \cdot \vec{B} = -\mu \check{\sigma} \cdot \vec{B} = -\mu (\check{\sigma}_x B_x + \check{\sigma}_y B_y + \check{\sigma}_z B_z) \\ &= -\mu \left[ \begin{pmatrix} 0 & 1 \\ 1 & 0 \end{pmatrix} B_x + \begin{pmatrix} 0 & -i \\ i & 0 \end{pmatrix} B_y + \begin{pmatrix} 1 & 0 \\ 0 & -1 \end{pmatrix} B_z \right] \\ &= -\mu \begin{pmatrix} B_z & B_x - iB_y \\ B_x + iB_y & B_z \end{pmatrix}. \end{aligned} \quad (1.58)$$

The coherent part of the nuclear potential operator  $\check{V}_N$ , on the other hand, is scalar in nature, assuming random orientations of any nuclear magnetic moments, and can be written as

$$\check{V}_N = \frac{2\pi\hbar^2}{m} \begin{pmatrix} Nb & 0 \\ 0 & Nb \end{pmatrix} = \frac{2\pi\hbar^2}{m} \begin{pmatrix} \rho_N & 0 \\ 0 & \rho_N \end{pmatrix} \quad (1.59)$$

where we have made use of the definitions of SLD  $\rho = Nb$  introduced earlier in Equations 1.5 and 1.6. The matrix elements of the magnetic potential operator of Equation 1.58 can also be described in terms of the products of a component magnetic scattering length  $p(x, y, z)$  and number density  $N$  of magnetic atoms:

$$\check{V}_M = \frac{2\pi\hbar^2}{m} \begin{pmatrix} Np_z & Np_x - iNp_y \\ Np_x + iNp_y & -Np_z \end{pmatrix} \quad (1.60)$$

where the magnitude of the magnetic scattering length  $p$  is associated with a given atomic magnetic moment. The magnetic scattering length  $p$  arises from the atom's unpaired electrons which are distributed about a volume of space orders of magnitude larger than that occupied by the nucleus. The volume occupied by the nucleus is so small in comparison, that the nuclear scattering length can, for almost all practical purposes, be considered to be constant, independent of  $Q$ . Although such is not the case for  $p$ , at the relatively small wavevector transfers typically of interest in specular PNR ( $Q$  values typically less than  $0.5 \text{ \AA}^{-1}$ ),  $p$  normally can be taken to be constant to a good enough approximation. Earlier in Equation 1.34 we defined a magnetic scattering length  $\rho_M$ . Here  $\rho_M = Np$ .

The total spin-dependent interaction potential operator for a magnetic material, including both nuclear and magnetic contributions (where, for simplicity, we assume a common density  $N$  of atomic scattering centers for both nuclear and magnetic interactions), is then

$$\check{V} = \frac{2\pi\hbar^2}{m} \begin{pmatrix} Nb + Np_z & Np_x - iNp_y \\ Np_x + iNp_y & Nb - Np_z \end{pmatrix} = \frac{2\pi\hbar^2}{m} \begin{pmatrix} \rho_{++} & \rho_{+-} \\ \rho_{-+} & \rho_{--} \end{pmatrix}. \quad (1.61)$$

Remember that we are considering specular reflection that is due only to variations in the SLD (nuclear and magnetic) along  $z$ , normal to the surface. Although this is a one-dimensional problem in this regard, the magnetization of the sample is a three-dimensional quantity and, as will become evident in

the following discussion, the direction of the magnetization in the sample has a significant effect on the reflectivity.

It is also important to remain cognizant of our conventional choice of the  $z$  direction as the quantization axis for the neutron spin, as realized by the particular form of the spin operator in Equation 1.38, and the fact that this direction coincides with the outward normal to the surface and  $Q$ .

Setting  $E = \hbar^2 k_0^2 / (2m)$ , the coupled equations of motion 1.56 can be rewritten in a form analogous to Equation 1.15 for the nonmagnetic case:

$$\begin{aligned} \left[ \frac{\partial^2}{\partial z^2} + \frac{Q^2}{4} - 4\pi\rho_{++}(z) \right] \psi_+(z) - 4\pi\rho_{+-}(z)\psi_-(z) &= 0 \\ \left[ \frac{\partial^2}{\partial z^2} + \frac{Q^2}{4} - 4\pi\rho_{--}(z) \right] \psi_-(z) - 4\pi\rho_{-+}(z)\psi_+(z) &= 0 \end{aligned} \quad (1.62)$$

where we have substituted  $Q = 2k_{0z}$ .

### The Wronskian Formula for Magnetic Films

In a later section we will deal with solving the coupled differential equations in Equation 1.62 and computing the reflectivity. First, however, we derive a general relationship between these solutions and the complex reflection amplitudes, which extends Equation 1.26 to the magnetic case and has several useful consequences. Some readers may wish to skip ahead and return to this material later.

We begin by reviewing notation and adding a few helpful refinements. For the time being, we will adopt the convention that the positive  $z$  direction points *opposite* of  $Q$  and into the body of the sample. The spinor wave function shown in Equation 1.32 can be denoted as

$$\Psi(k_{0z}, z) = \begin{pmatrix} \psi_+(k_{0z}, z) \\ \psi_-(k_{0z}, z) \end{pmatrix} \quad (1.63)$$

where the  $\psi_{\pm}(k_{0z}, z)$  satisfy Equations 1.62, now written in spinor form as

$$-\frac{\partial^2 \Psi(k_{0z}, z)}{\partial z^2} + 4\pi \left[ \rho(z) \mathbb{1} + \vec{\mathcal{B}}(z) \cdot \vec{\sigma} \right] \Psi(k_{0z}, z) = k_{0z}^2 \Psi(k_{0z}, z). \quad (1.64)$$

In Equation 1.64 the matrix  $\vec{\mathcal{B}}(z) \cdot \vec{\sigma} = m\check{V}_M / (2\pi\hbar^2)$ , where  $\check{V}_M$  is given by Equation 1.60;  $\vec{\sigma}$  is the vector Pauli matrix defined in Equation 1.38. Thus

the film's magnetic scattering length density is here represented as the vector “ $B$ ” field  $\vec{\mathcal{B}}(z)$ :

$$\vec{\mathcal{B}}(z) = -\mu m \vec{B} / (2\pi \hbar^2) = N p_x(z) \hat{x} + N p_y(z) \hat{y} + N p_z(z) \hat{z}. \quad (1.65)$$

The non-magnetic, or nuclear, scattering length density profile of the film is  $\rho(z) = \rho_N(z)$ , as in Equation 1.59, but we drop the  $N$  in this section. We have made the  $k_{0z}$ -dependence of the wave functions explicit for clarity, but as in other sections of this chapter, we remain flexible in the display of function arguments.

When written out in matrix form, analogously to Equation 1.57, the wave equation in this notation is

$$-\begin{pmatrix} \psi_+'' \\ \psi_-'' \end{pmatrix} + 4\pi \begin{pmatrix} \rho + \mathcal{B}_z & \mathcal{B}_x - i\mathcal{B}_y \\ \mathcal{B}_x + i\mathcal{B}_y & \rho - \mathcal{B}_z \end{pmatrix} \begin{pmatrix} \psi_+ \\ \psi_- \end{pmatrix} = k_{0z}^2 \begin{pmatrix} \psi_+ \\ \psi_- \end{pmatrix}, \quad (1.66)$$

where  $(\prime)$  stands for  $\partial/\partial z$ . The free-space solution corresponding to the incident beam is

$$\Psi_{0z}(k_{0z}, z) = e^{ik_{0z}z} \chi_0 = e^{ik_{0z}z} \begin{pmatrix} C_+ \\ C_- \end{pmatrix}, \quad (1.67)$$

which fully describes the incident beam in terms of its wave vector  $k_{0z}$  and spin state  $\chi_0$ . We consider here only the case of the free film. The generalization to non-vacuum, but non-magnetic, fronting and backing is not difficult.

## The Wronskian

Now consider the Wronskian function  $W(z)$ , composed of the physical solution  $\Psi(k_{0z}, z)$  of Equation 1.64 in the presence of a given magnetic film, and the incident wave function  $\Psi_0(k_{0z}, z)$ . This is defined as

$$W(z) = \Psi_0^\top(z) \Psi'(z) - \Psi_0'^\top(z) \Psi(z), \quad (1.68)$$

where  $^\top$  indicates the matrix transpose, *not* the hermitian conjugate  $^\dagger$ . In general terms, the Wronskian of two arbitrary continuous functions, say  $f(z)$  and  $g(z)$ , tests their linear independence from one another: *viz.*,  $f(z)$  and  $g(z)$  are linearly independent (*i.e.*, not proportional) if and only if  $W(z) = f(z)g'(z) - f'(z)g(z) \neq 0$ . In the scattering context, linear independence

essentially means that the two waves being compared propagate in different directions (recall that the differential operator  $\partial/\partial z$  can be related to the momentum along the  $z$  axis). For example, for  $z > L$ , *i.e.*, in the space behind the film (we are using the convention that the normal to the film is inward), both the transmitted wave and the incident wave are plane waves propagating in the same direction. Thus, in this domain they are linearly dependent, and  $W(z) = 0$ . On the other hand, in the fronting region the incident and reflected waves are plane waves moving in opposite directions with respect to the  $z$  axis, and thus  $W(z) \neq 0$  for  $z < 0$ ; in fact, we will see that  $W(z)$  is constant in the fronting. Now  $W(z)$  is continuous and has a continuous first derivative because it is composed of functions having this property, *viz.*, proper solutions of the wave equation. Thus as  $z$  increases into the film,  $W(z)$  goes continuously from a non-zero constant for  $z \leq 0$  to zero at  $z = L$  and then remains at zero for  $z > L$ . Roughly speaking,  $W(z)$  is a measure of reflected neutron current—*i.e.*, current in the direction opposite to the incident current—everywhere along the  $z$  axis, even within the film itself.

To be explicit, we start by differentiating  $W(z)$  in Equation 1.68. Thus

$$W'(z) = \partial (\Psi_0^\top \Psi' - \Psi_0'^\top \Psi) / \partial z = \Psi_0^\top \Psi'' - \Psi_0''^\top \Psi. \quad (1.69)$$

Only second derivatives survive on the RHS, since the terms depending on first derivatives cancel exactly. The second derivatives are cleared using Equation 1.67 for  $\Psi_0$  and the wave equation, Equation 1.64, for  $\Psi$ . These substitutions yield the equation

$$\begin{aligned} W'(z) &= 4\pi \Psi_0^\top \left( \rho \check{\mathbf{1}} + \vec{\mathcal{B}} \cdot \check{\sigma} - k_{0z}^2 \check{\mathbf{1}} \right) \Psi + k_{0z}^2 \Psi_0^\top \check{\mathbf{1}} \Psi \\ &= 4\pi \Psi_0^\top \left( \rho \check{\mathbf{1}} + \vec{\mathcal{B}} \cdot \check{\sigma} \right) \Psi. \end{aligned} \quad (1.70)$$

Integrating both sides of this with respect to  $z$ , from the front edge to the back edge of the film, we have

$$W(L) - W(0) = 4\pi \int_0^L \Psi_0^\top(z) \left[ \rho(z) \check{\mathbf{1}} + \vec{\mathcal{B}}(z) \cdot \check{\sigma} \right] \Psi(z) dz. \quad (1.71)$$

There is not much more that can be done in general with the RHS of Equation 1.71, except for an important refinement to be derived below, but we can readily replace the LHS with a more useful expression, knowing that  $W(z)$  is

continuous. Thus, note that  $W(0) = W(0^-)$ , where  $0^-$  means the limit as  $z \rightarrow 0$  from the left, and similarly, that  $W(L) = W(L^+)$ , where  $L^+$  means the limit as  $z \rightarrow L$  from the right. Furthermore, the wave functions for  $z < 0$  and for  $z > 0$  have canonical forms from which we can directly calculate  $W(z)$  in these regions. First consider the backing region. For  $z \geq L$  the solution consists only of the transmitted wave, which includes the incident wave and the forward scattered wave. Conventionally these two waves are combined into one, since in fact they are linearly dependent in  $z$ , *viz.*,

$$\Psi(k_{0z}, z) = e^{ik_{0z}z} \begin{pmatrix} C_+ t^{++} + C_- t^{-+} \\ C_- t^{--} + C_+ t^{+-} \end{pmatrix}, \quad (1.72)$$

where  $t^{\mu\nu}$  is the transmission coefficient for incident spin-state  $\mu$  and scattered (here transmitted) spin-state  $\nu$ , with  $|t^{\mu\nu}| \leq 1$ . The upper component of the spinor is a coherent superposition of the two ways a spin “up” state can be observed behind the film: transmission without spin-flip of an incident spin “up” state and transmission with spin-flip of an incident spin “down” state. Similarly, the lower component accounts for the channels producing a transmitted spin “down” state. Now to reduce the algebra, consider a simpler looking case where  $\Psi_0(z) = e^{ik_{0z}z} A$  and  $\Psi(z) = e^{ik_{0z}z} B$  for two constant but otherwise *arbitrary* spinors,  $A$  and  $B$ . Then  $\Psi_0^\top \Psi' - \Psi_0'^\top \Psi = (ik_{0z} - ik_{0z}) e^{ik_{0z}z} A^\top B = 0$ . Thus the actual contents of the spinor for the transmitted wave plays no role, and we have  $W(L) = 0$  quite generally, as anticipated earlier.

In the fronting region,  $z \leq 0$ , we have

$$\Psi(k_{0z}, z) = e^{ik_{0z}z} \begin{pmatrix} C_+ \\ C_- \end{pmatrix} + e^{-ik_{0z}z} \begin{pmatrix} C_+ r^{++} + C_- r^{-+} \\ C_- r^{--} + C_+ r^{+-} \end{pmatrix}, \quad (1.73)$$

where the  $r^{\mu\nu}$  are the channel-specific reflection amplitudes, defined analogously to the transmission coefficients  $t^{\mu\nu}$ . Here we have waves propagating in different directions, the incident and reflected waves, so  $W(z) \neq 0$  in the fronting region. In fact one easily finds that  $W(z) = 2ik_{0z} [C_+^2 r^{++} + C_-^2 r^{--} + C_+ C_- (r^{+-} + r^{-+})]$ , independently of  $z$ . Thus for  $z \leq 0$ ,  $W(z) = W(0)$ , a constant, consistent with the fact that  $W'(z) = 0$  in the fronting. For still more compact notation, introduce a matrix of reflection coefficients,

$$\check{\mathbb{R}} = \begin{pmatrix} r^{++} & r^{-+} \\ r^{+-} & r^{--} \end{pmatrix}. \quad (1.74)$$

Then Equation 1.71 can be written as

$$2ik_{0z}\Psi_0^T(0)\check{\mathbb{R}}\Psi_0(0) = 4\pi \int_0^L \Psi_0^T(z) \left[ \rho(z)\check{\mathbb{I}} + \vec{\mathcal{B}}(z) \cdot \check{\sigma} \right] \Psi(z) dz. \quad (1.75)$$

Equation 1.75 is rigorous, but it can be refined, as we shall soon see. It is fairly easy to show that in the absence of a magnetic field, Equation 1.75 is equivalent to the less notationally encumbered Equation 1.26.

### The Halperin Effect

As a formal device, the integration on the RHS of Equation 1.75 can be extended to the entire  $z$  axis, since the SLD profile of the film provides the explicit restriction to  $0 \leq z \leq L$ . Then recalling Equation 1.67, and temporarily writing  $k_{0z}\hat{z} = \vec{k}_0$ , we can write the integral as a Fourier transform (FT), *viz.*,

$$\begin{aligned} & \int_{-\infty}^{\infty} e^{i\vec{k}_0 \cdot \vec{r}} \left\{ \Psi_0^T(0) \left[ \rho(z\hat{z})\check{\mathbb{I}} + \vec{\mathcal{B}}(z\hat{z}) \cdot \check{\sigma} \right] \Psi(z\hat{z}) \right\} dz \\ &= \int_{-\infty}^{\infty} \Psi_0^T(0) \left[ \rho[\vec{k}_0 - \xi\hat{z}]\check{\mathbb{I}} + \vec{\mathcal{B}}[\vec{k}_0 - \xi\hat{z}] \cdot \check{\sigma} \right] \Psi[\xi\hat{z}] d\xi. \end{aligned} \quad (1.76)$$

On the RHS of Equation 1.76, we have used the (temporary) notation that  $f[\vec{Q}] = \text{FT}f(\vec{r})$  for any function  $f$ . To obtain the RHS, we used the standard product-convolution theorem of Fourier analysis.[36]

Recall from Equation 1.65 that the magnetic scattering length density  $\vec{\mathcal{B}}$  (in the current notation) is related to the internal magnetic field strength  $\vec{B}$  by  $\vec{\mathcal{B}}(\vec{r}) = \Lambda\vec{B}(\vec{r})$ , where

$$\Lambda = -\frac{\mu m}{2\pi\hbar^2}. \quad (1.77)$$

The internal magnetic field due to unpaired electron spins can be represented (in SI units) as

$$\vec{B}(\vec{r}) = \mu_0 \sum_i \vec{\nabla} \times \left( \frac{\vec{m}_i \times \hat{r}}{r^2} \right), \quad (1.78)$$

where  $\mu_0$  is the vacuum permeivity and  $\vec{m}_i$  is the magnetic moment of the  $i$ th spin. The Fourier transform of Equation 1.78 is

$$\vec{B}[\vec{Q}] = \int e^{i\vec{Q} \cdot \vec{r}} \vec{B}(\vec{r}) d^3r = \mu_0 \hat{Q} \times \left[ \vec{m}[\vec{Q}] \times \hat{Q} \right], \quad (1.79)$$

where

$$\vec{m}[\vec{Q}] = \sum_i \vec{m}_i e^{i\vec{Q}\cdot\vec{r}_i}. \quad (1.80)$$

The application of a standard identity to the vector cross product in Equation 1.79 gives

$$\vec{B}[\vec{Q}] = \mu_0 \left[ \vec{m}[\vec{Q}] - \left( \vec{m}[\vec{Q}] \cdot \hat{Q} \right) \hat{Q} \right] = \mu_0 \vec{m}_\perp[\vec{Q}], \quad (1.81)$$

where  $\vec{m}_\perp[\vec{Q}]$  denotes the component of  $\vec{m}[\vec{Q}]$  perpendicular to  $\vec{Q}$ . Therefore

$$\vec{B}[\vec{Q}] = \Lambda \mu_0 \vec{m}_\perp[\vec{Q}] = \vec{B}_\perp[\vec{Q}], \quad (1.82)$$

so that, taking account of the RHS of Equation 1.76, Equation 1.75 becomes

$$2ik_{0z} \Psi_0^\top(0) \check{\mathbb{R}} \Psi_0(0) = 4\pi \int_0^L \Psi_0^\top(z) \left[ \rho(z) \check{1} + \vec{B}_\perp(z) \cdot \check{\sigma}_\perp \right] \Psi(z) dz. \quad (1.83)$$

As seen from the form of the RHS, only the component of the film magnetization perpendicular to the neutron wave vector transfer causes spin-dependent reflection. This behavior is known as the ‘‘Halperin effect’’ in magnetic neutron scattering. Since for specular reflection the wave vector transfer  $\vec{Q} = -2k_0\hat{z}$  is perpendicular to the film, in Equation 1.83  $\vec{B}_\perp(z)$  is parallel to the film. Normally the Halperin effect is derived within the Born approximation, but in fact, as we see in Equation 1.83, it is exact. We refer to Equation 1.83 as the ‘‘Wronskian formula’’ for the spin-dependent neutron reflection amplitudes.

### Reflection Amplitudes in the Beam Polarization Frame

So far we have chosen the quantization axis for the neutron spin to be along the film normal, and the elements of  $\check{\mathbb{R}}$  specifically refer to this axis. But as discussed in detail in Sections 1.4.3 to 1.4.5, reflectivity measurements usually are made with respect to different polarization axes. We must be able, therefore, to relate the reflection amplitudes of Equation 1.83 to the measurement frame. There are several formalisms for doing this, usually with the aid of spinor rotation matrices, depending on the problem at hand. A general method will be worked out in Section 1.4.3 for the case of the transfer matrix formulation of the problem. Here we mention another approach which is perhaps less efficient but is easy to visualize.

The incident and reflected spinor wave functions defined in Equation 1.73 are completely general for any state of incident polarization, since the spinor coefficients,  $C_+$  and  $C_-$ , are arbitrary. Now, however, let us consider the spinor  $\chi = \begin{pmatrix} C_+ \\ C_- \end{pmatrix}$  as the “spin-up” state along the axis of polarization, and let the associated “spin-down” state be designated by  $\chi' = \begin{pmatrix} C'_+ \\ C'_- \end{pmatrix}$ , where  $C'_+$  and  $C'_-$  are determined by the pair,  $C_+$  and  $C_-$ . Namely, we specify  $\chi$  and  $\chi'$  to be the eigenstates of the matrix  $\tilde{\sigma} \cdot \hat{P}$ . Then the wavefunction in the fronting region can be represented as

$$\Psi(k_{0z}, z) = e^{ik_{0z}z} \begin{pmatrix} C_+ \\ C_- \end{pmatrix} + e^{-ik_{0z}z} \left\{ r^{\uparrow\uparrow} \begin{pmatrix} C_+ \\ C_- \end{pmatrix} + r^{\uparrow\downarrow} \begin{pmatrix} C'_+ \\ C'_- \end{pmatrix} \right\}, \quad (1.84)$$

where  $r^{\uparrow\uparrow}$  and  $r^{\uparrow\downarrow}$  are the non-spin-flip and spin-flip reflection amplitudes, respectively, relative to the polarization axis. Notice that we are careful to distinguish between the two quantization axes by using different index sets for them, where  $\{+, -\}$  refer to the film normal axis and  $\{\uparrow, \downarrow\}$  refer to the spin polarization axis. Thus, in the comparison of Equation 1.84 with Equation 1.73, which represents exactly the *same* wavefunction, we have two equations,

$$\begin{aligned} C_+ r^{\uparrow\uparrow} + C'_+ r^{\uparrow\downarrow} &= C_+ r^{++} + C_- r^{-+} \quad \text{and} \\ C_- r^{\uparrow\uparrow} + C'_- r^{\uparrow\downarrow} &= C_- r^{--} + C_+ r^{+-}, \end{aligned} \quad (1.85)$$

for the reflection amplitudes  $r^{\uparrow\uparrow}$  and  $r^{\uparrow\downarrow}$ . Similar equations determine  $r^{\downarrow\uparrow}$  and  $r^{\downarrow\downarrow}$ , should they be needed. For example, take the case of an incident beam completely polarized along the positive  $x$  axis in the sample coordinate system. Then  $C_+ = 1/\sqrt{2}$ ,  $C_- = 1/\sqrt{2}$ ,  $C'_+ = 1/\sqrt{2}$ , and  $C'_- = -1/\sqrt{2}$ ; therefore,

$$r^{\uparrow\uparrow} \begin{pmatrix} 1 \\ 1 \end{pmatrix} + r^{\uparrow\downarrow} \begin{pmatrix} 1 \\ -1 \end{pmatrix} = \begin{pmatrix} r^{++} + r^{-+} \\ r^{--} + r^{+-} \end{pmatrix}, \quad (1.86)$$

so that, solving for  $r^{\uparrow\uparrow}$  and  $r^{\uparrow\downarrow}$ , we have

$$\begin{aligned} r_x^{\uparrow\uparrow} &= \frac{1}{2} (r^{++} + r^{--}) + \frac{1}{2} (r^{-+} + r^{+-}) \\ r_x^{\uparrow\downarrow} &= \frac{1}{2} (r^{++} - r^{--}) + \frac{1}{2} (r^{-+} - r^{+-}). \end{aligned} \quad (1.87)$$

where  $r_x$  denotes the reflection amplitude for the  $x$  direction of polarization. The formulas for  $r_x^{\downarrow\downarrow}$  and  $r_x^{\downarrow\uparrow}$  are obtained from these by the interchange of  $\pm$  on the RHS. We will give an example of these formulas directly.

## The Born Approximation

In Section 1.2.5 we used the non-magnetic Wronskian formula, Equation 1.26, to derive the Born approximation for the specular reflection amplitude. We can do the same here for the magnetic case. The Born approximation replaces the exact spinor wavefunction  $\Psi(k_{0z}, z)$  with the incident wavefunction  $\Psi_0(k_{0z}, z)$  in Equation 1.83. The result of this approximation is

$$\begin{aligned} 2ik_{0z}\Psi_0^\top(0)\check{\mathbb{R}}_{\text{BA}}\Psi_0(0) &= 4\pi \int_0^L e^{2ik_{0z}z}\Psi_0^\top(0) \left( \rho(z)\check{\mathbf{1}} + \vec{\mathcal{B}}_\perp(z) \cdot \check{\sigma}_\perp \right) \Psi_0(0) dz \\ &= 4\pi\Psi_0^\top(0) \left( \rho[[Q]]\check{\mathbf{1}} + \vec{\mathcal{B}}_\perp[[Q]] \cdot \check{\sigma}_\perp \right) \Psi_0(0), \end{aligned} \quad (1.88)$$

where  $Q = 2k_{0z}$ . The spinor  $\Psi_0$  can be “factored out” of Equation 1.88 by rearranging it as

$$\Psi_0^\top(0) \left[ iQ\check{\mathbb{R}}_{\text{BA}} = 4\pi \left( \rho[[Q]]\mathbf{1} + \vec{\mathcal{B}}_\perp[[Q]] \cdot \check{\sigma}_\perp \right) \right] \Psi_0(0). \quad (1.89)$$

Since this holds for arbitrary polarization, the equality within the brackets must be satisfied, *i.e.*,

$$\check{\mathbb{R}}_{\text{BA}}(Q) = \frac{4\pi}{iQ} \left( \rho[[Q]]\check{\mathbf{1}} + \vec{\mathcal{B}}_\perp[[Q]] \cdot \check{\sigma}_\perp \right), \quad (1.90)$$

which in explicit matrix form is

$$\begin{pmatrix} r^{++}(Q) & r^{-+}(Q) \\ r^{+-}(Q) & r^{--}(Q) \end{pmatrix}_{\text{BA}} = \frac{4\pi}{iQ} \begin{pmatrix} \rho[[Q]] & \mathcal{B}_x[[Q]] - i\mathcal{B}_y[[Q]] \\ \mathcal{B}_x[[Q]] + i\mathcal{B}_y[[Q]] & \rho[[Q]] \end{pmatrix}. \quad (1.91)$$

Equation 1.91 is the magnetic generalization of Equation 1.27. We see at once from Equation 1.91 that  $r_{\text{BA}}^{++} = r_{\text{BA}}^{--} = r_{\text{BA}}$ , since there is now no spin dependence in the diagonal elements on the RHS. Such behavior is not true in general since the exact spinor in the medium,  $\Psi(k_{0z}, z)$ , induces a “diagonal” spin-dependence; but this is a “dynamical” effect, *i.e.*, one strictly outside Born approximation, and thus it must diminish as  $Q \rightarrow \infty$  where the Born approximation becomes asymptotically exact. Equation 1.91 reduces immediately to Equation 1.27 for  $\vec{\mathcal{B}}_\perp[[Q]] = 0$ .

## Helical Magnetization

A simple but interesting application of Equation 1.91 is a film having a twisting magnetization modeled by a continuous helix, such that the magnetic SLD varies with  $z$  as

$$\begin{aligned}\mathcal{B}_x(z) &= |\mathcal{B}| \cos(2\pi z/\mathcal{L}) \quad \text{and} \\ \mathcal{B}_y(z) &= |\mathcal{B}| \sin(2\pi z/\mathcal{L}),\end{aligned}\tag{1.92}$$

where  $\mathcal{L}$  is the pitch of the helix; a positive value of  $\mathcal{L}$  signifies right-handedness, a negative value, left-handedness. The phase of the helix is chosen here so that  $\vec{\mathcal{B}}(0) = |\mathcal{B}| \hat{x}$ . A straightforward calculation of the Fourier transform of the helix gives

$$\mathcal{B}_x[[Q]] \pm i\mathcal{B}_y[[Q]] = e^{i(Q \mp \mathcal{K})L/2} \text{sinc}\left(\frac{(Q \mp \mathcal{K})L}{2\pi}\right),\tag{1.93}$$

where  $\mathcal{K} = 2\pi/\mathcal{L}$  is the pitch wave number, and where  $\text{sinc}(x) = \sin(\pi x)/(\pi x)$ . We leave the behavior of the non-magnetic SLD profile  $\rho(z)$  unspecified. We then can insert Equation 1.93 into Equation 1.91 and, for the particular case of the incident beam fully polarized along the  $x$  axis, use Equation 1.88 to get

$$r_{\text{BA}x}^{\uparrow\uparrow}(Q) = \frac{4\pi}{iQ} \left( \rho[[Q]] + \frac{1}{2} e^{i(Q-\mathcal{K})L/2} \text{sinc}\left(\frac{(Q-\mathcal{K})L}{2\pi}\right) + \frac{1}{2} e^{i(Q+\mathcal{K})L/2} \text{sinc}\left(\frac{(Q+\mathcal{K})L}{2\pi}\right) \right)\tag{1.94}$$

and

$$r_{\text{BA}x}^{\uparrow\downarrow}(Q) = \frac{4\pi}{iQ} \left( \frac{1}{2} e^{i(Q-\mathcal{K})L/2} \text{sinc}\left(\frac{(Q-\mathcal{K})L}{2\pi}\right) - \frac{1}{2} e^{i(Q+\mathcal{K})L/2} \text{sinc}\left(\frac{(Q+\mathcal{K})L}{2\pi}\right) \right).\tag{1.95}$$

We can see from this that  $r_{\text{BA}x}^{\uparrow\uparrow}(Q)$  does not depend on the handedness of the helix (the sign of  $\mathcal{K}$ ), while  $r_{\text{BA}x}^{\uparrow\downarrow}(Q)$  only changes sign with handedness. Therefore,  $\left| r_{\text{BA}x}^{\uparrow\uparrow}(Q) \right|^2$  and  $\left| r_{\text{BA}x}^{\uparrow\downarrow}(Q) \right|^2$  are independent of handedness. (Nonetheless, handedness is observable in single-domain samples for the case where  $\vec{P} \parallel \vec{Q}$ , as discussed in Section 1.4.4.) However, the reflectivity does depend on the phase of the helix at  $z = 0$  relative to the incident neutron polarization. For example, it is not difficult to work out that twisting the helix in Equation 1.92 counter-clockwise by  $90^\circ$  takes  $\mathcal{B}_x[[Q]] \rightarrow -\mathcal{B}_y[[Q]]$  and  $\mathcal{B}_y[[Q]] \rightarrow \mathcal{B}_x[[Q]]$ . The resulting changes in Equations 1.94 and 1.95 are summarized by multiplying the terms involving  $Q \mp \mathcal{K}$  by  $\pm i$ , respectively. Thus

for a polarized beam,  $\left|r_{\text{BA}x}^{\uparrow\uparrow}(Q)\right|^2$ , but not  $\left|r_{\text{BA}x}^{\uparrow\downarrow}(Q)\right|^2$ , depends on the relative helical phase at the surface. Reflection of polarized neutron beams from twisting magnetic configurations will be discussed below in Sections 1.6.3 and 1.6.4 using the full dynamical theory.

### The Piecewise Continuous Solution Using the Transfer Matrix

Now we return to the problem of obtaining the explicit solution of Equations 1.62. We resume our convention that the positive  $z$  direction points *along*  $Q$ . As we saw earlier in Sections 1.2.3 and 1.2.4 for nonmagnetic films, it is possible to represent the given potential by a piecewise constant model using sufficiently fine subdivisions. Thus, just as in the nonmagnetic case, we begin by exactly solving the special problem of slab of uniform SLD. Now, however, the spin dependence of the problem makes the solution more complicated, as we shall see. We will need to generalize the  $2 \times 2$  transfer matrix of Equation 1.24 for a nonmagnetic film to one of dimension  $4 \times 4$  in order to handle spin-dependent reflection from magnetic material.

Therefore, let us again consider a slab of finite thickness and constant SLD, but having magnetic as well as nuclear components, so that in Equation 1.62  $\rho_{mn}(z) = \rho_{mn}$  (a constant). Here  $m$  and  $n$  each independently can be  $+$  or  $-$ , yielding up to four distinct values for  $\rho$  at one depth  $z$ . Combining the pair of coupled second-order Equations 1.62 above, two uncoupled fourth-order equations can be obtained:

$$\left(\frac{\partial^4}{\partial z^4} + F\frac{\partial^2}{\partial z^2} + G\right)\psi_{\pm}(z) = 0 \quad (1.96)$$

where

$$\begin{aligned} F &\equiv \frac{Q^2}{2} - 4\pi(\rho_{++} - \rho_{--}) \\ G &\equiv \left(\frac{Q^2}{4}\right)^2 - Q^2\pi(\rho_{++} + \rho_{--}) + (4\pi)^2(\rho_{++}\rho_{--} - \rho_{+-}\rho_{-+}). \end{aligned} \quad (1.97)$$

Substituting the trial solution  $\psi = \exp(Sz)$  in Equation 1.96 yields a characteristic equation for the coefficient  $S$  of the form

$$S^4 + FS^2 + G = 0. \quad (1.98)$$

The four unique roots of Equation 1.98 are found to be

$$\begin{aligned}
S_1 &= \sqrt{4\pi(Nb + Np) - Q^2/4} \\
S_2 &= -S_1 \\
S_3 &= \sqrt{4\pi(Nb - Np) - Q^2/4} \\
S_4 &= -S_3
\end{aligned} \tag{1.99}$$

where

$$(Np)^2 = (Np_x)^2 + (Np_y)^2 + (Np_z)^2. \tag{1.100}$$

General solutions of the original pair of coupled second-order differential wave equations 1.62 are then given by

$$\begin{aligned}
\psi_+(z) &= \sum_{j=1}^4 \mathcal{C}_j e^{S_j z} \\
\psi_-(z) &= \sum_{j=1}^4 \mathcal{D}_j e^{S_j z}
\end{aligned} \tag{1.101}$$

Substituting the expressions 1.101 above for the wave functions into the coupled wave equations 1.62 then gives a pair of algebraic equations which can be solved for the coefficients  $\mathcal{C}_j$  in terms of the  $\mathcal{D}_j$ :

$$\mathcal{D}_j = \mathcal{C}_j \frac{S_j^2 + Q^2/4 - 4\pi(\rho_{++} - \rho_{-+})}{S_j^2 + Q^2/4 - 4\pi(\rho_{--} - \rho_{+-})} \equiv \mathcal{C}_j \mu_j \tag{1.102}$$

Writing  $\rho_N = Nb$  and  $\rho_M = Np$  (where  $Np$  is defined in Equation 1.100) and using the definitions of  $\rho_{++}$ ,  $\rho_{--}$ ,  $\rho_{+-}$ , and  $\rho_{-+}$  from Equation 1.61 we obtain

$$\begin{aligned}
\mu_1 &= \mu_2 = \frac{Np - Np_z + Np_x + iNp_y}{Np + Np_z + Np_x - iNp_y} \\
\mu_3 &= \mu_4 = \frac{Np + Np_z - Np_x - iNp_y}{Np - Np_z - Np_x + iNp_y}
\end{aligned} \tag{1.103}$$

Returning to the general solutions for the wave functions  $\psi_+(z)$  and  $\psi_-(z)$  given in Equation 1.101, we can write at  $z = 0$

$$\begin{aligned}
\psi_+(0) &= \mathcal{C}_1 + \mathcal{C}_2 + \mathcal{C}_3 + \mathcal{C}_4 \\
\psi'_+(0) &= S_1\mathcal{C}_1 + S_2\mathcal{C}_2 + S_3\mathcal{C}_3 + S_4\mathcal{C}_4 \\
\psi_-(0) &= \mu_1\mathcal{C}_1 + \mu_2\mathcal{C}_2 + \mu_3\mathcal{C}_3 + \mu_4\mathcal{C}_4 \\
\psi'_-(0) &= S_1\mu_1\mathcal{C}_1 + S_2\mu_2\mathcal{C}_2 + S_3\mu_3\mathcal{C}_3 + S_4\mu_4\mathcal{C}_4
\end{aligned} \tag{1.104}$$

where the primes denote differentiation with respect to  $z$ . Making use of the relationships among the  $S_j$  and  $\mu_j$  derived previously, the above set of linear algebraic equations can be solved to find the coefficients  $\mathcal{C}_j$  in terms of the  $\mu_j$ ,  $S_j$ ,  $\psi(0)$ , and  $\psi'(0)$ . For example,

$$\mathcal{C}_1 = \frac{1}{2(\mu_3 - \mu_1)} \left( \mu_3 \psi_+(0) - \psi_-(0) + \frac{\mu_3}{S_1} \psi'_+(0) - \frac{1}{S_1} \psi'_-(0) \right). \quad (1.105)$$

In general, the  $\mathcal{C}_j$  can be written as

$$\mathcal{C}_j = \alpha_j \psi_+(0) + \beta_j \psi_-(0) + \gamma_j \psi'_+(0) + \delta_j \psi'_-(0) \quad (1.106)$$

where the coefficients  $\alpha_j$ ,  $\beta_j$ ,  $\gamma_j$ , and  $\delta_j$  can be expressed in terms of the  $S_j$  and  $\mu_j$ .

As a consequence of several of the expressions derived above, the general solutions for the wave functions at arbitrary values of  $z$ , given by Equations 1.101, can be expressed explicitly in terms of the known quantities  $\mu_j$ ,  $S_j$  and the wave functions and their first derivatives evaluated at  $z = 0$ . For example, after collecting and rearranging terms,

$$\begin{aligned} \psi_+(z) = & \quad (1.107) \\ & \psi_+(0) \sum_{j=1}^4 \alpha_j e^{S_j z} + \psi_-(0) \sum_{j=1}^4 \beta_j e^{S_j z} + \psi'_+(0) \sum_{j=1}^4 \gamma_j e^{S_j z} + \psi'_-(0) \sum_{j=1}^4 \delta_j e^{S_j z} \end{aligned}$$

and similarly for  $\psi_-(z)$ ,  $\psi'_+(z)$ , and  $\psi'_-(z)$ . We can, therefore, write a general matrix equation relating the spin-dependent wave functions and their first derivatives at arbitrary  $z$  to those evaluated at  $z = 0$ , assuming that the SLD is constant over that interval of length  $z$ .

$$\begin{pmatrix} \psi_+(z) \\ \psi_-(z) \\ \psi'_+(z) \\ \psi'_-(z) \end{pmatrix} = \begin{pmatrix} A_{11} & A_{12} & A_{13} & A_{14} \\ A_{21} & A_{22} & A_{23} & A_{24} \\ A_{31} & A_{32} & A_{33} & A_{34} \\ A_{41} & A_{42} & A_{43} & A_{44} \end{pmatrix} \begin{pmatrix} \psi_+(0) \\ \psi_-(0) \\ \psi'_+(0) \\ \psi'_-(0) \end{pmatrix} \quad (1.108)$$

The matrix coefficients  $A_{ij}$  are listed in Table 1.2.

As was done earlier in the case of reflection from nonmagnetic materials in Section 1.2, the boundary conditions that the wave functions and their first derivatives be continuous at any interface between regions of different constant SLD values can be imposed and applied in piecewise continuous

$$\begin{aligned}
A_{11} &= 2\Delta[\mu_3 \cosh(S_1\delta_z) - \mu_1 \cosh(S_3\delta_z)] \\
A_{21} &= 2\Delta[\mu_1\mu_3 \cosh(S_1\delta_z) - \mu_3\mu_1 \cosh(S_3\delta_z)] \\
A_{31} &= 2\Delta[\mu_3 \sinh(S_1\delta_z)S_1 - \mu_1 \sinh(S_3\delta_z)S_3] \\
A_{41} &= 2\Delta[\mu_1\mu_3 \sinh(S_1\delta_z)S_1 - \mu_3\mu_1 \sinh(S_3\delta_z)S_3] \\
\hline
A_{12} &= -2\Delta[\cosh(S_1\delta_z) - \cosh(S_3\delta_z)] \\
A_{22} &= -2\Delta[\mu_1 \cosh(S_1\delta_z) - \mu_3 \cosh(S_3\delta_z)] \\
A_{32} &= -2\Delta[\sinh(S_1\delta_z)S_1 - \sinh(S_3\delta_z)S_3] \\
A_{42} &= -2\Delta[\mu_1 \sinh(S_1\delta_z)S_1 - \mu_3 \sinh(S_3\delta_z)S_3] \\
\hline
A_{13} &= 2\Delta[\mu_3 \sinh(S_1\delta_z)/S_1 - \mu_1 \sinh(S_3\delta_z)/S_3] \\
A_{23} &= 2\Delta[\mu_1\mu_3 \sinh(S_1\delta_z)/S_1 - \mu_3\mu_1 \sinh(S_3\delta_z)/S_3] \\
A_{33} &= 2\Delta[\mu_3 \cosh(S_1\delta_z) - \mu_1 \cosh(S_3\delta_z)] \\
A_{43} &= 2\Delta[\mu_1\mu_3 \cosh(S_1\delta_z) - \mu_3\mu_1 \cosh(S_3\delta_z)] \\
\hline
A_{14} &= -2\Delta[\sinh(S_1\delta_z)/S_1 - \sinh(S_3\delta_z)/S_3] \\
A_{24} &= -2\Delta[\mu_1 \sinh(S_1\delta_z)/S_1 - \mu_3 \sinh(S_3\delta_z)/S_3] \\
A_{34} &= -2\Delta[\cosh(S_1\delta_z) - \cosh(S_3\delta_z)] \\
A_{44} &= -2\Delta[\mu_1 \cosh(S_1\delta_z) - \mu_3 \cosh(S_3\delta_z)]
\end{aligned}$$

where  $2\Delta \equiv 1/(\mu_3 - \mu_1)$  and  $\delta_z$  is defined to be the distance over which the SLD is constant.

Table 1.2: Elements of the transfer matrix for polarized neutron specular reflection.

$$\begin{aligned}
\psi_{+,I}(z) &\equiv I_+ = \mathcal{I}_+ e^{iQz/2}; & \psi'_{+,I}(z) &= \frac{iQ}{2} I_+ \\
\psi_{-,I}(z) &\equiv I_- = \mathcal{I}_- e^{iQz/2}; & \psi'_{-,I}(z) &= \frac{iQ}{2} I_- \\
\psi_{+,r}(z) &\equiv r_+ = \mathcal{R}_+ e^{-iQz/2}; & \psi'_{+,r}(z) &= -\frac{iQ}{2} r_+ \\
\psi_{-,r}(z) &\equiv r_- = \mathcal{R}_- e^{-iQz/2}; & \psi'_{-,r}(z) &= -\frac{iQ}{2} r_- \\
\psi_{+,t}(z) &\equiv t_+ = \mathcal{T}_+ e^{iQz/2}; & \psi'_{+,t}(z) &= \frac{iQ}{2} t_+ \\
\psi_{-,t}(z) &\equiv t_- = \mathcal{T}_- e^{iQz/2}; & \psi'_{-,t}(z) &= \frac{iQ}{2} t_-
\end{aligned}$$

Table 1.3: Neutron wave functions for polarized neutron specular reflection and transmission.

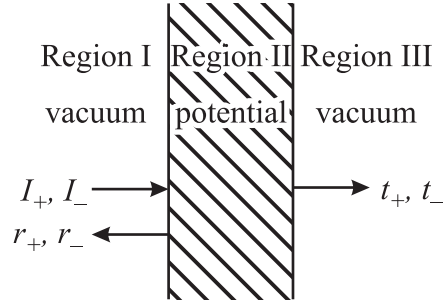


Figure 1.12: Schematic depiction of specular neutron reflection for polarized beams.

fashion to approximate an arbitrary SLD profile to any desired degree of accuracy. Using the explicit identifications tabulated in Table 1.3, the spin-dependent transmission and reflection coefficients can then be related by

$$\begin{pmatrix} t_+ \\ t_- \\ \frac{iQ}{2}t_+ \\ \frac{iQ}{2}t_- \end{pmatrix} = \prod_{l=N}^1 \begin{pmatrix} A_{11} & A_{12} & A_{13} & A_{14} \\ A_{21} & A_{22} & A_{23} & A_{24} \\ A_{31} & A_{32} & A_{33} & A_{34} \\ A_{41} & A_{42} & A_{43} & A_{44} \end{pmatrix}_l \begin{pmatrix} I_+ + r_+ \\ I_- + r_- \\ \frac{iQ}{2}(I_+ - r_+) \\ \frac{iQ}{2}(I_- - r_-) \end{pmatrix} \quad (1.109)$$

where

$$\prod_{l=N}^1 \check{A}_l = \check{A}_N \check{A}_{N-1} \cdots \check{A}_l \cdots \check{A}_2 \check{A}_1. \quad (1.110)$$

The matrix operator  $\check{A}_l$  corresponds to the  $l$ th layer or slab of thickness  $\delta_z$  over which the scattering length density is taken to be constant. The  $\delta_z$  appearing in the arguments of the hyperbolic functions of the transfer matrix elements  $A_{ij}$  (Table 1.2) refer specifically to the thickness of the  $l$ th slab. Slab  $l = 1$  is the first slab encountered by the incident beam. Note that the fronting and backing media surrounding the sample film have thus far been assumed to be vacuum. Equation 1.109 represents a system of simultaneous linear equations which can be solved for the spin-dependent reflection and transmission amplitudes for the specular reflection geometry depicted schematically in Figure 1.12. Further details of the solution shall be revealed in Section 1.6.1.

To summarize progress thus far, Equation 1.109 enables us to calculate the probabilities  $|r_+|^2$ ,  $|r_-|^2$  and  $|t_+|^2$ ,  $|t_-|^2$  of finding a reflected or transmitted neutron in the + or - spin basis state, respectively, for a specified incident beam initial polarization state defined by  $I = (I_+, I_-)$ . For example, Equation 1.109 can be used to compute the probability that a neutron will be reflected in the + spin state from a magnetic film of a given SLD depth profile if it were incident in the + spin state,  $I_+ = 1$  and  $I_- = 0$ , to begin with.

Remember that we have so far explicitly assumed that the Regions I and III (see Figure 1.12) surrounding the potential (Region II) are vacuum. Although a magnetic guide field is required in the surrounding Regions I and III of the “laboratory” in order to define an axis of quantization for the incident, reflected, and transmitted neutrons, we can assume a magnetic field and corresponding SLD of vanishingly small magnitude. However, it is important to realize that a normal (to the surface) component  $B_z$  of the magnetic induction  $\vec{B}$  within Region II, arising from the sample magnetization  $\vec{M}$ , cannot exist without identical  $B_z$  in the surrounding Regions I and III because the nature of the electromagnetic field is such that the normal component of  $\vec{B}$  across an infinite planar boundary must be continuous. Thus the one-dimensional formulation for specular reflection breaks down for films in which in-plane variations of the magnetization exist on a length scale which would give rise to significant discontinuous normal components of  $\vec{B}$ , arising, for example, from flux line closure between adjacent in-plane magnetic domains of different orientation. If a magnetic field component normal to the surface does exist, it is necessary, then, to consider magnetic SLD surrounding the sample film to ensure that the normal component is continuous.

### 1.4.2 Magnetic Media Surrounding Film

In order to consider cases in which a normal component of  $\vec{B}$  exists within the sample, Equation 1.109 must be generalized to include nonzero magnetic SLD in the fronting and backing surround (Regions I and III of Figure 1.12, respectively).

Whether the magnetic induction in the fronting or backing surrounding the sample is due to a magnetic material or a magnetic field applied in vacuum or nonmagnetic material, we can associate  $B$  with a magnetic scattering length density  $\rho$  as defined by Equation 1.34. The spin-dependent SLDs associated with fronting (F) and backing (B) surrounding media are in general

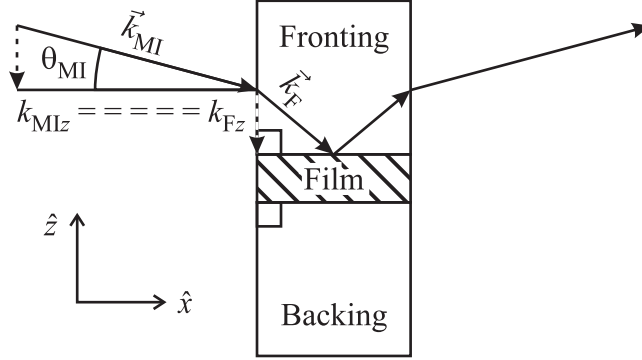


Figure 1.13: Schematic showing “side” entry of the incident beam into the “fronting” medium adjacent to the film of interest. The resulting relationship between wavevectors in the laboratory vacuum space and the fronting medium are derived in the text. Although not indicated in the drawing, it is assumed that the interaction of the incident neutron with the side face of the fronting medium and the surface of the film are not simultaneous, *i.e.*, any coherence between the two interfaces, which are typically separated by macroscopic distances, is taken to be negligible.

given by

$$\rho_F^\pm = \rho_{F,N} \pm \rho_{F,M}, \quad \rho_B^\pm = \rho_{B,N} \pm \rho_{B,M}. \quad (1.111)$$

Corresponding to the above values of the SLDs are spin-dependent wavevector components:

$$\begin{aligned} Q_F^\pm &= 2k_{Fz}^\pm = 2k_{0z}n_{Fz}^\pm = \sqrt{4k_{0z}^2 - 16\pi\rho_F^\pm} \\ Q_B^\pm &= 2k_{Bz}^\pm = 2k_{0z}n_{Bz}^\pm = \sqrt{4k_{0z}^2 - 16\pi\rho_B^\pm} \end{aligned} \quad (1.112)$$

As already mentioned above, it is required that any  $\vec{B}$  component along the normal to the surface of the film be continuous across each and every interface within the film as well as the boundaries with the surrounding fronting and backing regions.

It is important to realize that in practice, the fronting and backing media typically have the specific relationship to the sample film depicted in Figure 1.13 where the incident beam enters the fronting medium through a perpendicular “side” interface, *e.g.*, of a single-crystalline material such as

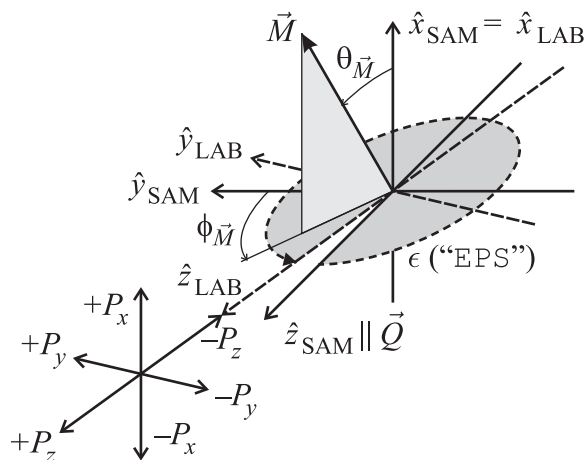


Figure 1.14: Vector diagram showing the relationship between laboratory and sample frames of reference as defined in the text and incorporated in the reflectivity program appearing in the appendix.

silicon or quartz. Across this orthogonal side boundary, the wavevector  $k_{\text{MI}z}^{\pm}$  measured on the instrument is equal to the wavevector  $k_{\text{F}z}^{\pm}$  in the fronting medium adjacent to the sample, since the  $z$  axis is parallel to the side surface of entry. The effective vacuum values  $k_{0z}$  that are required in the solution of Equation 1.15 can then be related to the measured values  $k_{\text{MI}z}^{\pm}$  by substituting  $k_{\text{MI}z}$  for  $k_{\text{F}z}$  in Equation 1.112:

$$k_{0z}^2 = (k_{\text{MI}z}^{\pm})^2 + 4\pi\rho_{\text{F}}^{\pm}. \quad (1.113)$$

### 1.4.3 Coordinate System Transformation

Up to now we have defined only a single coordinate system, one in which the quantization axis lies along  $z$ , normal to the film surface. The polarization states of incident, reflected, and transmitted neutrons are referred to this reference frame fixed to the film. It is useful to develop a self-consistent means of describing two separate axes of quantization; one in a “laboratory” coordinate system and the other in the “sample” reference frame. This is convenient for describing the vectorial distribution of the magnetization within the sample independently of the orientation of the polarization of the incident and reflected neutrons relative to a laboratory instrument.

Let us begin by considering the two different rectangular coordinate systems shown in Figure 1.14. The orientation of the magnetization vector  $\vec{M}$  at some depth  $z$  from the surface of the sample is determined by the angle  $\theta_{\vec{M}}$  from the sample  $x$  axis and by the angle  $\phi_{\vec{M}}$  between the projection of  $\vec{M}$  in the  $yz$  plane and the sample  $y$  axis. For specular reflection,  $\vec{Q}$  is normal to the  $xy$  plane of the sample. For  $\vec{M}$  lying in a plane parallel to the sample surface,  $\phi_{\vec{M}} = 0$  (or  $\phi_{\vec{M}} = \pi$ ). The laboratory coordinate system  $x$  axis coincides with that of the sample while the  $z$  axes, each of which represents the axis of quantization in the respective reference frame, are rotated from one another by an angle  $\epsilon$ .

Now the time-independent wave equation, referred to the sample coordinate system SAM, has the general form

$$\check{\mathcal{H}}_{\text{SAM}}\Psi_{\text{SAM}} = E\Psi_{\text{SAM}} \quad (1.114)$$

where the Hamiltonian operator  $\check{\mathcal{H}}_{\text{SAM}}$  represents kinetic plus potential energy and the scalar quantity  $E$  is the total energy of the system described by the wave function  $\Psi$ , as considered in previous sections. Equation 1.114 can be rewritten in the laboratory coordinate system LAB by applying the general rotation operator  $\check{U}_R$  of Equation 1.40:

$$\begin{aligned} \check{U}_R\check{\mathcal{H}}_{\text{SAM}}\check{U}_R^{-1}\check{U}_R\Psi_{\text{SAM}} &= E\check{U}_R\Psi_{\text{SAM}} = \\ \check{U}_R\check{\mathcal{H}}_{\text{SAM}}\check{U}_R^{-1}\Psi_{\text{LAB}} &= E\Psi_{\text{LAB}} \\ \check{\mathcal{H}}_{\text{LAB}}\Psi_{\text{LAB}} &= E\Psi_{\text{LAB}}. \end{aligned} \quad (1.115)$$

For the rotation pictured in Figure 1.14, the specific form of the rotation operator is given by

$$\begin{aligned} \check{U}_R &= e^{+i\check{\sigma}_x\epsilon/2} = \check{I}\cos(\epsilon/2) + i\begin{pmatrix} 0 & 1 \\ 1 & 0 \end{pmatrix}\sin(\epsilon/2) \\ &= \begin{pmatrix} \cos(\epsilon/2) & i\sin(\epsilon/2) \\ i\sin(\epsilon/2) & \cos(\epsilon/2) \end{pmatrix}. \end{aligned} \quad (1.116)$$

The inverse of the matrix of Equation 1.116 is

$$\check{U}_R^{-1} = \begin{pmatrix} \cos(\epsilon/2) & -i\sin(\epsilon/2) \\ -i\sin(\epsilon/2) & \cos(\epsilon/2) \end{pmatrix} \quad (1.117)$$

(the inverse of a rotation  $+\epsilon$  is a rotation  $-\epsilon$  [5]). We are now prepared to carry out a similarity transformation on a transfer matrix constructed in the

sample coordinate system. Doing so will enable us express the neutron wave functions in the laboratory coordinates. In other words, we would like to obtain a system of simultaneous equations which relate the spin-dependent reflection and transmission amplitudes to the incident neutron wave functions in the lab coordinates. In matrix notation, these equations are symbolically given by

$$\begin{pmatrix} t_{+\text{LAB}} \\ t_{-\text{LAB}} \\ \frac{iQ_{\text{B}}}{2}t_{+\text{LAB}} \\ \frac{iQ_{\text{B}}}{2}t_{-\text{LAB}} \end{pmatrix} = \check{A}_{\text{LAB}} \begin{pmatrix} I_{+\text{LAB}} + r_{+\text{LAB}} \\ I_{-\text{LAB}} + r_{-\text{LAB}} \\ \frac{iQ_{\text{F}}}{2}(I_{+\text{LAB}} - r_{+\text{LAB}}) \\ \frac{iQ_{\text{F}}}{2}(I_{-\text{LAB}} - r_{-\text{LAB}}) \end{pmatrix} \quad (1.118)$$

where

$$\check{A}_{\text{LAB}} = \check{U}_{\text{SAM} \rightarrow \text{LAB}} \check{A}_{\text{SAM}} \check{U}_{\text{SAM} \rightarrow \text{LAB}}^{-1}. \quad (1.119)$$

The rotation operator  $\check{U}_{\text{SAM} \rightarrow \text{LAB}}$  and its inverse can be constructed from Equations 1.116 and 1.117. Note that in order to simultaneously transform both the + and - wave function components and their first derivatives, as represented, *e.g.*, by the four element column vector on the LHS of Equation 1.118, a block diagonal matrix of the following form is required:

$$\check{U}_{\text{SAM} \rightarrow \text{LAB}} = \begin{pmatrix} \cos \frac{\epsilon}{2} & i \sin \frac{\epsilon}{2} & 0 & 0 \\ i \sin \frac{\epsilon}{2} & \cos \frac{\epsilon}{2} & 0 & 0 \\ 0 & 0 & \cos \frac{\epsilon}{2} & +i \sin \frac{\epsilon}{2} \\ 0 & 0 & +i \sin \frac{\epsilon}{2} & \cos \frac{\epsilon}{2} \end{pmatrix}. \quad (1.120)$$

The inverse of Equation 1.120 is

$$\check{U}_{\text{SAM} \rightarrow \text{LAB}}^{-1} = \begin{pmatrix} \cos \frac{\epsilon}{2} & -i \sin \frac{\epsilon}{2} & 0 & 0 \\ -i \sin \frac{\epsilon}{2} & \cos \frac{\epsilon}{2} & 0 & 0 \\ 0 & 0 & \cos \frac{\epsilon}{2} & -i \sin \frac{\epsilon}{2} \\ 0 & 0 & -i \sin \frac{\epsilon}{2} & \cos \frac{\epsilon}{2} \end{pmatrix}. \quad (1.121)$$

Thus we now have the equations necessary to compute the spin-dependent specular reflection and transmission amplitudes in the laboratory frame of reference for any layered magnetic structure. It should become evident, in the discussion and illustrative examples that follow, how immensely powerful PNR is as a probe of magnetic thin films and superlattices, in large part due to the accuracy of the theoretical description of the specular reflection process described above. A computer program, based on the formulas derived above,

is included in the appendix at the end of this chapter for calculating the spin-dependent reflectivities. (It should be noted that this program uses different, but equivalent, expressions for the  $\mu_j$ 's given in Equation 1.103 that are written exclusively in terms of the angles  $\theta_{\vec{M}}$  and  $\phi_{\vec{M}}$ , defined in Figure 1.14, as

$$\begin{aligned}\mu_1 &= \mu_2 = \frac{1 + \cos \theta_{\vec{M}} + i \sin \theta_{\vec{M}} \cos \phi_{\vec{M}} - \sin \theta_{\vec{M}} \sin \phi_{\vec{M}}}{1 + \cos \theta_{\vec{M}} - i \sin \theta_{\vec{M}} \cos \phi_{\vec{M}} + \sin \theta_{\vec{M}} \sin \phi_{\vec{M}}} \\ \mu_3 &= \mu_4 = \frac{-1 + \cos \theta_{\vec{M}} + i \sin \theta_{\vec{M}} \cos \phi_{\vec{M}} - \sin \theta_{\vec{M}} \sin \phi_{\vec{M}}}{-1 + \cos \theta_{\vec{M}} - i \sin \theta_{\vec{M}} \cos \phi_{\vec{M}} + \sin \theta_{\vec{M}} \sin \phi_{\vec{M}}}.\end{aligned}\quad (1.122)$$

These expressions appear explicitly in the lines of code.) It should also be mentioned that Equation 1.118 is applicable not only in the nanometer length scale range, where matter can be treated as a continuum of scattering length density, but also on the atomic scale corresponding to the higher wavevector transfers associated with atomic planes, as in the case of single-crystalline superlattice films grown by molecular beam epitaxy [37, 38]. Equation 1.118 is valid even at macroscopic length scales and can accurately predict the behavior of such neutron optical devices as resonance spin flippers for spatially oscillating magnetic fields. The universal application of the dynamical theory of spin-dependent neutron reflectivity to length scales differing by many orders of magnitude is remarkable.

#### 1.4.4 Selection Rules “of Thumb”

Despite its proven accuracy and range of applicability, even for simpler layered magnetic film structures, Equation 1.118 does not necessarily translate to particularly transparent analytic expressions of the reflection amplitudes. Nonetheless, at sufficiently large  $Q$  the Born approximation of the integral expressions for  $r^\pm$ , derived in detail in Section 1.4.1, are valid so that important symmetries and sensitivities to particular magnetic structures are recognizable in the form of more familiar structure factors. Moon *et al.* [39] described the spin-dependent reflection of neutrons from atomic crystals in the kinematic limit (Born approximation), assuming the incident neutrons to be in either a pure + or – spin basis state, *i.e.*,  $P_z = \pm 1$ , and that only the resultant + or – reflected intensities could be measured. In this section, we examine in explicit terms some of the more useful results of the formal presentation in Section 1.4.1.

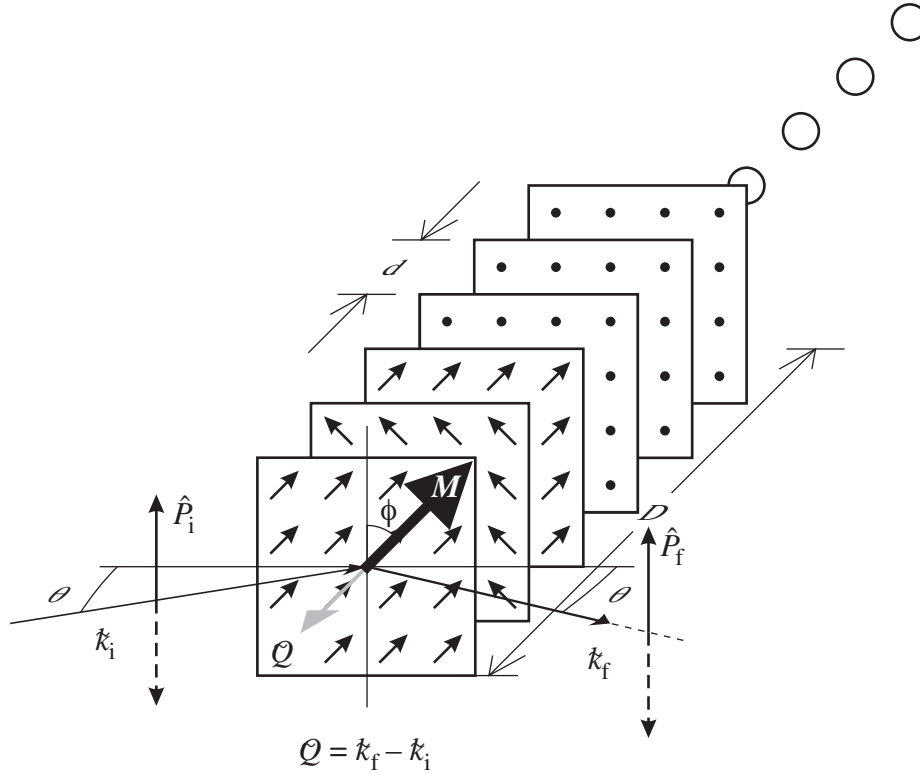


Figure 1.15: Schematic representation of the specular reflection of polarized neutrons from a layered film structure comprised of a finite series of atomic planes, as can be grown by molecular beam epitaxial techniques. The segment shown constitutes a “super” cell containing a number of ferromagnetic planes with alternating directions of the magnetization followed by several nonmagnetic planes (each dot or arrow indicates an atomic position). The entire cell can be repeated periodically to form a superlattice of total thickness  $L$ . Projections of each plane’s magnetization on the vertical axis parallel to the incident neutron polarization give rise to non-spin-flip scattering whereas horizontal components cause spin-flip scattering.

Consider the configuration shown in Figure 1.15 where the applied magnetic guide field defining the quantization axis is parallel to the neutron polarization  $\hat{P}$  and perpendicular to the wavevector transfer  $\vec{Q}$ . The magnetization vector  $\vec{M}$ , at any depth along the surface normal, lies in the plane of the film. (Because of the requirement that the normal component of  $\vec{B}$  be continuous across an infinite boundary between sample film and surrounding medium, as discussed earlier, any out-of-plane component of the magnetization cannot contribute to the scattering in the ideal case. This is the Halperin effect which was rigorously derived in Section 1.4.1 for the general dynamical problem.) In this geometry the Born approximation to the structure factor for non-spin-flip (NSF) reflection is proportional to

$$r_{\text{BA}}^{\pm\pm}(Q) \propto \int_0^L (\rho_{\text{N}}(z) \pm \rho_{\text{M}}(z) \cos(\phi(z))) e^{iQz} dz \quad (1.123)$$

where  $\phi$  is the angle defined in Figure 1.15 between the magnetization  $\vec{M}$  and the neutron polarization  $\hat{P}$  (parallel to the vertical in-plane axis of the sample) and  $L$  is the film thickness. Note the interference which can occur between nuclear and magnetic SLDs, as encountered earlier in the discussion of birefringence and the production of a polarized beam in Section 1.3.4. The spin-flip (SF) scattering, on the other hand, is given by

$$r_{\text{BA}}^{\pm\mp}(Q) \propto \int_0^L \rho_{\text{M}}(z) \sin(\phi(z)) e^{iQz} dz \quad (1.124)$$

and is purely magnetic in origin. Thus, Equations 1.123 and 1.124 imply that by measuring both NSF and SF reflectivities *vs.*  $Q$ , we can extract not only the magnitude of the magnetization as a function of depth, but its orientational depth profile as well.

Another special geometry, particularly useful in the examination of certain noncollinear magnetic structures, *e.g.*, a simple helix of a single chirality where the in-plane magnetization advances at a constant angular rate with depth, is that for which the neutron polarization vector  $\hat{P}$  lies completely along a direction parallel to  $\vec{Q}$ . (This is in contrast to the configuration for the helix considered in Section 1.4.1 in which the neutron polarization was taken to be perpendicular to  $\vec{Q}$ .) In this case the NSF reflectivity will be

entirely nuclear in origin whereas the SF scattering will be solely magnetic:

$$r_{\text{BA}}^{\pm\pm}(Q) \propto \int_0^L \rho_{\text{N}}(z) e^{iQz} dz, \text{ and} \quad (1.125)$$

$$r_{\text{BA}}^{\pm\mp}(Q) \propto \int_0^L \rho_{\text{M}}(z) [\sin(\phi(z)) \mp i \cos(\phi(z))] e^{iQz} dz. \quad (1.126)$$

Note that in this case ( $\vec{P} \parallel \vec{Q}$ ) the magnetic SF scattering is sensitive to the sense of rotation of the magnetization orientation angle  $\phi$  so that a helix with a left-handed helicity can be distinguished from one that is right-handed, for example. As we saw in Section 1.4.1, however, for  $\vec{P} \perp \vec{Q}$  differences in handedness are not observed in the reflectivities. Further discussion of kinematic magnetic structure factors can be found in other works [see, *e.g.*, [3, 9, 13]].

Recall our discussion in Section 1.2.6 regarding in-plane inhomogeneities in the nuclear SLD that give rise to nonspecular reflection. An analogous situation occurs with in-plane inhomogeneities in the magnetization, notably associated with ferromagnetic domains. Within an individual saturated ferromagnetic domain, all of the atomic magnetic moments are aligned parallel to a common direction. If the sample consists of single magnetic domains in-plane at every depth along the surface normal, then the reflectivity will be purely specular. If not, then both specular and nonspecular scattering can occur, depending on the in-plane areas of the domains relative to the effective lateral coherence length of the incident neutron wave packet. If the neutron coherence length in-plane is sufficiently larger than the average domain size, then the specular component of the reflectivity will be representative of the net magnetization which results from averaging over this collection of domains. In the opposite case, where the domain areas are far larger than the neutron in-plane coherence length, the specular contribution to the measured reflectivity will represent an incoherent sum of the reflectivities from individual domains, weighted by the relative area of each.

### 1.4.5 Three-Dimensional Polarization Analysis

It is possible to prepare an incident neutron in a mixed state, *i.e.*, one with both  $C_+ \neq 0$  and  $C_- \neq 0$  (as discussed in Section 1.3), have it interact with a magnetic sample placed within a region of zero applied field, and

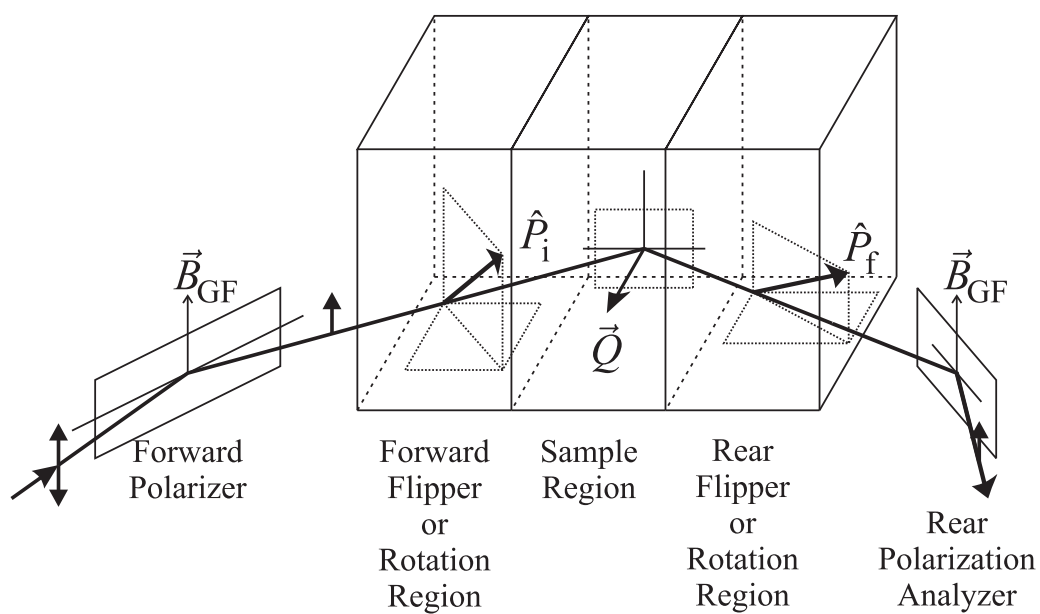


Figure 1.16: Schematic picture of experimental setup for selecting incident beam polarization and analysing the polarization of the scattered beam, as described in the text.

subsequently analyse its polarization state after reflection, albeit by statistical analysis of an ensemble of identically prepared incident neutrons. A schematic of the instrumental configuration for carrying out this general type of experiment is shown in Figure 1.16. This method is analogous to what is conventionally referred to as “zero-field polarimetry,” typically performed at higher wavevector transfers in the atomic lattice diffraction regime [40, 41]. The rotations of the neutron polarization which are performed in the regions preceding and following the sample volume can be realized with the rectangular magnetic solenoids described in Section 1.3 (either a single coil or two in succession with orthogonal rotation axes). This general type of polarimetry can be extended to measurements of the polarization states of transmitted neutrons as well, sometimes referred to as a neutron depolarization measurement [25, 35, 42]. In the dynamical regime, nonclassical polarization-dependent tunneling effects can occur for certain SLD profiles with magnetic barriers [43, 44].

#### 1.4.6 Elementary Spin-Dependent Reflectivity Examples

Table 1.4 lists values of neutron nuclear and magnetic scattering length densities for some common elements (corresponding x-ray densities are included for comparison). Figure 1.17 shows the SLD profiles of several prototypical magnetic multilayer structures and their corresponding spin-dependent neutron reflectivity curves assuming the measurement configuration of Figure 1.15: a) a bilayer, one layer of which is ferromagnetic and where the in-plane magnetization of each and every magnetic layer is aligned parallel to the neutron polarization; b) the same repeating unit bilayer of Figure 1.17a but with adjacent magnetic layers aligned antiparallel to one another and perpendicular to  $\hat{P}$ ; c) the bilayer of Figure 1.17a again, but with a canted, alternating sequence of magnetizations. Note that in the structure of Figure 1.17b the unit cell for the magnetic structure is double the length of the chemical bilayer thickness. In the more complicated arrangement of Figure 1.17c, the vertical magnetization components are equal and have a periodicity equal to that of the chemical modulation whereas the horizontal magnetizations have a commensurate but doubled period. In the reciprocal scattering space, the doubled spatial periodicity corresponds to peaks in the reflectivity which occur at approximately half the interval associated with the fundamental bi-

Element	$b$	$p$ ( $10^{-12}$ cm)	$f$		$N$ ( $10^{22}$ atom· cm $^{-3}$ )	$Nb$	$Np$ ( $10^{10}$ cm $^{-2}$ )		$Nf$	
			Re	Im			Re	Im		
			3.95							
			+ 0.07							
Si	0.42	0.00	= 4.02	0.09	5.00	2.10	0.00	20.1		
			7.33							
			- 0.33							
Fe	0.95	0.60	= 7.00	0.90	8.48	8.05	5.09	59.4		
			7.61							
			- 0.69							
Co	0.25	0.46	= 6.92	1.02	9.09	2.27	4.18	62.9		
			7.89							
			- 0.83							
Ni	1.03	0.16	= 7.06	0.14	9.13	9.40	1.46	64.5	1.3	
			8.17							
			- 0.57							
Cu	0.77	0.00	= 7.60	0.17	8.49	6.45	0.00	64.5	1.4	
			9.02							
			- 0.33							
Ge	0.82	0.00	= 8.69	0.25	4.41	3.62	0.00	38.3	1.1	

Table 1.4: Selected neutron and x-ray scattering lengths (from Refs. [9] and [54]) and densities for  $Q = 0$  and for a wavelength of 1.54 Å. The imaginary parts of the nuclear scattering lengths for neutrons are omitted because of their relatively small values.

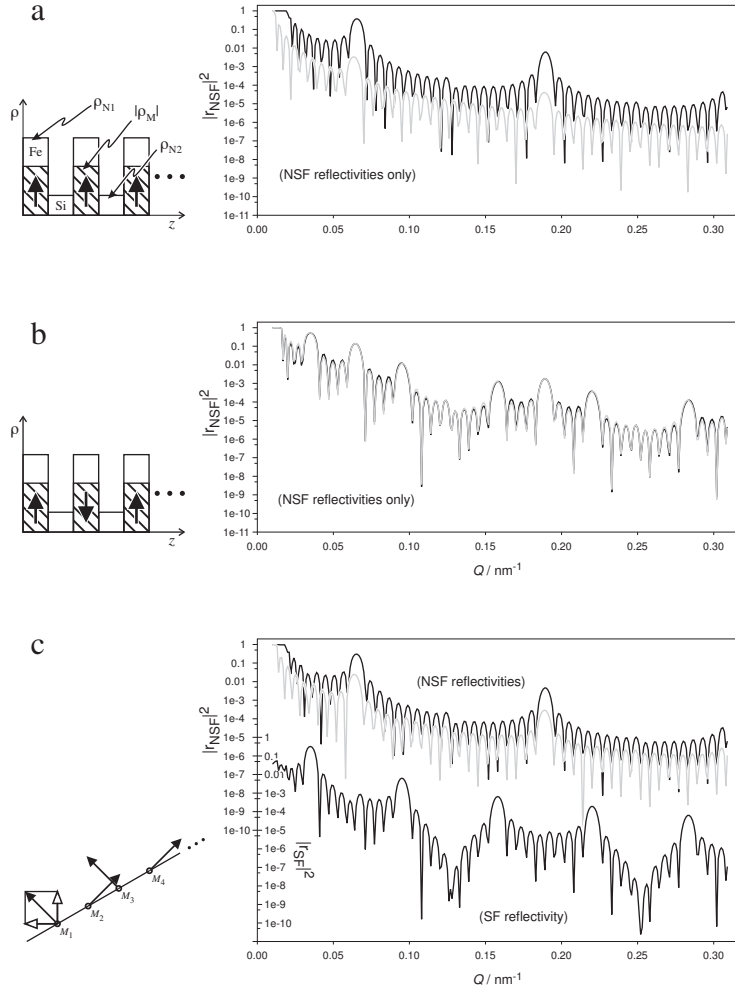


Figure 1.17: Polarized neutron reflectivity curves (NSF and SF) for several idealized SLD profiles of magnetic thin film structures that are described further in the text. The profile in panel c) has the same chemical modulation as those in panels a) and b) but its SLD profile shows only the magnetization directions in successive layers. In all three cases, there are ten chemical bilayer repeats and the fronting and backing media are taken to be vacuum for simplicity. Because each bilayer is made up of two different layers of equal thickness, the even order multiples of the fundamental multilayer Bragg reflection maximum (at  $Q \simeq 2\pi/D$ ) are suppressed.

layer period (the slight deviation is due to the dynamical effect of refraction). In these examples the bilayer thicknesses are constant and the widths of the principle reflections associated with this period are inversely proportional to the number of bilayer repeats: certain deviations from perfect periodicity can result in a broadening of the widths, although sufficiently small random fluctuations in bilayer thickness about a perfect periodic spacing primarily cause a decrease in peak height (static Debye-Waller effect). Further examples of PNR studies of magnetic thin film systems can be found in other references [4, 13, 31, 37]. Alternatively, the computer program provided in the appendix can be used to generate the spin-dependent reflectivities for any possible SLD profile and experimental configuration of interest.

Finally, it should be noted that polarized x-ray reflection (PXR) can also be a powerful probe of magnetic thin films and multilayers. PXR is similar in a number of significant ways to PNR, but in others, complementary (*e.g.*, the reflection of polarized x-rays can differentiate electron spin and orbital contributions to the magnetic scattering). Although the magnetic scattering is normally orders of magnitude weaker than that due to the electron charge, under certain resonance conditions the magnetic interaction can be comparable and element specific. Discussions of the magnetic scattering of x-rays can be found in both journals and texts [45, 46, 47, 48, 49].

## 1.5 Experimental methods

It is well beyond the scope of this chapter to discuss all of the experimental techniques pertaining to PNR, especially since a significant fraction of the methods apply to reflectometry in general. Furthermore, those aspects particular to the use of polarized neutron beams are common to other instruments, such as triple-axis and spin-echo inelastic scattering spectrometers (see, for example, the text by Williams [20]). Nonetheless, some discussion is in order.

In a significant fraction of PNR applications, a beam can be treated as a superposition of independent, noninteracting neutrons, each of which is described by a wavepacket. The wavepacket of each neutron, in turn, describes the uncertainty in that neutron's momentum and corresponding longitudinal and lateral coherence lengths (through the quantum mechanical uncertainty principle). The shape and size of the wavepacket is determined by how the neutron is prepared, *i.e.*, from where it originated and with what optical

elements, such as apertures and monochromating crystals, it interacted on its flight to the sample film. If the source and all of the interactions with a given set of optical elements are the same for every neutron, then the beam will consist of an ensemble of identical neutron “systems.” In a rigorous treatment, the two-component plane wavefunction used in the equations of motion derived above must then be replaced with a wavepacket, *e.g.*, made up of a Gaussian or other distribution of plane wave components. However, the neutron wavepackets in the beam may not all be identical because of interactions with discontinuous, extended elements, such as sources, moderators or a monochromating crystal with a “mosaic” distribution of microcrystallite blocks, which result in a distribution of different wavepacket sizes, shapes and nominal wavevector values. In this more complicated circumstance, in addition to accounting for the effects of each individual wave packet, the different neutron reflectivities (*i.e.*,  $|r|^2$  values) arising from the incoherent distribution of nonidentical wave packets must be averaged over. Nonetheless, in practice, the approximation typically made is to assume an expression for the reflectivity derived for the simple two-component plane wavefunction, as we have done above, and then average the calculated reflectivity over a distribution of wavevectors determined by an instrumental resolution function for an incoherent beam. Ordinarily, for a continuous source, the instrumental resolution function is primarily defined by a mosaic crystal monochromator in conjunction with a pair of horizontal and vertical apertures, the latter which limit the angular divergences of the beam. The widths of the distribution of neutron wavevector components are then straightforwardly calculated. In the case of pulsed sources using time-of-flight techniques, the instrumental resolution function depends on the angular divergences, pulse shape and frequency, as well as the distances from sample to detector. Discussions of coherence length and instrumental resolution can be found, for example, in References [50, 51, 52].

Similarly, consideration must be given, in practice, to the polarization of a beam of neutrons as opposed to the polarization of a single neutron. Suppose that the beam is a statistical ensemble or collection of  $N$  neutrons which have been prepared in exactly the same way (*i.e.*, such that each neutron is described by a pair of plane waves with an identical pair of corresponding wavevectors  $k_{\pm}$  and has the same probability of being found in either the spin  $+$  or spin  $-$  basis state). Each individual neutron, then, is represented by its own spinor wave function and density matrix operator  $\rho_j$  as defined by Equation 1.45. Now we can construct an ensemble wave function, which

has coefficients  $C_{E+}$  and  $C_{E-}$ , analogous to the single neutron quantities in Equations 1.32 and 1.42, representing the entire homogeneous collection of identical neutrons in the beam. Thus, for example, a beam or ensemble having a polarization of  $P_{Ex} = 1$  (with  $C_{E+} = 1/\sqrt{2}$  and  $C_{E-} = 1/\sqrt{2}$ ) represents a collection of neutrons in which each individual neutron has the same corresponding values of  $C_+$  and  $C_-$  as the ensemble, where the probability of finding any one of the neutrons of the ensemble in the  $+$  spin state is  $1/2$  and in the  $-$  spin state  $1/2$  as well. Note that this particular example does *not* imply a beam of neutrons in which one half are definitely in the  $+$  spin state and the other half in the  $-$  state. The latter case would correspond to an incoherent superposition of two distinct ensembles or component beams, each with one half the total number of particles, where one component beam is in a pure spin  $+$  state ( $C_{E+} = 1$  with every one of its member neutrons having  $C_+ = 1$ ) and the other in a pure spin  $-$  state ( $C_{E-} = 1$ ).

In general then, we need an ensemble of neutrons made up of identical replicas of one another to determine, statistically, the values  $C_+$  and  $C_-$  for an individual member, as was also discussed earlier in Section 1.3.5; we cannot determine the three-dimensional polarization vector of a single, isolated neutron (see again, for example, Reference [5]). If, on the other hand, a neutron beam does not consist of a collection of identical members with the same corresponding values of  $C_+$  and  $C_-$ , then the probabilistic determination of a physical quantity, such as the polarization, yields a value which represents the average over the entire inhomogeneous ensemble. In either case, the ensemble or beam polarization vector  $\vec{P}_E$  is given by

$$\vec{P}_E = \overline{\hat{P}} = \frac{1}{N} \sum_{j=1}^N \hat{P}_j = \frac{1}{N} \sum_{j=1}^N \langle \vec{\sigma} \rangle_j \quad (1.127)$$

where  $N$  is the number of particles in the collection. Note that  $\vec{P}_E$  is in general not a unit vector as  $\hat{P}$  is for a single particle.

Figure 1.18 shows a typical polarized neutron reflectometer configuration. For the relatively narrow angular beam divergences in the scattering plane, defined by  $\vec{k}_i$  and  $\vec{k}_f$ , that are common in PNR, multilayer polarizers are well matched. Alternating layers of a saturated ferromagnetic layer and a non-magnetic spacer, such as Fe and Si, respectively, can yield relatively high polarizations ( $\sim 95\%$  or better) and reflectivities ( $\sim 95\%$ ) of one spin state over the required angular range of beam divergence if a graded sequence of bilayer thicknesses is deposited to form a so-called “supermirror” (see, for

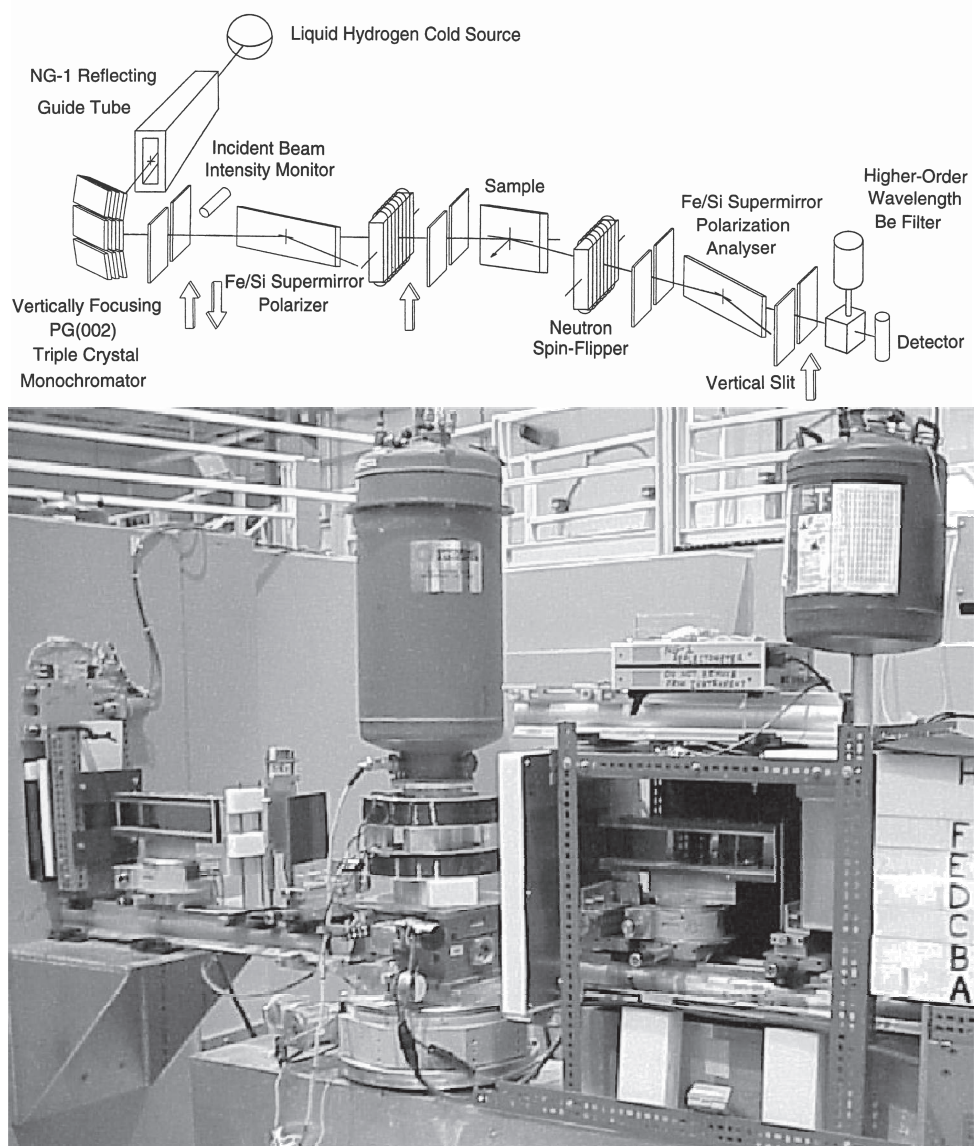


Figure 1.18: Schematic and photograph of the polarized neutron reflectometer on the NG-1 guide tube at the NIST Center for Neutron Research.

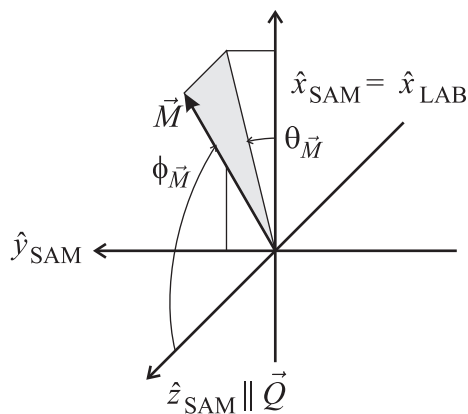


Figure 1.19: An alternate parameterization for the three-dimensional neutron polarization vector  $\hat{P}$  optimized for zero magnetization out of the sample plane.

example, Reference [53, 21]. Spin turning devices or “flippers” constructed of flat solenoidal coils are also efficient ( $\sim 99\%$ ). Nonetheless, accurate quantitative methods which correct for imperfect polarizers and spin turn devices must often be applied in practice (see, for example, References [20] and [37]).

## 1.6 An Illustrative Application of PNR

An excellent example of the application of the theoretical formalism and experimental methodology of PNR which we have presented here is illustrated in the reflection from magnetic twists where the interpretation of the raw data is not necessarily obvious. But before we delve into the details of that system, it would be good to summarize our results thus far, and recast them into a slightly different form which will be more suitable to noncollinear magnetic structures.

### 1.6.1 Symmetries of Reflectance Matrices

Recall that the description of a homogeneous slab can be characterized by the four-dimensional linear equation given by Equation 1.109, the solution of which yields reflection amplitudes for NSF and SF processes. A magnetic

helix consists of a layered system where each layer is uniformly magnetized in the  $xy$  plane. As layers are stacked along  $z$ , the moment in successive layers is rotated about  $z$  relative to the magnetization in the layer below. For such a system it will be convenient for us to rotate our spherical coordinate system so that the polar axis is along the quantization axis  $z$ , as shown in Figure 1.19. In this figure we have adopted a convention different from Figure 1.14 for naming the polar and azimuthal angles. Now the polar angle is labeled  $\phi_{\vec{M}}$  and the azimuthal angle is labeled  $\theta_{\vec{M}}$ . In this way a smoothly varying direction of in-plane magnetization  $\vec{M}$  can be described as a function of only  $\theta_{\vec{M}}$ . From now on we will drop the  $\vec{M}$  subscript when it is convenient to do so. In this coordinate system we can write the single-layer transfer matrix  $\check{A}_z$  as

$$2\check{A}_z = \begin{matrix} & & & & (1.128) \\ \left[ \begin{array}{cccc} \tilde{c}_1 + \tilde{c}_3 & e^{-i\theta}(\tilde{c}_1 - \tilde{c}_3) & \frac{\tilde{s}_1}{s_1} + \frac{\tilde{s}_3}{s_3} & e^{-i\theta} \left( \frac{\tilde{s}_1}{s_1} - \frac{\tilde{s}_3}{s_3} \right) \\ e^{i\theta}(\tilde{c}_1 - \tilde{c}_3) & \tilde{c}_1 + \tilde{c}_3 & e^{i\theta} \left( \frac{\tilde{s}_1}{s_1} - \frac{\tilde{s}_3}{s_3} \right) & \frac{\tilde{s}_1}{s_1} + \frac{\tilde{s}_3}{s_3} \\ \tilde{s}_1 s_1 + \tilde{s}_3 s_3 & e^{-i\theta}(\tilde{s}_1 s_1 - \tilde{s}_3 s_3) & \tilde{c}_1 + \tilde{c}_3 & e^{-i\theta}(\tilde{c}_1 - \tilde{c}_3) \\ e^{i\theta}(\tilde{s}_1 s_1 - \tilde{s}_3 s_3) & \tilde{s}_1 s_1 + \tilde{s}_3 s_3 & e^{i\theta}(\tilde{c}_1 - \tilde{c}_3) & \tilde{c}_1 + \tilde{c}_3 \end{array} \right] \end{matrix}$$

with  $\tilde{c}_j = \cosh(s_j \delta_z)$ ,  $\tilde{s}_j = \sinh(s_j \delta_z)$ ,  $s_1 = \sqrt{4\pi(Nb + Np) - Q^2/4}$ ,  $s_3 = \sqrt{4\pi(Nb - Np) - Q^2/4}$ , and  $\theta$  is the angle with respect to  $x$  of the projection of  $\vec{B}$  into the  $xy$  plane. The scattering vector  $\vec{Q}$  lies along  $z$ . In this and subsequent expressions in Section 1.6.1 we always choose the principle root for the solution of the radical. This root is the one whose complex phase  $\eta$  is one-half that of the argument of the radical. Negative real arguments have  $\eta = \pi$ . The transfer matrix  $\check{A}_z$  is a  $4 \times 4$  matrix of complex numbers. The product transfer matrix  $\check{A}$ , which describes a layered system  $L_1, L_2, \dots, L_n$ , is given by Equation 1.110 when the neutron encounters layer  $L_1$  first. However, we recognize that, fundamentally, our system is described by 2-dimensional spinors. Eliminating  $t$  from Equation 1.109 leads to an equation of the form

$$\check{u}\check{\epsilon} \begin{pmatrix} r_+ \\ r_- \end{pmatrix} = \check{v}\check{\epsilon} \begin{pmatrix} I_+ \\ I_- \end{pmatrix} = \check{v}\check{\epsilon}\psi. \quad (1.129)$$

Here we allow ourselves the explicit possibility of having the quantization axis in which we measure  $I_+$ ,  $I_-$ ,  $r_+$ , and  $r_-$  be different from that which we used

to define  $\check{A}$ . The operator  $\check{\epsilon}$  transforms the coordinates from the laboratory frame to the sample frame in which  $\check{A}$ ,  $\check{u}$ , and  $\check{v}$  have been defined, as was discussed in Section 1.4.3. Common choices for  $\check{\epsilon}$  are the identity matrix, and one which describes a polarization axis  $\hat{\epsilon} = \hat{Q} \times \hat{k} / |\hat{Q} \times \hat{k}|$  where  $\vec{k}$  is the incident wave-vector. This  $\check{\epsilon}$  has the form  $\check{\epsilon} = \sqrt{2} \begin{bmatrix} 1 & -i \\ -i & 1 \end{bmatrix}$ . The inversion of Equation 1.129 leads to the actual  $2 \times 2$  linear operator  $\check{R}$  which we desire:

$$\check{R} \equiv \check{\epsilon}^{-1} \check{u}^{-1} \check{v} \check{\epsilon}. \quad (1.130)$$

The matrices  $u$  and  $v$  have elements

$$\begin{pmatrix} v \\ u \end{pmatrix}_{ij} = \pm (\zeta_i A_{i j} - A_{i+2 j}) + \xi (\zeta_i A_{i j+2} - A_{i+2 j+2}) \quad (1.131)$$

where the upper sign is chosen for  $v$  and the lower sign is chosen for  $u$ . The lingering effect of  $t$  is that we must correct for the relative index of refraction of the fronting media to the backing media. Part of the correction has already been assumed in the construction of  $\check{A}_z$ ; the final correction is supplied by  $\zeta_i^2 = \xi^2 + 4\pi(\rho_{i,\text{backing}} - \rho_{i,\text{fronting}})$  where  $\xi = iQ/2$ . We allow for polarization dependent refraction effects in the surround, choosing the value for spin-up when  $i = 1$  and the value for spin-down when  $i = 2$ . When constructing Equation 1.128, we implicitly added  $\rho_i$  to  $Q^2$  in  $s_j$ .

One surprising result is that reflection from helices with the beam incident from one side of the film may be different from reflection with the beam incident on the other side. For the vast majority of other systems encountered, such is not the case. Certainly, there are generic reasons to expect differences in “front” and “back” reflectivity that are not specific to noncollinear magnetic films. For example, the scattering vector  $\vec{Q}$  must be corrected for refraction effects from the incident medium, and if the sample is backed by a thick silicon substrate on one side and air (or vacuum) on the other, the reflectivities will be subtly different. The main difference would be the observation of different critical edges for the front side and the back side. Or, if one side of the sample contains a stronger neutron absorber than the other, then a difference between front and back reflectivities will also occur. On the other hand, noncollinear magnetic films in which the fronting and backing media are identical and which contain no strong neutron absorbers can produce reflectivities from the front and back that are grossly different. That is, even if the only inhomogeneity is due to variations in direction of the magnetization, there still can be strong differences in the reflectivity measured from

the front side and that measured from the back side. Noncollinear magnetic structures are special in that they may give rise to asymmetric reflectivities that are unrelated to the aforementioned common effects.

### 1.6.2 Basis-Independent Representation

Let us formalize more precisely the concepts we have been discussing. We can divide the universe of reflectivity samples into three classes: samples with no magnetism ( $p = 0$ ), samples with collinear magnetism ( $p \neq 0, \theta = 0$ , for some suitable choice of orientation of the  $x$  axis), and samples with noncollinear magnetism (all the rest). In this section we will concentrate on magnetic helices. In these samples  $\theta$  is a linear function of the depth  $z$  into the sample. Magnetic structures like this are expected for layered exchange-spring magnets in certain ranges of applied magnetic fields. Exchange-spring magnets are two-component systems consisting of a hard ferromagnetic material ( $\text{Fe}_{0.45}\text{Pt}_{0.55}$ , for example) and a softer ferromagnetic material ( $\text{Fe}_{0.20}\text{Ni}_{0.80}$  is a typical choice). Hard and soft here refer to the materials' magnetic anisotropy, which indicates the difficulty in changing the direction of magnetization in a magnetically saturated specimen. Soft ferromagnets reorient much more easily than hard ferromagnets. These two-component systems were proposed by Kneller and Hawig [55] to solve a long-standing problem of permanent-magnet materials science. It is a quirk of nature that soft ferromagnets typically have much larger saturation magnetizations than hard ferromagnets. As a result, quite strong ferromagnets can be made from soft material, but they are readily demagnetized. Hard ferromagnets are much weaker, so you need a greater volume to get the same magnetic dipole moment. Since miniature permanent magnets are integral components of devices such as computer hard disks, cellular telephones, and miniature stereo headphones, solving the problem of producing tiny, hard to demagnetize permanent magnets is important. In a bilayer of soft ferromagnet on top of hard ferromagnet, strong exchange across the interface couples the magnetization. At saturation, both layers are fully aligned. As a reverse field is applied, the soft layer demagnetizes first while the bottom of the hard layer stays aligned in the original direction. As a result, a smooth twist develops across the thickness of the bilayer. These samples exhibit strong spin-flip scattering, non-spin-flip splitting, and the reflectivity from the back side is different from the front side, especially near the critical angle, as shown in Figure 1.22. To understand the origins of this effect in general is quite difficult. But by

abstracting the essential features we can make progress. First, we shall again make some slight adjustments which will reduce our  $4 \times 4$  matrix of scalars into a  $2 \times 2$  matrix of spinor operators.

The construction of Equation 1.128 as a  $2 \times 2$  block matrix comprised of  $2 \times 2$  blocks suggests a form for  $\check{A}_z$  developed by Rühm, Toperverg and Dosch [56], called a “supermatrix.” In this formalism the  $2 \times 2$  blocks are replaced with one 2-dimensional spinor operator. Reversing the order of operands under the square root in the definition of  $s_j$  introduces a factor of  $\sqrt{-1}$  which can be absorbed into the hyperbolic trigonometric functions, changing them into ordinary trigonometric functions. With this modification, the transfer matrix for layer  $m$  (Equation 1.128) becomes

$$\check{A}_m = \frac{1}{2} \left[ \begin{array}{c|c} \check{\mathcal{A}} & \check{\mathcal{B}} \\ \hline \check{\mathcal{C}} & \check{\mathcal{A}} \end{array} \right] \quad (1.132)$$

where

$$\begin{aligned} \check{\mathcal{A}} &= \frac{1}{2} \left[ \begin{array}{cc} \tilde{c}_1 + \tilde{c}_3 & e^{-i\theta} (\tilde{c}_1 - \tilde{c}_3) \\ e^{i\theta} (\tilde{c}_1 - \tilde{c}_3) & \tilde{c}_1 + \tilde{c}_3 \end{array} \right], \\ \check{\mathcal{B}} &= \frac{1}{2} \left[ \begin{array}{cc} s_1^{-1} \tilde{s}_1 + s_3^{-1} \tilde{s}_3 & e^{-i\theta} (s_1^{-1} \tilde{s}_1 - s_3^{-1} \tilde{s}_3) \\ e^{i\theta} (s_1^{-1} \tilde{s}_1 - s_3^{-1} \tilde{s}_3) & s_1^{-1} \tilde{s}_1 + s_3^{-1} \tilde{s}_3 \end{array} \right], \text{ and} \\ \check{\mathcal{C}} &= \frac{1}{2} \left[ \begin{array}{cc} -(s_1 \tilde{s}_1 + s_3 \tilde{s}_3) & -e^{-i\theta} (s_1 \tilde{s}_1 - s_3 \tilde{s}_3) \\ -e^{i\theta} (s_1 \tilde{s}_1 - s_3 \tilde{s}_3) & -(s_1 \tilde{s}_1 + s_3 \tilde{s}_3) \end{array} \right]. \end{aligned} \quad (1.133)$$

Equation 1.132 can be rewritten as

$$\begin{aligned} \check{A}_m &= \left[ \begin{array}{cc} \cos(\check{p}_m \delta_z) & \check{p}_m^{-1} \sin(\check{p}_m \delta_z) \\ -\check{p}_m \sin(\check{p}_m \delta_z) & \cos(\check{p}_m \delta_z) \end{array} \right] \\ &\equiv \check{S}_m \end{aligned} \quad (1.134)$$

where  $\check{p}_m$  is an *operator* which expresses the polarization axis of the neutron in this layer of uniformly magnetized matter oriented at an angle  $\theta$  with respect to the  $x$ -axis. Equation 1.109 is now a  $2 \times 2$  matrix equation of these operators. In writing Equation 1.132 we have halved the number of dimensions, hiding them implicitly in the operator. The operator  $\check{p}_m$  is related to

the original Hamiltonian via the following relations:

$$\begin{aligned}
\check{p}_m^2 &= \Xi \begin{bmatrix} \cos \gamma & i e^{-i\theta} \sin \gamma \\ i e^{-i\theta} \sin \gamma & \cos \gamma \end{bmatrix}, \\
\cos \gamma &= \Upsilon/\Xi, \quad \sin \gamma = \Omega/\Xi, \\
\Xi^2 &= \Upsilon^2 + \Omega^2, \\
\Upsilon &= p_0^2 - 2mV_m/\hbar^2, \text{ and} \\
\Omega &= -2im\mu B/\hbar^2.
\end{aligned} \tag{1.135}$$

In the absence of magnetization ( $\Omega = 0$ ),  $\check{p}_m^2$  becomes a multiple of the identity operator, and the reflectivity reduces to the well-known scalar result [6].

### 1.6.3 Front–Back Reflectivity of Idealized Twists

As our final step in motivating the essential difference between front and back reflectometry for non-collinear systems, we cut the system down to the bare essentials:

1. a free-standing film (so as to remove refraction effects on the neutron wavefunction),
2. composed of only two layers,
3. where both layers have the same thickness,
4. both layers have the same magnitude of magnetization, and
5. the top layer is oriented at angle  $+\theta$  to the  $x$ -axis, the bottom at angle  $-\theta$  to  $x$ .

The sample is depicted in Figure 1.20a). Our choice of  $\theta$  means that the average magnetization  $\overline{\vec{M}}$  lies along  $x$ . Rühm, Toperverg, and Dosch [56] make use of the fact that the  $2 \times 2$  reflectance operator  $\check{R}$ , given by Equation 1.130, can be decomposed into a sum of scalar multiples of the identity operator  $\check{\sigma}_0$  and the three Pauli spin operators  $\check{\sigma}_x$ ,  $\check{\sigma}_y$ , and  $\check{\sigma}_z$ :  $\check{R} = \frac{1}{2}(R_0 + \vec{R} \cdot \vec{\sigma})$ , where  $\vec{R}$  is a normal Cartesian three-vector, and  $\vec{\sigma}$  is given by Equation 1.38. They showed that the non-spin-flip reflectivity  $R^{\text{NSF}} = \frac{1}{4} \left| R_0 + \vec{R} \cdot \hat{P} \right|^2$ , where  $\hat{P}$  is

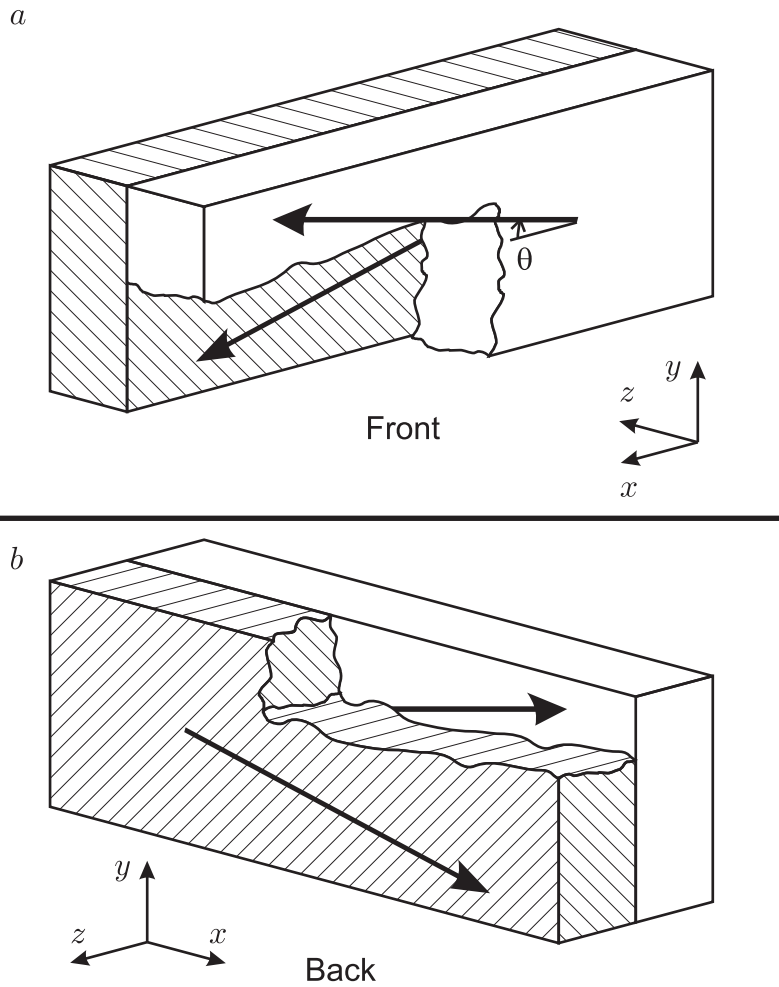


Figure 1.20: A simple free-standing bilayer with non-collinear magnetization. Each layer is uniformly magnetized in the  $xy$  plane. The  $x$  component of each layer is identical, but the  $y$  component differs in sign between the two layers. Panel a) shows the view seen by a neutron associated with front reflectivity and Panel b) shows the view seen by a neutron associated with back reflectivity.

the polarization of the incident neutron. Applying the simplifications made above, we find that

$$R^{\text{NSF}} = \frac{1}{4} |R_0 + R_x P_x \cos \theta + R_y P_y \sin \theta|^2. \quad (1.136)$$

$R_0$ ,  $R_x$  and  $R_y$  are fractions with numerators which include multiples of  $\cos \theta$  and  $\cos(2\theta)$  and share a common denominator consisting of multiples of  $\cos \theta$  and  $\cos(2\theta)$ , but otherwise no explicit dependence on  $\theta$ . When the magnetization is confined to the  $xy$  plane,  $R_z = 0$ .

The reflectivity of Equation 1.136 corresponds to the case in which the neutron encounters the top layer first. When the neutron encounters the bottom layer first, the only change we need to make is the transformation  $\theta \rightarrow -\theta$ , as shown in Figure 1.20b. We can examine the effect of this change for various configurations of the polarization of the incident neutron. Our discussion is facilitated if we first expand Equation 1.136 to first order in  $\theta$ :  $R^{\text{NSF}} = \frac{1}{4} |R_0 + R_x P_x + \theta R_y P_y|^2$ . We see that if  $\hat{P} \parallel \hat{x}$ , then  $R^{\text{NSF}} = \frac{1}{4} |R_0 + R_x P_x|^2$  is independent of  $\theta$ . This result is familiar for collinear magnetism: when the neutron polarization is in the plane of the film, we cannot tell whether the magnetic moments lie to the left or to the right of  $\hat{P}$ . Therefore, we cannot see a difference between front and back reflectivity. Now suppose that  $\hat{P} \parallel \hat{y}$ . Then  $R_{\text{front}}^{\text{NSF}} = \frac{1}{4} |R_0 + \theta R_y P_y|^2$  and  $R_{\text{back}}^{\text{NSF}} = \frac{1}{4} |R_0 - \theta R_y P_y|^2$ , which are different when  $\theta \neq 0$ . Recall that the use of spin-flippers gives the experimenter the ability to measure two non-spin-flip reflectivities. Let us associate  $R^{++}$  with polarization  $\hat{P}$  and  $R^{--}$  with polarization  $-\hat{P}$ . Then  $R_{\text{front}}^{++} = \frac{1}{4} |R_0 + \theta R_y P_y|^2$  and  $R_{\text{front}}^{--} = \frac{1}{4} |R_0 - \theta R_y P_y|^2$ , but the latter is seen to be identical to the expression  $R_{\text{back}}^{++} = \frac{1}{4} |R_0 - \theta R_y P_y|^2$  which we get by taking  $\theta \rightarrow -\theta$  for  $R_{\text{front}}^{++} \rightarrow R_{\text{back}}^{++}$ . So for  $\hat{P} \perp \vec{M}$ , the two non-spin-flip reflectivities interchange on interchanging the side of the sample first encountered by the neutron. If  $\hat{P}$  is at some arbitrary angle  $\phi$  with respect to  $\hat{x}$ , then we would expect the following table of values

$4R$	++	--
front	$ R_0 + R_x \cos \phi + \theta R_y \sin \phi ^2$	$ R_0 - R_x \cos \phi - \theta R_y \sin \phi ^2$
back	$ R_0 + R_x \cos \phi - \theta R_y \sin \phi ^2$	$ R_0 - R_x \cos \phi + \theta R_y \sin \phi ^2$

which generally takes on four distinct values when  $\theta \neq 0$ . For collinear structures, of course,  $\theta = 0$ , and there is no difference between front and back reflectivities for any one spin state.

Let us now examine the spin-flip scattering, as derived by Rühm, Toperverg, and Dosch [56]. We find that  $R^{\text{SF}} = \frac{1}{4}(|R_x|^2 + \theta^2|R_y|^2 + |R_x P_x + \theta R_y P_y|^2 + \text{Im}((R_x R_y^* - R_y R_x^*)\theta P_z))$  for small  $\theta$ . We can apply the same sort of inspection of this result for different polarizations of the incident neutron as we did for  $R^{\text{NSF}}$ . When external magnetic field is applied in the  $xy$  plane of the sample (as is typical for exchange-spring magnets), the polarization of the neutron will also lie in the  $xy$  plane. If in addition,  $p_x = 0$ ,  $R^{\text{SF}} = \frac{1}{4}(|R_x|^2 + \theta^2|R_y|^2 + |\theta R_y P_y|^2)$ ; conversely, if  $p_y = 0$ ,  $R^{\text{SF}} = \frac{1}{4}(|R_x|^2 + \theta^2|R_y|^2 + |R_x P_x|^2)$ . In both cases, we see that  $R^{\text{SF}}$  is an even function of  $\theta$ . Therefore, the front and back reflectivity are the same. But, if  $\hat{P}$  is at some arbitrary angle  $\phi$  with respect to  $\hat{x}$ , then we find the term  $|R_x P_x + \theta R_y P_y|^2$  introduces a difference between  $R_{\text{front}}^{\text{SF}}$  and  $R_{\text{back}}^{\text{SF}}$  when  $\theta \rightarrow -\theta$ .

Some noncollinear magnetic configurations exist in the absence of an applied magnetic field. In this case we might be free to place the polarization axis along  $z$ . We know from Equation 1.136 that when  $P_x = P_y = 0$ ,  $R^{\text{NSF}}$  gives information from only  $R_0$ , independent of  $P_z$ , so the non-spin-flip reflectivity is independent of incident spin state and which side the neutrons encounter first. Now the spin-flip reflectivity  $R^{\text{SF}} = \frac{1}{4}(|R_x|^2 + \theta^2|R_y|^2 + \text{Im}((R_x R_y^* - R_y R_x^*)\theta P_z))$  has a contribution which changes sign when  $\theta \rightarrow -\theta$ . Rather than changing the sign of  $\theta$ , we could merely change the sign of the polarization  $P_z$ , which is exactly what the spin flipper does. When there is noncollinear magnetism, and the polarization is along  $z$ ,  $R_{\text{front}}^{+-} \neq R_{\text{front}}^{-+} = R_{\text{back}}^{+-}$ . Historically, checking the difference between  $R_{\text{front}}^{+-}$  and  $R_{\text{front}}^{-+}$  has been the way to detect magnetic twists, as discussed in Section 1.4.4. The elegance of the front/back technique is that it allows us this same determination when  $P_z = 0$ . Unfortunately, the technique cannot tell us the chirality of the twist, but it does detect its presence. That is, we can measure  $|\text{d}\theta/\text{d}z|$ , but not its sign.

Let's now consider a three-layer film, pictured in Figure 1.21. Again, we impose similar restrictions on the parameters of the film that we did for the bilayer, except for the following. Let the topmost and bottommost layers have their magnetization lie at angle  $-\theta$  to  $x$ , while the middle layer has twice the thickness and its moments lie at angle  $\theta$  to  $x$ . The net magnetization  $\vec{M}$  still lies along  $x$ . By construction, there is no net chirality so that the front and back reflectivities are identical.

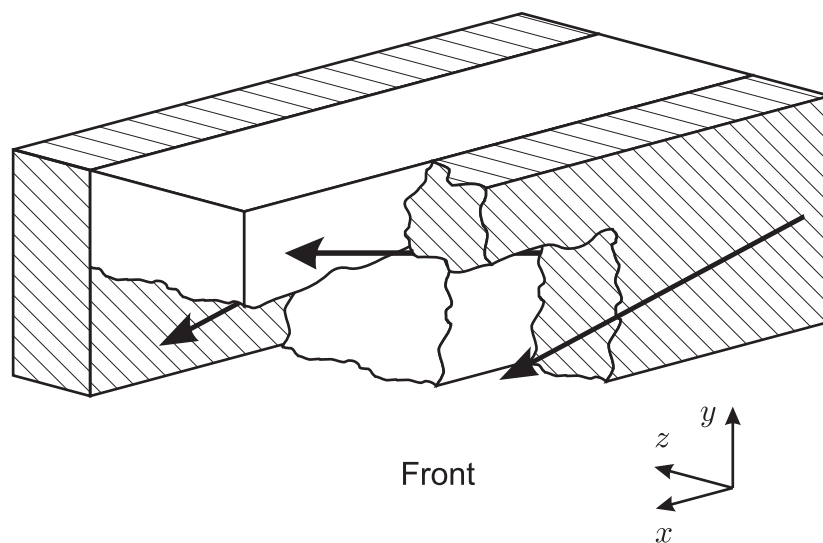


Figure 1.21: The bilayer of Figure 1.20 has had an additional copy of the hatched layer applied to the other side of the unhatched layer. Now the sample contains a magnetic mirror plane parallel to the  $xy$  plane and located at the center of the unhatched layer. Neutrons see the same potential regardless of whether they encounter the back or front first.

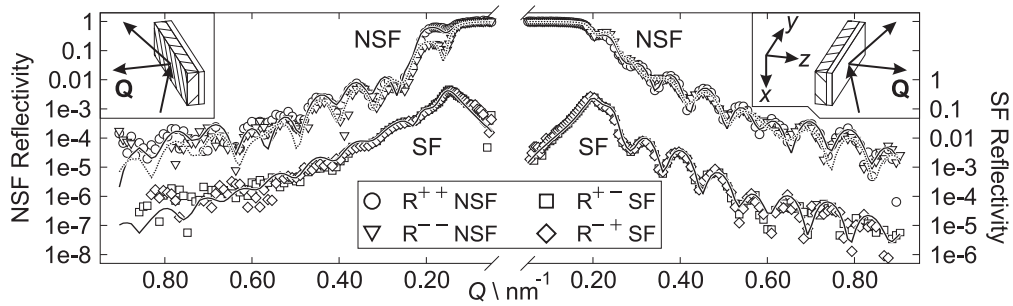


Figure 1.22: Reflectivity and fits from an FePt–FeNi exchange-spring magnet at 16 mT. The front (back) reflectivity is shown on the right (left) with  $Q$  increasing towards the right (left). The non-spin-flip (NSF) reflectivities are plotted against the left axis. The spin-flip (SF) reflectivities are plotted against the right axis, which is shifted by 2 orders of magnitude. The insets show the scattering geometry appropriate for that reflecting off that side of the sample.

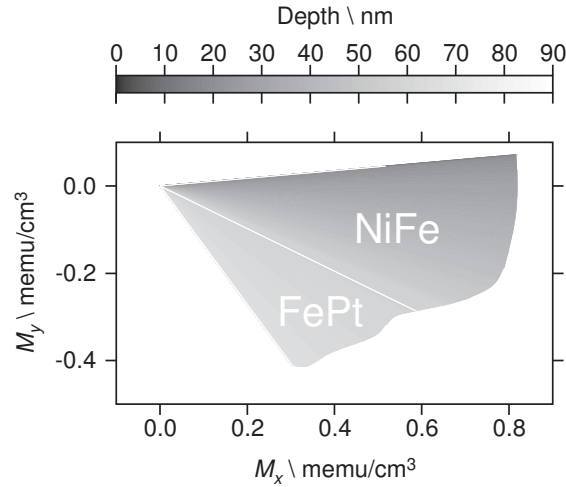


Figure 1.23: The magnetic structure from the fits shown in Figure 1.22. The original saturating field was applied along  $-y$ . The white line shows the interface between the FePt and the NiFe.

#### 1.6.4 PNR of Actual Systems

Now we are prepared to put these principles to use on real materials. The first system we shall examine is a permalloy ( $\text{Ni}_{80}\text{Fe}_{20}$ ) film on an  $\text{Fe}_{55}\text{Pt}_{45}$

film. This bilayer is buffered on each side with Pt, and the substrate is glass. Further details can be found in Reference [57]. Permalloy is a soft ferromagnet, while FCT (face-centered tetragonal) FePt is a hard ferromagnet. At the thicknesses deposited (50.0 nm permalloy, 20.0 nm FePt), the two layers couple strongly into an exchange-spring magnet. To align the layers, a magnetic field of 900 mT is applied along  $-y$ . The interesting effects emerge when the sign of the field is changed and very small fields are applied along  $+y$ . The presence of the magnetic field selects a polarization  $\hat{P} = \hat{y}$ . The four spin-dependent reflectivities from both the front and the back surfaces measured at 16 mT are plotted in Figure 1.22. Reflectivity from the front surface is plotted on the right side with  $Q$  increasing towards the right, and the reflectivity from the back surface is plotted on the left side with  $Q$  increasing towards the left. To clarify the differences between spin-flip (SF) and non-spin-flip (NSF) reflectivities, the SF reflectivities have been shifted down relative to the NSF reflectivities. The axis for the NSF reflectivity is at the left edge of the figure and the axis for the SF reflectivity is at the right edge of the figure. Figure 1.23 shows a plan-view of the vector magnetization at this field, where the vector from FePt to NiFe comes out of the figure. The vector magnetization was determined by fitting all the reflectivities in Figure 1.22 simultaneously. The magnetization at the bottom of the hard FePt is still close to  $-y$  while that of the top of the soft NiFe has twisted towards  $+y$ .

Exploring the parameter space of the vector magnetization as a function of the opening angle  $\theta$  leads us to some qualitative conclusions without actually fitting the data. For example, note the splitting between the two NSF reflectivities in Figure 1.22. The splitting is quite pronounced in the back reflectivity and almost non-existent in the front reflectivity. For this system, the large difference between these two splittings is the signature of the non-collinear magnetism. The fact that the splitting is bigger at the back coincides with the fact that the net magnetization lies closer to  $-y$  than to  $+y$ , *i.e.*, the exchange spring is just beginning to wind up. Looking forward to Figure 1.24 (which shows the reflectivity measured at 26 mT), we see the splitting is more pronounced on the front, which indicates the net magnetization is now closer to  $+y$  than to  $-y$ .

Returning to Figure 1.22, note that the amplitude of the Kiessig fringes in the SF reflectivities is also different. Those for the back reflectivity are damped relative to the front. Although the counting statistics for the back reflectivity are reduced because of attenuation from the glass substrate (a single-crystalline Si or Al<sub>2</sub>O<sub>3</sub> substrate would have been preferable), the in-

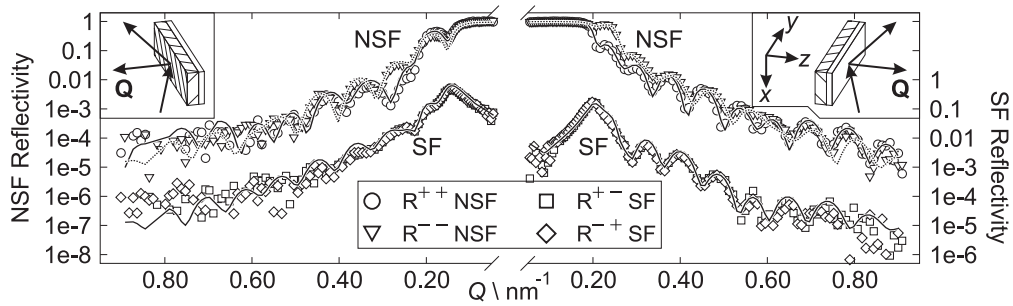


Figure 1.24: Reflectivity and fits for the exchange-spring after increasing the field in Figure 1.22 to 26 mT. Note the splitting in the NSF reflectivity near the critical angle has moved from the back side in Figure 1.22 to the front side here.

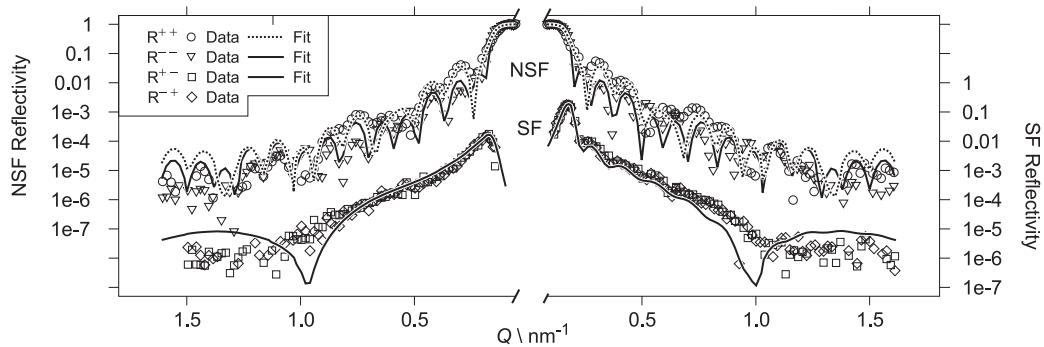


Figure 1.25: The reflectivity and fits from an Co ferrite film on a CoFe film at 47 mT. There are only subtle differences in the non-spin-flip reflectivity, but a strong asymmetry exists for the front-back spin-flip reflectivity.

creased relative background is not enough to account for the damping. The back SF reflectivity is damped because the moments at the back of the sample are more aligned with  $-y$ , while those at the front are more aligned with  $+x$ , and thereby contribute more features to the spin-flip scattering. In Figure 1.24 the back SF reflectivity is still damped relative to the front—the FePt spins are still more closely pinned to  $-y$  and the NiFe spins are aligned closer to  $+x$ . (This can be demonstrated by simple model calculations.)

As the magnetic anisotropy of the hard layer is increased, we expect that

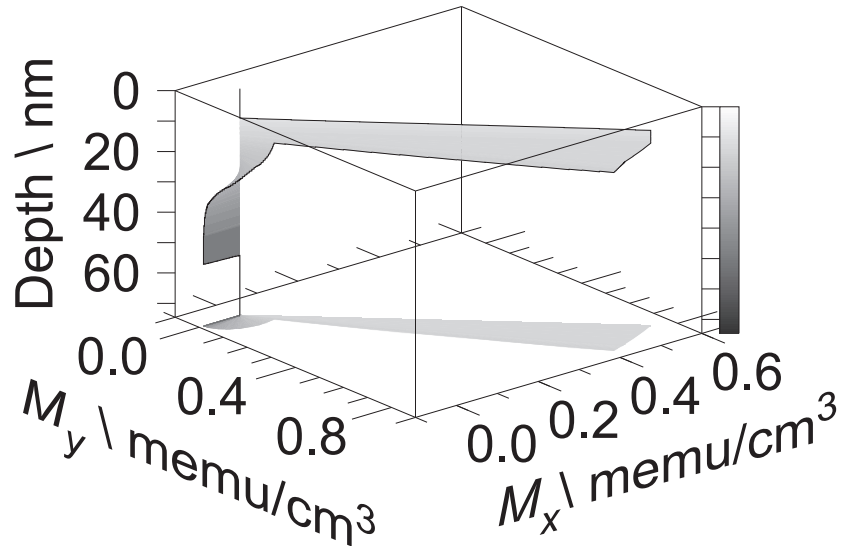


Figure 1.26: The magnetic structure from the fits shown in Figure 1.25.

the twist will be found more predominantly in the soft layer. A system such as Ta(10.0 nm) on CoFe<sub>10</sub>(6.0 nm) on CoFe<sub>2</sub>O<sub>4</sub>(37.5 nm) on Si is an example of a soft ferromagnet (CoFe<sub>10</sub>) coupled to a ferrimagnet (CoFe<sub>2</sub>O<sub>4</sub>). A ferrimagnet still exhibits a net magnetic moment, but at the atomic level neighboring magnetic sites have alternating direction of magnetic moment, just like antiferromagnets. The anisotropy of a ferrimagnet is thus typically greater than for hard ferromagnets. More details of this system can be found in Reference [58]. Figure 1.25 shows the reflectivity measured at 47 mT after saturating at  $-900$  mT. Here note that the NSF reflectivities look very symmetrical, but there is a peak in  $R_{\text{front}}^{\text{SF}}$  which is missing in  $R_{\text{back}}^{\text{SF}}$ . The fitted structure is shown in Figure 1.26, where the soft ferromagnet occupies the depth from 10 nm to 16 nm. Here the two layers are canted with respect to each other, so there is no mirror plane. The SF reflectivities show the expected asymmetry, but why are the NSF reflectivities so symmetric? The most likely answer is that the interplay between the nuclear potential (which is not independent of depth in these real-world samples) and the magnetic potential complicates our earlier findings for free-standing films of homogeneous nuclear character. The symmetry of the measured reflectivity is indeed that predicted by the program of the appendix. In the FePt–FeNi system,

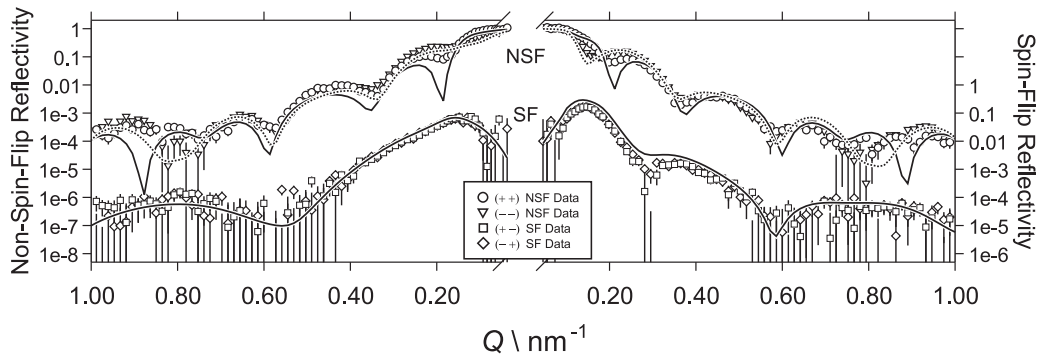


Figure 1.27: Reflectivity and fits from an FeMn–Co exchange-biased film at 23 mT. Despite the difference in the front–back spin-flip-reflectivity, the fitted magnetic structure is collinear. The interplay between chemical and magnetic potentials is the most likely cause for the asymmetry.

the nuclear potential  $Nb$  was always greater than the magnetic potential  $Np$ . When the saturated magnetic SLD  $Np_{\text{sat}} > Nb$ , then  $Nb \pm Np$  can approach and cross zero as the direction of magnetization in a layer changes. This necessarily complicates the systematic dependence of reflectivity with field.

A final example is provided by replacing the ferrimagnet with an antiferromagnet. An example of such a system is Co on FeMn [59]. When the soft Co couples to the antiferromagnetic FeMn, exchange biasing occurs. Exchange biasing, which occurs only when the antiferromagnet is cooled below its ordering temperature in the presence of a magnetic field, leads to hysteresis loops which are no longer symmetric about the origin and may lead to different magnetic reversal processes when going from large positive fields to large negative fields and back again [60]. The anisotropy of the antiferromagnetic FeMn, once ordered, is so large that we would not expect any significant change in the local magnetization in the antiferromagnet while an external field is applied. Because the net magnetization of the antiferromagnet is zero, we will observe negligible magnetic scattering in reflectivity experiments at sufficiently small angles. However, we can detect how the soft Co demagnetizes. In particular, we are interested in knowing if a twist develops in the Co due to the pinning of Co magnetization at the Co–FeMn interface.

Figure 1.27 shows the reflectivity of a Co film 12 nm thick deposited on

8 nm of FeMn. The FeMn is deposited on Cu, and this trilayer systems is buffered on either side with Nb. The reflectivity was measured at 22.7 mT after cooling the system in a field of  $-242$  mT [61]. Again the NSF reflectivities are not dramatically different, and although the splitting on the front side is slightly greater than that from the back side, this might be due to the Si substrate at one side *vs.* air at the other. There is again a peak in the front SF reflectivities, and smooth decay in the back SF reflectivities, much as in Figure 1.24. However, here it is found that a uniformly canted Co layer, with no twist, is the best fit to the reflectivity [61]. Again, the interplay of the nuclear potential and magnetic potential of this real system complicates the simplified models presented earlier.

What lessons should be learned from these three examples? Chiefly, that although trivial model structures with a high degree of symmetry produce features in the reflectivity characteristic of twists, canted layers, and other structures, real-world materials can complicate the issue. Before measuring the reflectivity, one ought first to simulate the possible reflectivity under various conditions (including: side of neutron incidence, polarization orientation, fronting media, backing media and magnetic field) using programs similar to that found in the appendix. After exploring the parameter space for a particular sample, key features shall often appear near certain values of  $Q$  and in certain reflectivities. Furthermore, the scattering from one side of the sample may be particularly sensitive to a magnetic configuration, while the other side may be rather insensitive. Armed with this knowledge, experiments targeted to the material at hand can be successfully crafted.

## Appendix

This appendix contains the FORTRAN77 source code for a program which will calculate the reflection and transmission amplitudes of neutron scattering from a series of slabs of constant SLD. A copy of the code is also available in the World Wide Web in links from <http://www.ncnr.nist.gov/programs/reflect/>. The National Institute of Standards and Technology supplies this code freely to the public. Although considerable effort has been expended to ensure the accuracy of the code, the reader assumes all risk in compiling, using, and interpreting the results of the code.

```
PROGRAM GEPORE
C *****
```

```

c
c Program "gepore.f" (GEneral POLarized REflectivity) calculates the
5 c spin-dependent neutron reflectivities (and transmissions) for
c model potentials, or scattering length density profiles, assuming
c the specular condition.
c
c In the present version, both nuclear and magnetic, real scattering
10 c length densities can be input, whereas imaginary components of the
c nuclear potential cannot. Also, magnetic and nuclear incident, or
c "fronting", and substrate, or "backing", media can be included. A
c description of the input parameters is given below:
c
c
15 c
c     NL = # of distinct layers or "slabs" of uniform scattering
c           length density (SLD)
c
c     NC = # of "unit cell" repeats
20 c
c     QS = first wavevector transfer at which reflectivities and
c           transmissions are calculated (Angstroms-1)
c
c     DQ = increment in Q (A-1)
25 c
c     NQ = # of Q-values at which reflectivities and transmissions
c           are calculated
c
c     EPS = angle, in radians, between the laboratory guide field
30 c           or quantization axis and the sample axis of
c           quantization, defined to be the z-axis, which is parallel
c           to Q: note that the x-axes of the laboratory and sample
c           coordinate systems are taken to be coincident. The sense
c           of rotation is the following: EPS is the angle FROM the
35 c           sample z-axis TO the lab z-axis rotating CCW about the
c           x-axis as viewed from the positive side of the x-axis.
c           For the lab z-axis to be aligned with the positive y-axis
c           of the sample, for example, EPS must be 3pi/2 radians.
c
c     IP, IM = complex numbers describing the polarization state
40 c           of the incident neutron relative to the lab-
c           oratory axis of quantization: e.g., spin "+" is
c           represented by IP = (1.0,0.0) and IM =
c           (0.0,0.0) whereas a neutron in the pure spin
45 c           "-" state is given by IP = (0.0,0.0) and IM =
c           (1.0,0.0). Note that in this program, the incident,
c           reflected, and transmitted amplitudes and intensities

```

```

c          are referred to the laboratory frame: a similarity
c          transformation is then performed on the transfer
50 c          matrix to go from the sample system, in which it was
c          originally formulated, to the lab system. This is
c          different from what is done in predecessors of this
c          program, such as "r6dp.f", in which the amplitudes &
c          intensities are rotated from lab to sample reference
55 c          frame and back (with the transfer matrix correspond-
c          ing to the sample scattering potential remaining
c          unchanged in the sample coordinate system).
c
c          ROINP = nuclear + magnetic SLD of incident medium for "+" spin
60 c
c          ROINM = " - " " " " " "-" "
c
c          ROSUP = " + " " substrate " "+" "
c
65 c          ROSUM = " - " " " " " "-" "
c
c          The parameters defined above are input into the program
c          through the file "inpt.d".
c
70 c          Another input file called "tro.d" contains information about each
c          individual layer comprising the sample. Starting with the first
c          layer encountered by the incident beam, the following quantities
c          for the jth layer are supplied in the format as shown:
c
75 c          T(J) BN(J) PN(J) THE(J) PHI(J)
c
c          .
c          .
c          .
80 c
c          where
c
c          T(J) = layer thickness in A
c
85 c          BN(J) = nuclear SLD in A-2 (e.g., 8.05e-06 for Fe)
c
c          PN(J) = magnetic SLD in A-2 (e.g., 5.085e-06 A-2 -- for Fe --
c          corresponds to a B-field of ~ 22,000. Gauss)
c
90 c          THE(J) = angle in radians that the layer magnetization
c          direction makes wrt the + x-axis of the sample:
c          note that the sample z-axis is parallel to Q

```

```

c          so that the sample x- and y-axes lie in the plane
c          of the laminar film sample.  THE(J) must be defined
95 c          in the interval between zero and pi.
c
c          PHI(J) = angle, in radians, of the projection of the layer
c          magnetization in the sample coordinate system's
c          (y,z)-plane relative to the sample y-axis.  The
100 c          sense of rotation is CCW FROM the y-axis TO the
c          magnetization projection about the x-axis as view-
c          from the positive side of the x-axis.  PHI(J) can
c          be defined in the interval between zero and 2pi.
c
105 c It must be noted that in the continuum reflectivity calculation
c performed by this program, Maxwell's equations apply, specifically
c the requirement that the component of the magnetic induction, B,
c normal to a boundary surface be continuous.  Neither the program
c nor the wave equation itself automatically insure that this is so:
110 c this condition must be satisfied by appropriate selection of the
c magnetic field direction in the incident and substrate media,
c defined by the angle "EPS", and by the values of PN(J), THE(J),
c and PHI(J) specified in the input.
c
115 c Be aware that earlier versions of this program, such as "r6dp.f",
c do not allow for magnetic incident or substrate media AND ALSO
c require that PHI(J) be zero or pi only so that no magnetization
c in the sample is parallel to Q or normal to the plane of the film.
c
120 c The output files contain the spin-dependent reflectivities and
c transmissions, relative to the laboratory axis of quantization --
c which is the same in the incident and substrate media -- as follows:
c
c          qrp2.d -- probability that the neutron will be reflected in
125 c          the plus spin state
c
c          qrm2.d -- probability that the neutron will be reflected in
c          the minus spin state
c
130 c          qtp2.d -- probability that the neutron will be transmitted
c          in the plus spin state
c
c          qtm2.d -- probability that the neutron will be transmitted
c          in the minus spin state
135 c
c all of the above as a function of Q in A-1.
c

```

```

c Also output are the files:
c
140 c      qrpmpms.d -- the reflectivities and transmissions, in the
c              above order, and their sums as a function of Q
c
c      sum.d -- Q, sum of reflectivities and transmissions
c
145 c      rpolx.d -- x-component of the polarization of the reflected
c              neutron vs. Q
c
c      tpolx.d -- x-component of the polarization of the transmitted
c              neutron vs. Q
150 c
c      rpoly.d -- y-component of the polarization of the reflected
c              neutron vs. Q
c
c      tpoly.d -- y-component of the polarization of the transmitted
155 c              neutron vs. Q
c
c      rpolz.d -- z-component of the polarization of the reflected
c              neutron vs. Q
c
160 c      tpolz.d -- z-component of the polarization of the transmitted
c              neutron vs. Q
c
c      rrem.d -- Q, Re(r"-")
c
165 c      rimm.d -- Q, Im(r"-")
c
c      rrep.d -- Q, Re(r"+")
c
c      rimp.d -- Q, Im(r"+")
170 c
c      where
c
c              reflectivity = Re(r)**2 + Im(r)**2
c
175 c *****
c
c      IMPLICIT REAL*8(A-H,O-Z)
c      DIMENSION T(1000),BN(1000),PN(1000)
c      DIMENSION THE(1000),PHI(1000)
180 c      DIMENSION A(4,4),B(4,4),C(4,4)
c      DIMENSION S(4),U(4),ALP(4),BET(4),GAM(4),DEL(4)
c      DIMENSION CST(4,4)

```

```

COMPLEX*16 IP,IM,CI,CR,CO,ARG1,ARG2
COMPLEX*16 ZSP,ZSM,ZIP,ZIM,YPP,YMM,YPM,YMP
185 COMPLEX*16 S,U,ALP,BET,GAM,DEL,EF,A,B,C
COMPLEX*16 RM,RP,TP,TM,RMD,RPD,X
COMPLEX*16 P1,P2,P3,P4,P5,P6,P7,P8,P9,P10,P11,P12
COMPLEX*16 ARGZSP,ARGZSM,ARGZIP,ARGZIM
COMPLEX*16 CST
190 COMPLEX*16 CC,SS,SCI
COMPLEX*16 FANGP,FANGM
PI=3.141592654
CI=(0.0,1.0)
CR=(1.0,0.0)
195 CO=(0.0,0.0)
OPEN(UNIT=10,NAME='inpt.d',STATUS='OLD',FORM='FORMATTED')
READ(10,*)NL,NC,QS,DQ,NQ,EPS,IP,IM,ROINP,ROINM,ROSUP,ROSUM
WRITE(*,*)NL,NC,QS,DQ,NQ,EPS,IP,IM,ROINP,ROINM,ROSUP,ROSUM
CLOSE(10)
200 OPEN(UNIT=11,NAME='tro.d',STATUS='OLD',FORM='FORMATTED')
READ(11,*)(T(J),BN(J),PN(J),THE(J),PHI(J),J=1,NL)
CLOSE(11)
IF(NQ.GT.1000)GO TO 900
IF(NL.GT.1000)GO TO 900
205 OPEN(UNIT=14,NAME='qrm2.d',STATUS='UNKNOWN',FORM='FORMATTED')
OPEN(UNIT=15,NAME='qrp2.d',STATUS='UNKNOWN',FORM='FORMATTED')
OPEN(UNIT=16,NAME='qtm2.d',STATUS='UNKNOWN',FORM='FORMATTED')
OPEN(UNIT=17,NAME='qtp2.d',STATUS='UNKNOWN',FORM='FORMATTED')
OPEN(UNIT=20,NAME='qrpmtpms.d',STATUS='UNKNOWN',FORM='FORMATTED')
210 OPEN(UNIT=21,NAME='sum.d',STATUS='UNKNOWN',FORM='FORMATTED')
OPEN(UNIT=31,NAME='rrem.d',STATUS='UNKNOWN',FORM='FORMATTED')
OPEN(UNIT=32,NAME='rirm.d',STATUS='UNKNOWN',FORM='FORMATTED')
OPEN(UNIT=33,NAME='rrep.d',STATUS='UNKNOWN',FORM='FORMATTED')
OPEN(UNIT=34,NAME='rimp.d',STATUS='UNKNOWN',FORM='FORMATTED')
215 OPEN(UNIT=41,NAME='rpolx.d',STATUS='UNKNOWN',FORM='FORMATTED')
OPEN(UNIT=42,NAME='tpolx.d',STATUS='UNKNOWN',FORM='FORMATTED')
OPEN(UNIT=43,NAME='rpoly.d',STATUS='UNKNOWN',FORM='FORMATTED')
OPEN(UNIT=44,NAME='tpoly.d',STATUS='UNKNOWN',FORM='FORMATTED')
OPEN(UNIT=45,NAME='rpolz.d',STATUS='UNKNOWN',FORM='FORMATTED')
220 OPEN(UNIT=46,NAME='tpolz.d',STATUS='UNKNOWN',FORM='FORMATTED')
CC=CR*COS(EPS/2.)*COS(EPS/2.)
SS=CR*SIN(EPS/2.)*SIN(EPS/2.)
SCI=CI*COS(EPS/2.)*SIN(EPS/2.)
DO 600 IQ=1,NQ
225 DO 200 I=1,4
DO 180 J=1,4
B(I,J)=(0.0,0.0)

```

```

180 CONTINUE
200 CONTINUE
230 B(1,1)=(1.0,0.0)
      B(2,2)=(1.0,0.0)
      B(3,3)=(1.0,0.0)
      B(4,4)=(1.0,0.0)
      Q=QS+(IQ-1)*DQ
235 QP=DSQRT(Q*Q+16.*PI*ROINP)
      QM=DSQRT(Q*Q+16.*PI*ROINM)
      SUMT=0.0
      DO 400 IC=1,NC
      DO 300 L=1,NL
240 SUMT=SUMT+T(L)
      ARG1=CR*(4.*PI*(BN(L)+PN(L))-QP*QP/4.)
      ARG2=CR*(4.*PI*(BN(L)-PN(L))-QM*QM/4.)
      S(1)=CDSQRT(ARG1)
      S(3)=CDSQRT(ARG2)
245 U1NR=+1.+COS(THE(L))-SIN(THE(L))*SIN(PHI(L))
      U1NI=+SIN(THE(L))*COS(PHI(L))
      U1DR=+1.+COS(THE(L))+SIN(THE(L))*SIN(PHI(L))
      U1DI=-SIN(THE(L))*COS(PHI(L))
      U(1)=(U1NR*CR+U1NI*CI)/(U1DR*CR+U1DI*CI)
250 U3NR=-2.+U1NR
      U3NI=U1NI
      U3DR=-2.+U1DR
      U3DI=U1DI
      U(3)=(U3NR*CR+U3NI*CI)/(U3DR*CR+U3DI*CI)
255 S(2)=-S(1)
      S(4)=-S(3)
      U(2)=U(1)
      U(4)=U(3)
      ALP(1)=U(3)/(2.*U(3)-2.*U(1))
260 BET(1)=-ALP(1)/U(3)
      GAM(1)=ALP(1)/S(1)
      DEL(1)=-ALP(1)/(U(3)*S(1))
      ALP(2)=ALP(1)
      BET(2)=-ALP(1)/U(3)
265 GAM(2)=-ALP(1)/S(1)
      DEL(2)=ALP(1)/(U(3)*S(1))
      ALP(3)=-U(1)*ALP(1)/U(3)
      BET(3)=ALP(1)/U(3)
      GAM(3)=-U(1)*ALP(1)/(U(3)*S(3))
270 DEL(3)=ALP(1)/(U(3)*S(3))
      ALP(4)=-U(1)*ALP(1)/U(3)
      BET(4)=ALP(1)/U(3)

```

```

GAM(4)=U(1)*ALP(1)/(U(3)*S(3))
DEL(4)=-ALP(1)/(U(3)*S(3))
275 DO 240 I=1,4
DO 220 J=1,4
C(I,J)=(0.0,0.0)
A(I,J)=(0.0,0.0)
220 CONTINUE
280 240 CONTINUE
DO 260 J=1,4
EF=CDEXP(S(J)*T(L))
A(1,1)=A(1,1)+ALP(J)*EF
A(1,2)=A(1,2)+BET(J)*EF
285 A(1,3)=A(1,3)+GAM(J)*EF
A(1,4)=A(1,4)+DEL(J)*EF
A(2,1)=A(2,1)+ALP(J)*U(J)*EF
A(2,2)=A(2,2)+BET(J)*U(J)*EF
A(2,3)=A(2,3)+GAM(J)*U(J)*EF
290 A(2,4)=A(2,4)+DEL(J)*U(J)*EF
A(3,1)=A(3,1)+ALP(J)*S(J)*EF
A(3,2)=A(3,2)+BET(J)*S(J)*EF
A(3,3)=A(3,3)+GAM(J)*S(J)*EF
A(3,4)=A(3,4)+DEL(J)*S(J)*EF
295 A(4,1)=A(4,1)+ALP(J)*U(J)*S(J)*EF
A(4,2)=A(4,2)+BET(J)*U(J)*S(J)*EF
A(4,3)=A(4,3)+GAM(J)*U(J)*S(J)*EF
A(4,4)=A(4,4)+DEL(J)*U(J)*S(J)*EF
260 CONTINUE
300 DO 290 I=1,4
DO 280 J=1,4
DO 270 K=1,4
C(I,J)=C(I,J)+A(I,K)*B(K,J)
270 CONTINUE
305 280 CONTINUE
290 CONTINUE
DO 294 I=1,4
DO 292 J=1,4
B(I,J)=C(I,J)
310 292 CONTINUE
294 CONTINUE
300 CONTINUE
400 CONTINUE
CST(1,1)=C(1,1)*CC+C(2,2)*SS+(C(2,1)-C(1,2))*SCI
315 CST(1,2)=C(1,2)*CC+C(2,1)*SS+(C(2,2)-C(1,1))*SCI
CST(2,1)=C(2,1)*CC+C(1,2)*SS+(C(1,1)-C(2,2))*SCI
CST(2,2)=C(2,2)*CC+C(1,1)*SS+(C(1,2)-C(2,1))*SCI

```

```

CST(1,3)=C(1,3)*CC+C(2,4)*SS+(C(2,3)-C(1,4))*SCI
CST(1,4)=C(1,4)*CC+C(2,3)*SS+(C(2,4)-C(1,3))*SCI
320 CST(2,3)=C(2,3)*CC+C(1,4)*SS+(C(1,3)-C(2,4))*SCI
CST(2,4)=C(2,4)*CC+C(1,3)*SS+(C(1,4)-C(2,3))*SCI
CST(3,1)=C(3,1)*CC+C(4,2)*SS+(C(4,1)-C(3,2))*SCI
CST(3,2)=C(3,2)*CC+C(4,1)*SS+(C(4,2)-C(3,1))*SCI
CST(4,1)=C(4,1)*CC+C(3,2)*SS+(C(3,1)-C(4,2))*SCI
325 CST(4,2)=C(4,2)*CC+C(3,1)*SS+(C(3,2)-C(4,1))*SCI
CST(3,3)=C(3,3)*CC+C(4,4)*SS+(C(4,3)-C(3,4))*SCI
CST(3,4)=C(3,4)*CC+C(4,3)*SS+(C(4,4)-C(3,3))*SCI
CST(4,3)=C(4,3)*CC+C(3,4)*SS+(C(3,3)-C(4,4))*SCI
CST(4,4)=C(4,4)*CC+C(3,3)*SS+(C(3,4)-C(4,3))*SCI
330 DO 480 I=1,4
DO 470 J=1,4
C(I,J)=CST(I,J)
470 CONTINUE
480 CONTINUE
335 RMD=(0.0,0.0)
RPD=(0.0,0.0)
RM=(0.0,0.0)
RP=(0.0,0.0)
TM=(0.0,0.0)
340 TP=(0.0,0.0)
ARGZSP=CR*(QP*QP-16.*PI*ROSUP)
ZSP=(CI/2.)*CDSQRT(ARGZSP)
ARGZSM=CR*(QM*QM-16.*PI*ROSUM)
ZSM=(CI/2.)*CDSQRT(ARGZSM)
345 ARGZIP=CR*(QP*QP-16.*PI*ROINP)
ZIP=(CI/2.)*CDSQRT(ARGZIP)
ARGZIM=CR*(QM*QM-16.*PI*ROINM)
ZIM=(CI/2.)*CDSQRT(ARGZIM)
X=-1.*CR
350 YPP=ZIP*ZSP
YMM=ZIM*ZSM
YPM=ZIP*ZSM
YMP=ZIM*ZSP
P1=ZSM*C(2,1)+X*C(4,1)+YPM*C(2,3)-ZIP*C(4,3)
355 P2=ZSP*C(1,1)+X*C(3,1)-YPP*C(1,3)+ZIP*C(3,3)
P3=ZSP*C(1,1)+X*C(3,1)+YPP*C(1,3)-ZIP*C(3,3)
P4=ZSM*C(2,1)+X*C(4,1)-YPM*C(2,3)+ZIP*C(4,3)
P5=ZSM*C(2,2)+X*C(4,2)+YMM*C(2,4)-ZIM*C(4,4)
P6=ZSP*C(1,1)+X*C(3,1)-YPP*C(1,3)+ZIP*C(3,3)
360 P7=ZSP*C(1,2)+X*C(3,2)+YMP*C(1,4)-ZIM*C(3,4)
P8=ZSM*C(2,1)+X*C(4,1)-YPM*C(2,3)+ZIP*C(4,3)
P9=ZSP*C(1,2)+X*C(3,2)-YMP*C(1,4)+ZIM*C(3,4)

```

```

P10=ZSM*C(2,1)+X*C(4,1)-YPM*C(2,3)+ZIP*C(4,3)
P11=ZSM*C(2,2)+X*C(4,2)-YMM*C(2,4)+ZIM*C(4,4)
365 P12=ZSP*C(1,1)+X*C(3,1)-YPP*C(1,3)+ZIP*C(3,3)
RM=RM+IP*P1*P2
RM=RM-IP*P3*P4
RM=RM+IM*P5*P6
RM=RM-IM*P7*P8
370 RMD=RMD+P9*P10
RMD=RMD-P11*P12
RM=RM/RMD
RP=RP+RM*P9
RP=RP+IP*P3
375 RP=RP+IM*P7
RPD=-P2
RP=RP/RPD
TP=C(1,1)*(IP+RP)+C(1,2)*(IM+RM)
TP=TP+C(1,3)*ZIP*(IP-RP)+C(1,4)*ZIM*(IM-RM)
380 TM=C(2,1)*(IP+RP)+C(2,2)*(IM+RM)
TM=TM+C(2,3)*ZIP*(IP-RP)+C(2,4)*ZIM*(IM-RM)
FANGP=ZSP*SUMT
FANGM=ZSM*SUMT
TP=TP*CDEXP(-FANGP)
385 TM=TM*CDEXP(-FANGM)
RM2=(DREAL(RM))**2+(DIMAG(RM))**2
RP2=(DREAL(RP))**2+(DIMAG(RP))**2
TP2=(DREAL(TP))**2+(DIMAG(TP))**2
TM2=(DREAL(TM))**2+(DIMAG(TM))**2
390 QV=QS+(IQ-1)*DQ
PRXUN=2.0*DREAL(RP)*DREAL(RM)
PRXUN=PRXUN+2.0*DIMAG(RP)*DIMAG(RM)
PRYUN=2.0*DREAL(RP)*DIMAG(RM)
PRYUN=PRYUN-2.0*DIMAG(RP)*DREAL(RM)
395 PTXUN=2.0*DREAL(TP)*DREAL(TM)
PTXUN=PTXUN+2.0*DIMAG(TP)*DIMAG(TM)
PTYUN=2.0*DREAL(TP)*DIMAG(TM)
PTYUN=PTYUN-2.0*DIMAG(TP)*DREAL(TM)
PRX=PRXUN/(RP2+RM2)
400 PRY=PRYUN/(RP2+RM2)
PRZ=(RP2-RM2)/(RP2+RM2)
PTX=PTXUN/(TP2+TM2)
PTY=PTYUN/(TP2+TM2)
PTZ=(TP2-TM2)/(TP2+TM2)
405 WRITE(31,*)QV,DREAL(RM)
WRITE(32,*)QV,DIMAG(RM)
WRITE(33,*)QV,DREAL(RP)

```

```

WRITE(34,*)QV,DIMAG(RP)
SUM=RP2+RM2+TP2+TM2
410 WRITE(20,*)QV,RP2,RM2,TP2,TM2,SUM
WRITE(21,*)QV,SUM
WRITE(14,*)QV,RM2
WRITE(15,*)QV,RP2
WRITE(16,*)QV,TM2
415 WRITE(17,*)QV,TP2
WRITE(41,*)QV,PRX
WRITE(42,*)QV,PTX
WRITE(43,*)QV,PRY
WRITE(44,*)QV,PTY
420 WRITE(45,*)QV,PRZ
WRITE(46,*)QV,PTZ
600 CONTINUE
900 CONTINUE
CLOSE(14)
425 CLOSE(15)
CLOSE(16)
CLOSE(17)
CLOSE(20)
CLOSE(21)
430 CLOSE(31)
CLOSE(32)
CLOSE(33)
CLOSE(34)
CLOSE(41)
435 CLOSE(42)
CLOSE(43)
CLOSE(44)
CLOSE(45)
CLOSE(46)
440 STOP
END

```

# Bibliography

- [1] J. W. von Goethe, *Faust*, Parts I (1808) and II (1832), B. Taylor, trans., (Washington Square Press, New York, 1964) p22.
- [2] D. T. Pierce, J. Unguris and R. J. Celotta, *MRS Bulletin* **13**, 19 (1988).
- [3] C. F. Majkrzak, J. Kwo, M. Hong, Y. Yafet, D. Gibbs, C. L. Chien and J. Bohr, *Advances in Physics* **40**, 99 (1991).
- [4] M. R. Fitzsimmons, S. D. Bader, J. A. Borchers, G. P. Felcher, J. K. Furdyna, A. Hoffmann, J. B. Kortright, I. K. Schuller, T. C. Schulthess, S. K. Sinha, M. F. Toney, D. Weller and S. Wolf, *J. Magn. and Magn. Mat.*, in press.
- [5] E. Merzbacher, *Quantum Mechanics*, 2nd Ed. (Wiley, New York, 1970).
- [6] M. Born and E. Wolf, *Principles of Optics*, 6th Ed. (Pergamon Press, Oxford, 1980) p51.
- [7] S. Yamada, T. Ebisawa, N. Achiwa, T. Akiyoshi and S. Okamoto, *Annual Report*, Res. Reactor Inst. Kyoto Univ. **11**, 8 (1978).
- [8] P. Croce and B. Pardo, *Nowv. Rev. Opt. Appl.* **1**, 229 (1970).
- [9] G. E. Bacon, *Neutron Diffraction*, 3rd Ed., (Oxford University Press, London, 1975).
- [10] L. Koester, *Springer Tracts in Modern Physics* **80**, (1977).
- [11] V. F. Sears, *Neutron Optics*, (Oxford University Press, Oxford, 1989).
- [12] C. F. Majkrzak, N. F. Berk and U. A. Perez-Salas, *Langmuir* **19**, 7796 (2003).

- [13] C. F. Majkrzak, J. F. Ankner, N. F. Berk and Doon Gibbs, in *Magnetic Multilayers*, Edited by L. H. Bennett and R. E. Watson, (World Scientific, Singapore, 1994) p299.
- [14] N. F. Berk, unpublished.
- [15] S. K. Sinha, E. B. Sirota, S. Garoff and H. B. Stanley, *Phys. Rev. B* **38**, 2297 (1988).
- [16] R. Pynn, *Phys. Rev. B* **45**, 602 (1992).
- [17] F. Mezei, *Physica B* **137**, 295 (1986).
- [18] R. P. Feynman, F. L. Vernon, Jr. and R. W. Hellwarth, *J. Appl. Phys.* **28**, 49 (1957).
- [19] K. Blum, *Density Matrix Theory and Its Applications*, (Plenum Press, New York, 1981).
- [20] W. G. Williams, *Polarized Neutrons*, (Oxford, London, 1988).
- [21] C. F. Majkrzak, *Physica B* **213&214**, 904 (1995).
- [22] E. E. Anderson, *Modern Physics and Quantum Mechanics*, (Saunders, Philadelphia, 1971) p366.
- [23] V. G. Baryshevskii and M. I. Podgoretskii, *Soviet Phys. JETP* **20**, 704 (1965) or *J. Exp. The. Phys. (U.S.S.R.)* **47**, 1050 (1964).
- [24] I. I. Gurevich and L. V. Tarasov, *Low-Energy Neutron Physics*, (North Holland, Amsterdam, 1968).
- [25] M. Th. Rekveldt, *J. Phys. (Paris)* **C1**, 579 (1971).
- [26] F. Mezei, *Z. Phys.* **255**, 146 (1972).
- [27] S. K. Mendiratta and M. Blume, *Phys. Rev. B* **14**, 144 (1976).
- [28] P. J. Sivadriere, *Acta Crystallogr.* **A31**, 340 (1975).
- [29] V. A. Belyakov and R. Ch. Bokun, *Fiz. Tverd. Tela (Leningrad)* **18**, 2399 (1976) [*Sov. Phys.—Solid State* **18**, 1399 (1976)].

- [30] O. Scharpf, *J. Appl. Crystallogr.* **11**, 626 (1978).
- [31] G. P. Felcher, R. O. Hilleke, R. K. Crawford, J. Haumann, R. Kleb and G. Ostrowski, *Rev. Sci. Instrum.* **58**, 609 (1987).
- [32] C. F. Majkrzak and N. F. Berk, *Phys. Rev. B* **40**, 371 (1989).
- [33] C. F. Majkrzak, *Physica B*. **156&157**, 619 (1989).
- [34] G. M. Drabkin, *J. Exptl. Theoret. Phys., (U.S.S.R.)* **43**, 1107 (1962).
- [35] M. T. Rekveldt, in *Magnetic Neutron Scattering*, Edited by A. Furrer, (World Scientific, Singapore, 1995) p211.
- [36] G. Arfken, *Mathematical Methods for Physicists*, 2nd Ed., (Academic Press, NY, 1971).
- [37] C. F. Majkrzak, *Physica B* **221**, 342 (1996).
- [38] C. F. Majkrzak, in *Magnetic Neutron Scattering*, Edited by A. Furrer, (World Scientific, Singapore, 1995) p78.
- [39] R. M. Moon, T. Riste and W. C. Koehler, *Phys. Rev.* **181**, 920 (1969).
- [40] F. Tasset, P. J. Brown and J. B. Forsyth, *J. Appl. Phys.* **63**, 3606 (1988).
- [41] P. J. Brown, V. Nunez, F. Tasset and P. Radhakrishna, *J. Phys.: Condens. Matter* **2**, 9409 (1990).
- [42] A. I. Okorokov, V. V. Runov and A. G. Gukasov, *Nucl. Instrum. and Meth.* **157**, 487 (1978).
- [43] M. Buttiker, *Phys. Rev. B* **27**, 6178 (1983).
- [44] V. Nunez, C. F. Majkrzak and N. F. Berk, *MRS Symp. Proc.* **313**, 431 (1993).
- [45] M. Blume and D. Gibbs, *Phys. Rev. B* **37**, 1779 (1988).
- [46] M. Blume, *J. Appl. Phys.* **57**, 3615 (1985).
- [47] J. B. Kortright, D. D. Awschalom, J. Stohr, S. D. Bader, Y. U. Idzerda, S. S. P. Parkin, I. K. Schuller and H. C. Siegmann, *J. Magnetism and Magnetic Materials* **207**, 7 (1999).

- [48] G. H. Lander, in *Magnetic Neutron Scattering*, Edited by A.Furrer, (World Scientific, Singapore, 1995) p.255.
- [49] S. W. Lovesey, *J. Phys. C: Solid State Phys.* **20**, 5625 (1987).
- [50] H. Rauch and S. A. Werner, *Neutron Interferometry*, (Clarendon Press, Oxford, 2000).
- [51] S. K. Sinha, M. Tolan and A. Gibaud, *Phys. Rev. B* **57**, 2740 (1998).
- [52] C. F. Majkrzak, N. F. Berk, S. Krueger and U. Perez-Salas, in *Techniques and Applications of Neutron Scattering in Biology*, Edited by J. Fitter, T. Gutberlet and J. Katsaras, (Springer-Verlag, Berlin, submitted).
- [53] F. Mezei and P. A. Dagleish, *Comm. Phys.* **2**, 41 (1977).
- [54] *International Tables for X-ray Crystallography*, Vol. IV, Eds. J. A. Ibers and W. C. Hamilton, Published for IUC (Kynoch Press, Birmingham, England, 1974).
- [55] E. F. Kneller, R. Hawig, *IEEE Trans. Magn.* **27**, 3588 (1991).
- [56] A. Rühm, B. P. Toperverg, H. Dosch, *Phy. Rev. B* **60**, 16073 (1999).
- [57] K. V. O'Donovan, J. A. Borchers, C. F. Majkrzak, O. Hellwig and E. E. Fullerton, *Phys. Rev. Lett.* **88**, 067201 (2002).
- [58] K. V. O'Donovan, J. A. Borchers, S. Maat, M. J. Carey and B. A. Gurney, *J. Appl. Phys.*, accepted (2004).
- [59] J. Bass and W. P. Pratt, *J. Magn. Magn. Mat.* **200**, 274, 1999.
- [60] M. R. Fitzsimmons, P. Yashar, C. Leighton, I. K. Schuller, J. Nogues, C.F. Majkrzak and J. A. Dura, *Phys. Rev. Lett.* **84**, 3986 (2000); C. Leighton, M. R. Fitzsimmons, P. Yashar, A. Hoffmann, J. Nogues, J. Dura, C. F. Majkrzak and I. K. Schuller *Phys. Rev. Lett.* **86**, 4394 (2001).
- [61] J. A. Borchers, private communication.